Localized waves in discrete excitable mechanical systems

Jose Eduardo Morales Morales

Communauté
UNIVERSITÉ Grenoble Alpes

THÈSE

Pour obtenir le grade de

DOCTEUR DE LA COMMUNAUTÉ UNIVERSITÉ GRENOBLE ALPES

Spécialité : **Mathématiques appliquées**

Arrêté ministériel : 7 Août 2006

Présentée par

José Eduardo Morales Morales

Thèse dirigée par **Guillaume James**
et codirigée par **Arnaud Tonnelier**

préparée au sein **d'INRIA Grenoble et Laboratoire Jean Kuntzmann** et de **l'Ecole Doctorale Mathématiques, Sciences et Technologies de l'Information, Informatique**

Ondes localisées dans des systèmes mécaniques discrets excitables

Thèse soutenue publiquement le **29 Novembre 2016**,
devant le jury composé de :

M, Hidde de Jong
DR, INRIA Grenoble Rhône-Alpes, Président
Mme, Anna Vainchtein
PR, Université de Pittsburgh, Rapporteur
M, Jean-Pierre Françoise
PR, Université Pierre et Marie Curie, Rapporteur
M, Michael Herrmann
PR, Université de Münster, Examinateur
M, Bruno Lombard
CR, CNRS LMA Marseille, Examinateur
M, Guillaume James
PR, Grenoble INP, Directeur de thèse
M, Arnaud Tonnelier
CR, INRIA Grenoble Rhône-Alpes, Co-Directeur de thèse

Abstract/Résumé

abstract: This thesis analyses localized travelling waves for some classes of nonlinear lattice differential equations describing excitable mechanical systems. These systems correspond to an infinite chain of blocks connected by springs and sliding on a surface in the presence of a nonlinear velocity-dependent friction force. We investigate both the Burridge-Knopoff model (with blocks attached to springs pulled at constant velocity) and a chain of free blocks sliding on an inclined plane under the effect of gravity. For a class of non-monotonic friction functions, both systems display a large response to perturbations above a threshold, one of the main properties of excitable systems. This response induces the propagation of either solitary waves or fronts, depending on the model and parameter regime. We study these localized waves numerically and theoretically for a broad range of friction laws and parameter regimes, which leads to the analysis of nonlinear advance-delay differential equations. Phenomena of propagation failure and oscillations of the travelling wave profile are also investigated. The introduction of a piecewise linear friction function allows one to construct localized waves explicitly in the form of oscillatory integrals and to analyse some of their properties such as shape and wave speed. An existence proof for solitary waves is obtained for the excitable Burridge-Knopoff model in the weak coupling regime.

keywords: localized travelling waves, solitary waves, fronts, lattice differential equations, excitable mechanical systems, Burridge-Knopoff model, nonlinear friction, advance-delay differential equations, piecewise linear dynamical systems, propagation failure.

résumé: Cette thèse étudie des ondes localisées pour certaines classes d'équations différentielles non linéaires décrivant des systèmes mécaniques excitables. Ces systèmes correspondent à une chaîne infinie de blocs reliés par des ressorts et qui glissent sur une surface en présence d'une force de frottement non linéaire dépendant de la vitesse. Nous analysons à la fois le modèle de Burridge-Knopoff (avec des blocs attachés à des ressorts tirés à une vitesse constante) et une chaîne de blocs libres glissant sur un plan incliné sous l'effet de la gravité. Pour une classe de fonctions de frottement non-monotones, ces deux systèmes présentent une réponse de grande amplitude à des perturbations au-dessus d'un certain seuil, ce qui constitue l'une des principales propriétés des systèmes excitables. Cette réponse provoque la propagation d'ondes solitaires ou de fronts, en fonction du modèle et des paramètres. Nous étudions ces ondes localisées numériquement et théoriquement pour une grande gamme de lois de frottement et de régimes de paramètres, ce qui conduit à l'analyse d'équations différentielles non linéaires avec avance et retard. Les phénomènes d'extinction de propagation et d'apparition d'oscillations sont également étudiés pour les ondes progressives. L'introduction d'une fonction de frottement linéaire par morceaux permet de construire explicitement des ondes localisées sous la forme d'intégrales oscillantes et d'analyser certaines de leurs propriétés telles que la forme et la vitesse des ondes. Une preuve de l'existence d'ondes solitaires est obtenue pour le modèle de Burridge-Knopoff pour un couplage faible.

mots-clés: ondes progressives localisées, ondes solitaires, fronts, équations différentielles sur réseau, systèmes mécaniques excitables, modèle de Burridge-Knopoff, frottement non linéaire, équations différentielles avec avance-retard, systèmes dynamiques linéaires par morceaux, extinction de propagation.

Para mis padres

Acknowledgements

I would like to thank profoundly and sincerely Guillaume James and Arnaud Tonnelier for their teachings and guidance during the last years. Words are not enough for describing my appreciation and gratitude towards them. I deeply enjoyed the thesis subject they proposed me which was full of stimulating questions and problems that I enjoyed to investigate, analyse and understand.

Thank you to Anna Vainchtein, Jean-Pierre Françoise, Michael Herrmann, Hidde de Jong and Bruno Lombard for accepting the invitation as members of the jury for my thesis defence. I was very honoured with their participation and the feedbacks they provided me during the conclusion of my thesis trajectory.

My time in the BIPOP-Team at Inria Rhône-Alpes was a very pleasant and enjoyable experience. I want to thank all the members of the team for their friendliness. Special thanks to Jan Michalczyk, Alexander Sherikov, Alejandro Blumentals, Alexandre Vieira, Mounia Haddouni and Narendra Akhadkar for their friendship and nice moments we passed together.

I want to thank my family and Veli for supporting me during the development of my thesis. Thank you my parents for providing me their unconditional love. Their teachings and personal values they transmitted me have always helped me to reach all my objectives.

Finally, I would like to express in general my profound admiration and respect to the different scientific communities all around the world. I believe that the passion for science has always been the main force for leading the humankind forward.

Contents

Chapter 1

Introduction

1.1 Wave propagation in excitable systems

An excitable unit is a dynamical system which is able to react to perturbations. Weak perturbations, i.e. below a threshold value, lead to small responses. If the perturbation surpasses a threshold value then the system undergoes over time a large excursion in the state space before arriving (or returning) to an equilibrium point (see Fig. 1.1). Excitable systems are commonly described by non-linear dynamical systems where, in the simple case, two variables are involved

$$\begin{aligned} \frac{du}{dt} &= F(u,y), \\ \frac{dy}{dt} &= G(u,y), \end{aligned} \tag{1.1}$$

where u may be seen as an activator and v as an inhibitor (or a recovery variable). The FitzHugh-Nagumo model, which describes the firing of a nerve cell, is given by the previous kind of equations and constitutes the prototypical example of an excitable system where large amplitude trajectories and oscillatory dynamics are prevailing [1, 2]. The qualitative analysis of the dynamics in the phase plane helps to understand the threshold effect. In particular, the nullcline configuration and the vector field direction allow to identify the threshold manifold that separates subthreshold regions from regions where the system has a large amplitude response. The coupling of excitable units defines an excitable medium where it is possible to transmit the perturbation from one unit to another. Different architectures may be found and the coupling of ODE

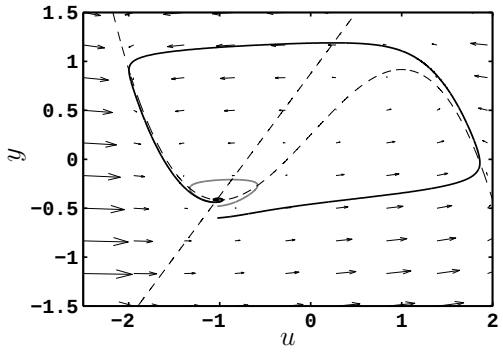

Figure 1.1: Phase space of the FitzHugh-Nagumo model $\dot{u} = u - u^3/3 - y + I$, $\dot{y} = 0.08(u + 0.7 - 0.8y)$. The responses of the nerve cell for different stimuli are shown in the phase plane. The nullclines are plotted (dotted lines). A small perturbation produces a small trajectory (grey line), whereas a stronger perturbation elicits a significant response (black line).

systems defined by (1.1) could result in a PDE system of the form

$$\begin{aligned} \frac{\partial u}{\partial t} &= d\frac{\partial^2 u}{\partial x^2} + k\frac{\partial^2 y}{\partial x^2} + F(u,y), \\ \frac{\partial y}{\partial t} &= G(u,y), \end{aligned} \tag{1.2}$$

where the spatial coupling includes: (i) a diffusive coupling corresponding to the term $\partial^2 u/\partial x^2$ where d is the diffusion coefficient and (ii) an elastic coupling corresponding to the term $\partial^2 y/\partial x^2$ where k is the stiffness coefficient. Other coupling types, as linear cross-diffusion, may also be included in the y-equation of (1.2) [3]. Diffusively coupled excitable systems appear in biological, chemical or ecological contexts. A well known example is Nagumo's equation that captures some of the complex behaviours observed in reaction-diffusion processes [1, 4, 5].

Excitable models with elastic (or dispersive) coupling are less abundant and they mainly occur in a mechanical context. In most cases, the u variable represents a velocity and y a position. A typical example is the Burridge-Knopoff model which has been considered in the geoscience field in order to reproduce statistical features of earthquakes dynamics [6, 7]. Cross-diffusion models have been developed for biophysical and biomedical applications such as the modelling of bacteria population growth or predator-prey interactions [5, 8]. It has been shown that spatially continuous models exhibit a wide variety of dynamical behaviours including propagating fronts, solitary waves, periodic wave trains, spiral waves, or chaotic behaviours [4].

Discrete excitable models. Several excitable systems are spatially discrete by

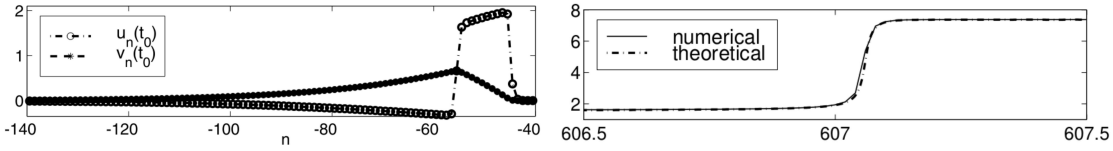

Figure 1.2: Examples of pulse (left) and front (right) profiles from the discrete FitzHugh Nagumo equation and the discrete Nagumo equation, respectively, and reproduced from [16, 17]. The pulse is plotted respect to the n coordinate, and the front respect to the $n - ct$ coordinate where c is the wave speed.

nature rather than continuous as encountered in electronic networks, chemical systems [9–11], species invasion models [12], or biological neurons [13]. Discrete media are frequently idealized as continuous media in order to simplify the mathematical analysis by replacing the infinite system of ODEs by a PDE. However, a continuous approximation cannot capture all the dynamical features of discrete media, specially at low coupling strength [14, 15]. In this case, discrete media have to be described using lattice differential equations. The discrete counterpart of (1.2) reads

$$\begin{aligned} \frac{du_n}{dt} &= d\Delta_d u_n + k\Delta_d y_n + F(u_n, y_n), \qquad n \in \mathbb{Z}, \\ \frac{dy_n}{dt} &= G(u_n, y_n), \end{aligned} \tag{1.3}$$

where $\Delta_d x_n = x_{n+1} - 2x_n + x_{n-1}$ is the discrete Laplacian. Similar spatio-temporal dynamics are found in both continuous and discrete models. For example, Fig. 1.2 illustrates the propagation of pulses and fronts in spatially discrete versions of the FitzHugh-Nagumo and Nagumo models [16, 17]. However the well known phenomenon of propagation failure or pinning effect that describes the inability of a wave to propagate is inherent to the lattice structure [13]. Analysis of discrete excitable systems has been mainly done for diffusively coupled systems. The discrete version of the Nagumo equation [4] is a prototypical example of such systems where the analysis of travelling waves and propagation failure has been well documented [18–21]. Keener presented a rigorous proof of propagation failure at weak coupling strength [13]. Erneux and Nicolis developed an asymptotic method to describe propagation failure [22]. Existence theorems for travelling fronts and travelling pulses have been proved [14, 16, 23]. Comparatively little insight has been obtained for discrete elastic excitable models and propagating phenomena have been not much explored [6, 7, 24]. In particular, propagation failure has not been addressed.

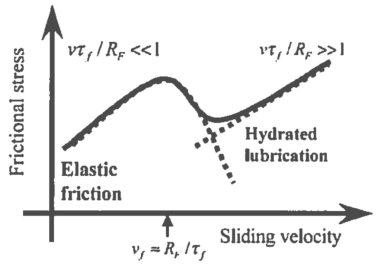

Figure 1.3: Schematic representation of a friction stress as a function of the sliding velocity for a gel that is adhesive to the substrate in liquid. The friction force presents a spinodal-type profile. (Figure obtained from [28]).

Discrete excitable elastic models. The Burridge-Knopoff model is a discrete elastic system that has been introduced in 1967 to describe statistical features of earthquake dynamics. The interaction of two plates is modelled as a block-spring chain subject to a friction law. Cartwright et al. have revisited the BK model via the introduction of a spinodal friction function. This friction function is velocity-strengthening at both low and high slipping velocities and velocity-weakening for intermediate slipping velocities (see Fig. 1.3 for a typical profile). This type of friction law is motivated by laboratory experiments on materials such as metal, rocks, hydrogels and rubber polymers, and from theoretical arguments [25–29]. Theoretical studies mainly rely on the continuum approximation for which propagating fronts, global oscillations and self-sustained travelling shock waves have been reported [6]. However, the existence of travelling pulse solutions has not been explored [7, 24] and the excitable properties of the model have been investigated only partially. In particular the influence of the non-monotonic friction force on propagating patterns is still unclear.

1.2 Objectives of the thesis and methods

In this thesis we study localized travelling waves for some classes of nonlinear lattice differential equations describing excitable mechanical systems. We consider two specific systems but the mathematical tools used and developed in this thesis could be used as well for other applications. The two systems that we analyse correspond to an infinite chain of blocks connected by springs and sliding over a surface in the presence of a nonlinear velocity-dependent friction force. We investigate both a chain of free blocks sliding on an inclined plane under the effect of gravity (chapter 2) and the BK model (chapters 3 and 4). For a class of non-monotonic friction functions, both systems

display a large response to perturbations above a threshold, one of the main properties of excitable systems. This response induces the propagation of either solitary waves or fronts, depending on the model and parameter regime. We study these localized waves numerically and theoretically for a broad range of friction laws and parameter regimes, which leads to the analysis of nonlinear advance-delay differential equations. Phenomena of propagation failure and oscillations of the solitary wave profile are also investigated in the BK model (chapter 3). The introduction of a piecewise linear friction function allows one to construct explicitly front solutions (chapter 2) and solitary waves (chapter 3) in the form of oscillatory integrals and to analyse some of their properties such as shape and wave speed. An existence proof for solitary waves is obtained for the excitable Burridge-Knopoff model in the weak coupling regime (chapter 4). Chapter 5 lists several open problems and perspectives opened by this work.

1.3 Spring-block chain sliding under gravity

In chapter 2 we study the dynamics of an infinite chain of identical blocks sliding on a slope under the effect of gravity (see Fig. 1.4). The blocks are coupled to their nearest neighbours through linear springs of stiffness k. We denote by $F(v)$ the friction force exerted on a block sliding at velocity v, G the tangential component of the gravity force and m the mass of the blocks. The velocity V corresponds to the constant sliding state $F(V) = G$ (we shall use V as a bifurcation parameter instead of G). We consider the spatially uniform constant sliding state as our reference state. We denote by $y_n(t)$ a perturbation of the position of the n^{th} block and $u_n = \frac{dy_n}{dt}$ a perturbation of the constant sliding velocity. The dynamical equations are

$$\begin{aligned} \frac{dy_n}{dt} &= u_n, \\ m\frac{du_n}{dt} &= k\Delta_d y_n - F(V + u_n) + G, \qquad n \in \mathbb{Z}, \end{aligned} \tag{1.4}$$

where $\Delta_d y_n = y_{n+1} - 2y_n + y_{n-1}$ is the discrete Laplacian.

We are not aware of previous studies of nonlinear waves in this lattice dynamical system. Equation (1.4) will be analysed for spinodal friction laws $F(v)$ qualitatively similar to the one represented in Fig. 1.3.

In the case of a single block (or if $k = 0$), the spinodal friction law leads to bistability between two constant sliding velocities. The coupling of such bistable units results in

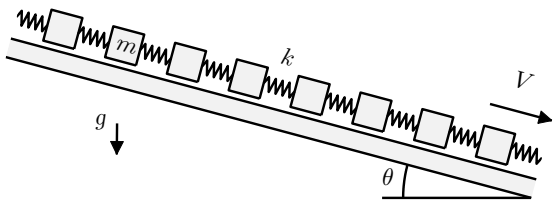

Figure 1.4: Schematic representation of the chain sliding on a slope. The steady state corresponds to $F(V) = G$ with $G = mg\sin\theta$.

an excitable network that supports moving fronts and pulses. Numerically, we observe in a certain range of pulling velocities V that the pulses broaden during propagation. Pulses with a fixed width are also observed for a specific sliding velocity $V = V^*$.

Equation (1.4) is studied analytically for a piecewise linear friction law $F(v)$. We construct a front solution by Fourier transform and derive a nonlinear equation for its wave speed c. The equation is solved numerically and analytically in the small coupling limit.

We observe that $c \to 0$ for $k \to 0$, hence propagation failure does not occur at low coupling. This property contrasts with known results on front propagation in discrete bistable diffusive systems, where pinning occurs at low coupling [13–16, 19, 30].

Using the explicit front solution, we explain the dynamics of pulse propagation on system (1.4). Broadening pulses merely consist of two fronts propagating with different wave speeds. Pulses with constant width correspond to both fronts propagating with the same wave speed. We analytically compute the sliding velocity $V = V^*$ for which pulses with constant width exist.

Finally, we discuss a connection between system (1.4) and the BK model. The latter sustains propagating pulses under the same friction laws and parameter values. The fronts of system (1.4) can be used to approximate transition layers of pulse solutions of the BK model.

1.4 Travelling pulses in the discrete excitable BK model

Chapter 3 is devoted to the BK model that describes the frictional interaction of two surfaces, one being pulled at a constant speed V and the second discretized as a chain of blocks. We first provide a summary of different types of friction laws considered in previous work on the BK model and review the different types of wave phenomena

that have been analysed. The main part of chapter 3 addresses the propagation of localized waves in the BK model within a simplified physical framework. We assume that the blocks are identical (with mass γ) and experience a friction force described by a nonlinear function $F(v)$ where v denotes the sliding velocity (see Fig. 1.5). The blocks are connected to nearest neighbours by Hookean springs of stiffness k_c and to the upper plate by springs of stiffness k_p (this effect was absent in system (1.4)). Using the dimensionless coupling parameter $k = k_c/k_p$, the governing equations are

$$\begin{aligned} \frac{dy_n}{dt} &= u_n, \\ \gamma\frac{du_n}{dt} &= k\Delta_d y_n - F(V+u_n) - y_n, \end{aligned} \tag{1.5}$$

where $n \in \mathbb{Z}$. The spatial discreteness of the BK model is appropriate to describe the frictional dynamics of micropatterned surfaces similar to the ones presented in Fig. 1.6. Other applications include earthquake modelling, nonlinear transmission lines and mechanical oscillator networks.

We show that for a class of non-monotonic friction forces, similar to the one depicted in Fig. 1.3, the BK model supports the propagation of solitary waves. We explore numerically and analytically the characteristics of these travelling waves such as their waveforms and wave speeds. Propagation failure phenomenon at weak coupling is studied.

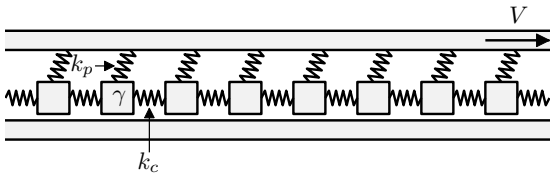

Figure 1.5: The mechanical interpretation of the Burridge-Knopoff model, where V is the pulling velocity or slip rate of the loader plate, γ is the mass of a block, k_c and k_p are the stiffness of the Hookean springs.

The critical coupling value k^* that determines propagation failure is investigated for different pulling velocities V. The properties of the waves are qualitatively explained using the geometry of single-block excitability.

Two special regimes are explored in detail: a bistability regime and the continuum limit. A bistability regime appears close to the transition when the friction law switches from a velocity-strengthening regime for large sliding velocities to a velocity weakening regime. In this regime, a stable focus coexists with self-sustained oscillations inducing

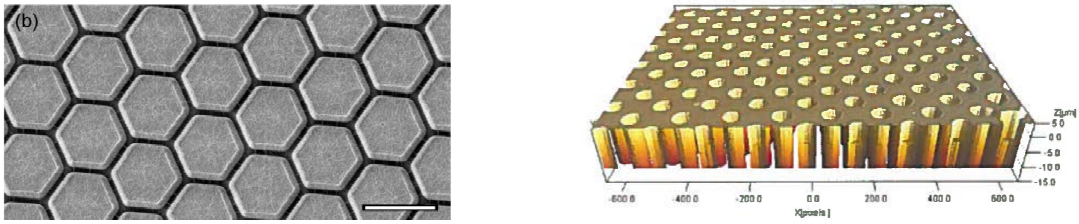

Figure 1.6: Micropattern surfaces fabricated for slip control under wet conditions. Left figure reproduced from [31] and right figure reproduced from [32].

complex propagating patterns. The continuum limit is approached numerically and analytically as $k \gg 1$. Near the continuum limit, model (1.5) takes the form of a PDE

$$\gamma \frac{\partial^2 y}{\partial t^2} + F\left(V + \frac{\partial y}{\partial t}\right) + y = \frac{\partial^2 y}{\partial x^2} + \text{h.o.t}, \tag{1.6}$$

for which we seek travelling wave solutions. We show that smooth solitary waves do not exist in the continuum limit but weak solutions (shocks) exist. Numerical simulations of the BK model with $k \gg 1$ suggest the existence of solitary waves with shock-like profiles that are related to the existence of the weak solutions obtained in the formal continuum limit.

Finally, we construct analytically a formal solitary wave solution for a piecewise-linear friction force with a jump discontinuity. The solution satisfies an advance-delay differential equation and can be expressed using Fourier transform. We are interested in studying the simplest type of solitary waves, i.e., a solution that crosses the jump discontinuity only twice. For suitable parameter values, we show that stable solitary waves coexist with slower solitary waves not observed in dynamical simulations (and presumably unstable). The propagation failure that occurs at low coupling corresponds to a fold bifurcation between these two solution branches. We also determine parameter values for which spurious solutions occur in our formal calculations. This is the reason why we establish an existence theorem for solitary waves under specific assumptions in chapter 4.

1.5 Existence theorem for solitary waves in the BK model

Chapter 4 presents an existence theorem for solitary waves in the Burridge Knopoff model with the piecewise-linear friction force

$$F(v) = \frac{v}{a} - \alpha H(v - a), \quad v > 0, \tag{1.7}$$

where H denotes the Heaviside function. Block velocities take the form $u_n(t) = \varphi(\xi)$ with $\xi = n - ct$ (c denotes the wave speed) and $\lim_{\xi\to\pm\infty} \varphi(\xi) = 0$. Using this Ansatz, equation (1.5) yields the advance-delay differential equation

$$c^2\gamma\varphi''(\xi) = k\Delta_d\varphi(\xi) + c\frac{d}{d\xi}F(V + \varphi(\xi)) - \varphi(\xi), \tag{1.8}$$

with derivatives taken in the sense of distributions (due to the discontinuity of F at $v = a$). We further assume that solitary waves possess the following structure with only two discontinuity crossings

$$\begin{cases} \varphi(0) = \varphi(\xi_1) = a - V \\ V + \varphi(\xi) < a \ \text{ if } \ \xi \in]\xi_1, 0[\\ V + \varphi(\xi) > a \quad \text{otherwise.} \end{cases} \tag{1.9}$$

Under assumption (1.9), equation (1.8) takes the form of an affine advance-delay differential equation which can be solved by Fourier transform and the two equality constraints in (1.9) determine the velocity c and the parameter ξ_1 of the solitary wave. In order to prove the existence of solitary waves, the main difficulty is then to check the inequality constraints in (1.9). This step is not straightforward because φ is defined through an oscillatory integral in the above setting. We overcome this difficulty in the limit $k \approx 0$, where (1.8) becomes close to an ODE. We prove the following result.

Theorem 1 (Existence of solitary waves)**.** *Assume $\gamma < \frac{1}{4a^2}$. Fix $c > \frac{b}{a\gamma \ln\left(\frac{1+b}{1-b}\right)}$ with $b = \sqrt{1 - 4a^2\gamma}$. Then there exist functions $\bar{V}(k)$ and $\xi_1(k)$ such that the following result holds. For all k small enough, for $V = \bar{V}(k) = a + \mathcal{O}(k)$, there exists a solution of (1.7)-(1.8)-(1.9) such that $\lim_{\xi\to\pm\infty} \varphi(\xi) = 0$. This solution takes the following form when $k \to 0$:*

$$\varphi(\xi) = \alpha c\,[K(\xi - \xi_1) - K(\xi)] + \mathcal{O}(k) \tag{1.10}$$

where K denotes the fundamental solution of the operator $c^2\gamma\frac{d^2K}{d\xi^2} - \frac{c}{a}\frac{dK}{d\xi} + K$. We have in addition when $k \to 0$

$$\xi_1 = \mathcal{O}(\ln k). \tag{1.11}$$

The assumption $\gamma < \frac{1}{4a^2}$ in Theorem 1 sets the analysis in the overdamped regime which allows to simplify, to some extent, the verification of the inequality constraints. The proof is based on an asymptotic expansion of φ for $k \approx 0$, ODE techniques to study inner approximations of φ near the two discontinuities of φ' (at $\xi = 0$ and $\xi = \xi_1$),

and outer approximations of φ (based on the explicit form of K). Using the above expansions, we also derive a lower bound on the coupling constant k in order to have existence of solitary waves of the type (1.9), in the case where the pulling velocity V is fixed and close to a.

Chapter 2

Travelling waves in a block-spring chain sliding down a slope

2.1 Introduction

Spatially discrete extended systems have a wide range of applications such as the description of vibration in crystals or micromechanical arrays [33–35]. The type of coupling between the elements is a distinctive feature of the application domain. In mechanical systems, ideal mass spring systems with nearest-neighbours coupling are frequently introduced to approximate the macroscopic behaviour of deformable systems [36]. In this work we consider the dynamics of an infinite chain of blocks coupled by Hookean springs that slides down a slope due to gravity (see Fig. 2.1). Each block is subjected to a nonlinear friction force. We consider a friction law of spinodal type (see Fig. 1.3 for an example). Such friction laws have been reported to induce excitable dynamics reminiscent of neural excitability [6], i.e., a perturbation above a certain threshold produces a large excursion in the phase space before returning to the equilibrium state. In biology, it is well documented that a large class of excitable media is able to support nonlinear solitary waves [37]. It has been recently shown that excitable mechanical systems also have the capacity to induce self-sustained solitary waves [6, 7, 24].

In many studies, the analysis of discrete travelling patterns heavily relies on a continuum approximation of the original model. In the spring-block model presented here, we directly tackle the discrete nature of the equations and use an idealized piecewise-linear friction force to derive exact expressions for propagating waves. This approach

has been used in a variety of contexts to study travelling waves in lattices, see e.g. [14, 19, 20, 38–45]. The structure of this chapter is as follows. We first derive the governing equations for the chain of elastically coupled blocks. Then we study the dynamical properties of an isolated block and demonstrate that a bistable behaviour exists when a spinodal friction force is considered. For the coupled system, numerical simulations show that the bistability property induces travelling patterns, as fronts and pulses. For a piecewise-linear friction force we construct the travelling fronts analytically. The link between fronts and pulse waves is also studied. We then conclude by connecting the results to the dynamics of the BK model.

2.2 The Model

Let us consider an isolated block of mass m and position $x(t)$ that slips down a slope under gravity and subject to a velocity-dependent friction force $F\left(\frac{dx}{dt}\right)$. The dynamical equations read

$$m\frac{d^2x}{dt^2} + F\left(\frac{dx}{dt}\right) = G \tag{2.1}$$

where G is the tangential component of the gravity force. A steady state of (2.1) exists when the block achieves a constant velocity motion $\frac{dx}{dt} = V$ where $F(V) = G$. Let us consider an infinite chain of identical blocks linearly coupled through Hookean springs of stiffness k that slips at the constant speed V over an inclined surface (see Fig. 2.1). The dynamical equations in a frame moving at velocity V are given by:

$$\begin{aligned} \frac{dy_n}{dt} &= u_n, \\ m\frac{du_n}{dt} &= k\Delta_d y_n - F(V+u_n) + G, \qquad n \in \mathbb{Z} \end{aligned} \tag{2.2}$$

where y_n represents the displacement of the n^{th} block from the steady sliding state and u_n its velocity. The term $\Delta_d y_n = y_{n+1} - 2y_n + y_{n-1}$ is the discrete Laplacian.

The system may be interpreted as a variant of the Burridge-Knopoff model [46] where the shear stress described by the local potential is replaced by a constant tangential force induced by gravity. The dynamics of system (2.2) is explored for three normalized non-monotonic friction laws F_ε, F_c and F_0, depicted in Fig. 2.2**A**-**C** and given by

$$\begin{aligned} F_\varepsilon(v) &= \left[1 - \alpha + \sqrt{N(v)}\right]\frac{v}{\sqrt{\varepsilon + v^2}}, \\ F_c(v) &= 3.2v^3 - 7.2v^2 + 4.8v, \\ F_0(v) &= v/a - \alpha H(v-a), \end{aligned} \tag{2.3}$$

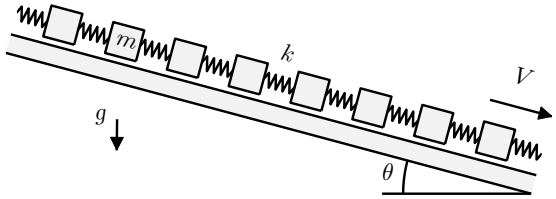

Figure 2.1: Mechanical representation of the block-spring slider model where m is the mass, k is the spring constant and V is the sliding velocity. The steady state corresponds to $F(V) = G$ with $G = mg\sin\theta$.

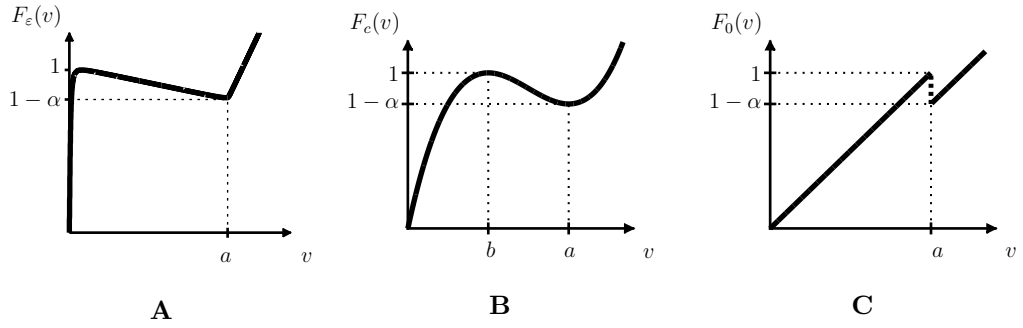

Figure 2.2: Non-monotonic friction laws. **A** Coulomb-like friction force F_ε, where $\varepsilon = 10^{-4}$. **B** The cubic friction force $F_c(v)$, where $b = 0.5$, $a = 1$ and $\alpha = 0.2$. **C** The piecewise linear friction force $F_0(v)$.

where $N(v) = \varepsilon + 4\max(|v| - a, 0)^2 + \alpha^2 \max(a - |v|, 0)^2$, and H is the Heaviside step function. For convenience, the cubic friction force F_c is given for $a = 1$ where a is the location of the local minimum, i.e. the transition point from velocity-weakening ($v < a$) to velocity-strengthening ($v > a$) regime. The friction function F_ε describes a regularized generalized Coulomb law as $\varepsilon \to 0$. The cubic friction force F_c describes a smooth spinodal friction law similar to the one introduced in [7]. The piecewise linear function F_0 captures some properties of these friction laws. It reduces the velocity-weakening region to a jump discontinuity and is convenient for analytical computations.

2.3 Bistable dynamics of a single block

For a single block, (2.2) reads

$$\begin{aligned} \frac{dy}{dt} &= u. \\ m\frac{du}{dt} &= -F(V+u)+F(V). \end{aligned} \tag{2.4}$$

The y-nullcline is defined by $u = 0$ whereas the u-nullcline is obtained by solving $F(V + u) = F(V)$ so that the vertical axis $u = 0$ always defines in the (u, y) plane the set of fixed points for an isolated block. It is easy to check that the two associated eigenvalues are given by $\lambda_1 = \frac{-F'(V)}{m}$, $\lambda_2 = 0$ so that the equilibrium straight line is stable (but not asymptotically stable). In (2.4), the dynamics of the velocity u does not depend on the position y so that system (2.4) behaves as a one dimensional dynamical system whose bifurcation diagram is shown in Fig. 2.3 for the three friction laws (2.3) where V is taken as the bifurcation parameter.

For $V \in (a, V_{\max})$, where $V_{\max}$ is the velocity value such that $F(V_{\max})$ equals the local maximum in F and $V_{\max} > a$, there exist three fixed points $U_1 < U_2 < U_3 = 0$ whose stability is governed by the eigenvalue $\mu_i = \frac{-F'(V+U_i)}{m}$, $i \in \{1, 2, 3\}$, respectively. A saddle-node bifurcation occurs at $V = V_{\max}$ and a transcritical bifurcation takes place at $V = a$. For $V \in (a, V_{\max})$, the two fixed points U_1 and U_3 are stable whereas U_2 is unstable and behaves as an excitation threshold. For an initial condition below U_2 the trajectory of the system tends towards $U_3 = 0$, whereas for a sufficiently strong perturbation the system reaches asymptotically the state U_1 illustrating the excitable dynamics of an isolated block. Depending on the initial state, the system can switch from a neighbourhood of U_3 to U_1 and vice versa. For the cubic friction force $F_c(v)$, the threshold is given by

$$U_2 = -\frac{3}{2}V + \frac{9}{8} + \frac{1}{8}\Delta(V) \tag{2.5}$$

where $\Delta(V) = \left(-48V^2 + 72V - 15\right)^{1/2}$ (one has $\Delta(V) \in \mathbb{R}$ for $V \in [1/4, 5/4]$). We have

$$U_1 = -\frac{3}{2}V + \frac{9}{8} - \frac{1}{8}\Delta\left(V\right),$$

and $V_{\max} = 5/4$. For the friction force $F_0(v)$, the threshold is simply defined as

$$U_2 = a - V, \tag{2.6}$$

the stable fixed point U_1 is given by

$$U_1 = -\alpha a, \tag{2.7}$$

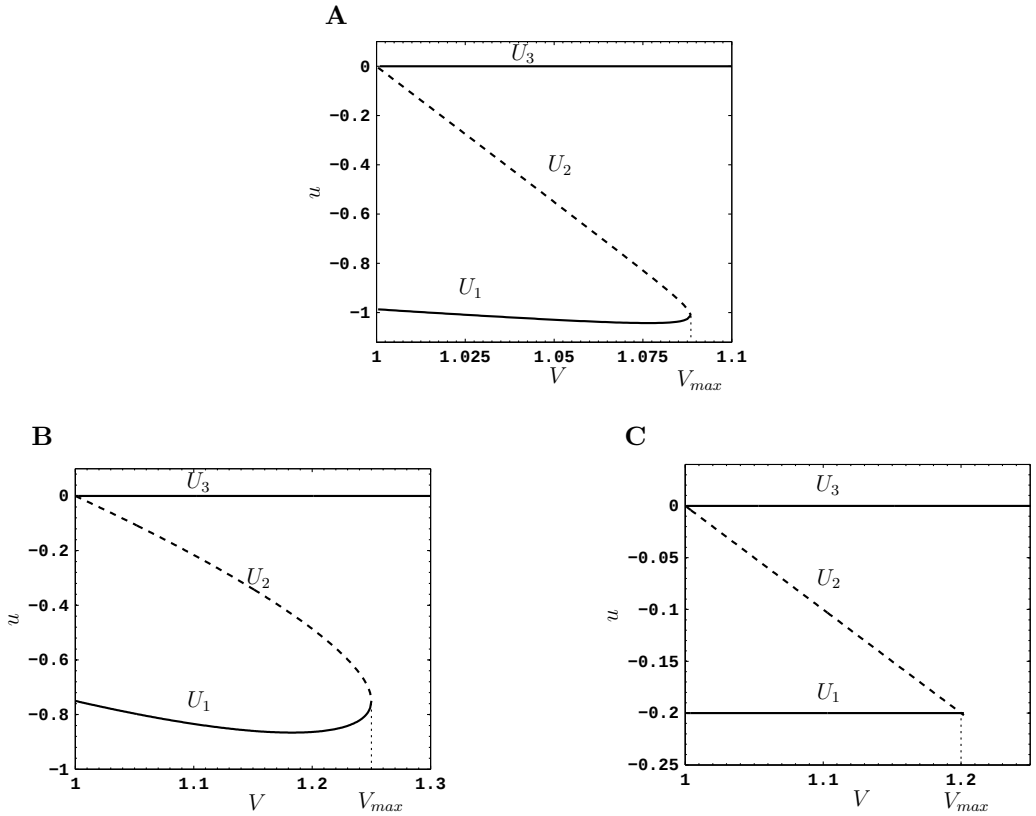

Figure 2.3: Bifurcation diagrams of the single block model. Stationary state, u, as a function of the sliding velocity, V, for **A** regularized generalized Coulomb friction force F_ε ($a = 1$, $\alpha = 0.2$, $\varepsilon = 10^{-4}$) **B** the cubic friction force F_c ($a = 1$, $b = 0.5$, $\alpha = 0.2$) and **C** the piecewise linear friction force F_0 ($a = 1$, $\alpha = 0.2$). Solid lines represent stable states (denoted U_1 and U_3) and dotted lines are for unstable states (U_2).

and we have $V_{\max} = a(1 + \alpha)$. For the regularized generalized Coulomb law F_ε, as $\varepsilon \to 0$ the threshold converges to

$$U_2 = (a - V)\left[1 + \frac{2}{\alpha}\right]$$

and the stable fixed point U_1 to

$$U_1 = -V$$

and we have $V_{\max} = a(1 + \frac{\alpha}{2})$. In the following we are interested in the excitability regime where the velocity of the single block has two stable steady states and we fix a V value in the interval delimited by the two bifurcation points, i.e. $V \in]a, V_{\max}[$. As we will show in the sequel, the bistability property is a key feature for the existence of travelling fronts in the block-spring chain.

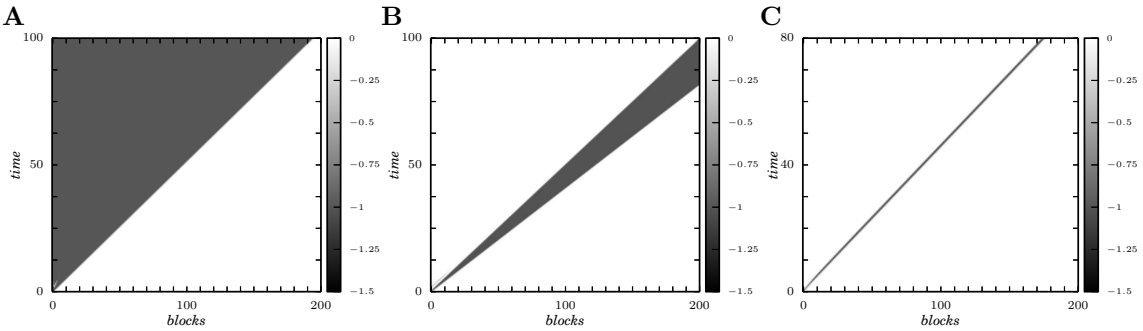

Figure 2.4: Numerical simulations of equation (2.8) with the regularized Coulomb friction force F_ε with the same parameters as in Fig. 2.3. We display spatiotemporal plots of the velocity variable u_n of **A** a travelling front ($k = 0.5$ and $V = 1.01$), **B** a broadening pulse ($k = 1$ and $V = 1.025$), **C** a steadily propagating pulse solution ($k = 1$ and $V = 1.046$). An initial perturbation $u_0(0) = -10$ is applied on the first block of the chain. Computations are performed for $m = 0.15$.

2.4 Travelling waves

Let us consider the block-spring slider model with the regularized generalized Coulomb law F_ε. We choose parameters so that each block exhibits a bistable behaviour. The parameters of the friction law are those of Fig. 2.3**A**. Model (2.2) can be rewritten in terms of velocity as

$$m\frac{d^2u_n}{dt^2} = k\Delta_d u_n - \frac{du_n}{dt}F'(V + u_n). \tag{2.8}$$

We initialize the network by applying a suitable perturbation to the steady state $U_3 = 0$. A localized perturbation is applied on the first block at the left edge of the network, see Fig. 2.4 for more details. We consider a finite chain of blocks with free boundary conditions. For the numerical simulations, we use the adaptive Lsoda solver with a time step $\Delta t = 0.001$ and with a minimal error tolerance of $1.5e-8$.Unless stated otherwise we take for the numerical simulations $m = 0.15$, this value was considered in the study of the BK model in chapter 3 and allows a direct comparison of the dynamics between both models. We observe the existence of travelling fronts as shown in Fig. 2.4**A**. In addition, two types of pulse solutions are observed: (i) pulse waves with expanding width and (ii) pulse waves with constant shape as plotted in Fig. 2.4**B** and **C**, respectively.

Propagating fronts (similar to the one shown in Fig. 2.4**A**) are the dominant pattern when the threshold is close to the resting state, i.e., for V close to a ($|U_2| \ll 1$). The speed of the propagating front increases with the coupling value k but, at the same

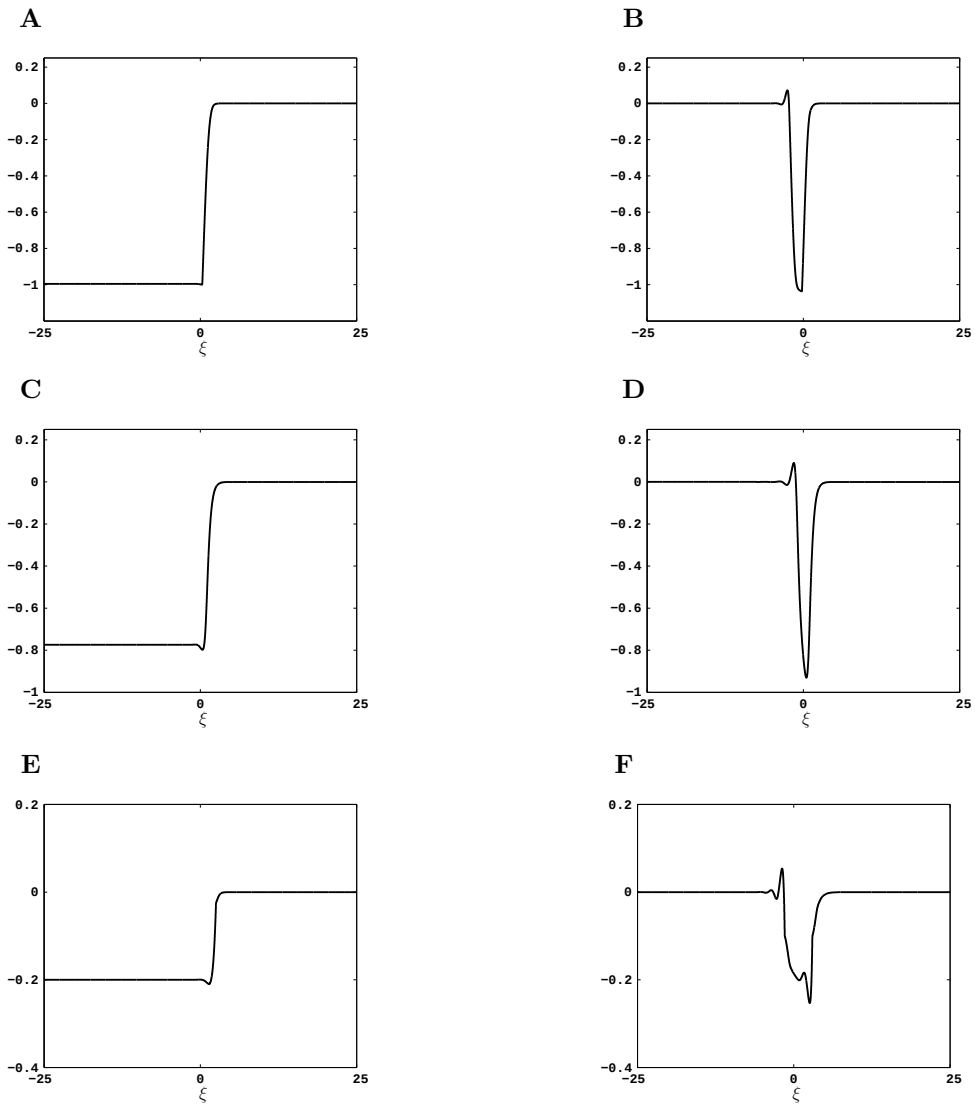

Figure 2.5: Plots of the velocity waveforms $u_n(t)$ of the block-spring model in the travelling wave coordinate $\xi = n - ct$. The wave profiles in **A,B** are obtained with the regularized generalized Coulomb law F_ε and correspond to the travelling waves shown in Fig. 2.4**A,C**, respectively. Plots **C** and **D** represent the wave profiles obtained with the cubic friction force, F_c. Plots **E** and **F** represent the wave profiles obtained with the piecewise linear friction law F_0. The wave speed is **A** $c = 1.95$, **B** $c = 2.21$, **C** $c = 3.06$, **D** $c = 3.16$, **E** $c = 3.16$ **F** $c = 1.45$. For the piecewise linear law, we use $a = 1$ and $\alpha = 0.2$. Other parameters are those of Fig. 2.4 for **A-B** and we take **C** $V = 1.025$, $k = 1$ **D** $V = 1.18$, $k = 2$, **E**, $V = 1.025$, $k = 1$, **F** $V = 1.1$, $k = 1$.

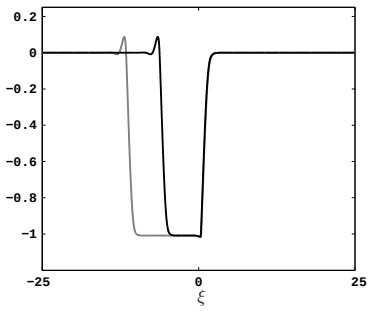

Figure 2.6: Plot of the velocity waveforms $u_n(t)$ of the block-spring model. The two localized pulses correspond to a snapshot of the travelling pattern shown in Fig. 2.4**B** at two different locations ($n = 25$, $n = 50$). The initial front propagates at speed $c = 2.45$ and the rear front at $c = 2$. Other parameters are those of Fig. 2.4**B**

time, the parameter range where front waves exist shrinks (without vanishing). As the sliding velocity increases, a front to pulse transition occurs where the excitation spreads over the network and leads to pulses with expanding width (see Fig. 2.4**B**). The rate of expansion of the enlarging pulse decreases as the sliding velocity increases leading to the existence of a pulse with constant width as shown in Fig. 2.4**C**. For $V \to V_{\max}$, the threshold approaches the fixed point U_1 and a perturbation fails to produce a travelling pattern. Qualitatively similar results are obtained for the cubic friction force F_c and for the piecewise linear friction force F_0.

The profiles of the travelling waves observed in Fig. 2.4**A,C** are shown in Fig. 2.5**A,B**, respectively, and are compared with those obtained with the cubic law (Fig. 2.5**C,D**) and the piecewise-linear law (Fig. 2.5**E,F**). The travelling patterns for the three friction forces have similar shapes and mainly contrast in their amplitude that is determined by the distance between the two stable fixed points. A non-monotonic wave profile is observed for the travelling fronts with the existence of a dip behind the front (see Fig. 2.5**C,E**) whereas the dip is too small to be seen in Fig. 2.5**A**. Interestingly, similar profiles were obtained for travelling fronts in a chain of bistable oscillators [47]. Qualitatively, these results are not affected by the mass parameter (simulations not shown).

The enlarging pulse observed in Fig. 2.4**B** may be seen as the superposition of two travelling fronts with two different propagating speeds (see Fig. 2.6). The initial front is qualitatively similar to the waveform shown in Fig. 2.5**A** and is followed by a travelling front that propagates in the same direction but with a lower speed and that connects the two stable states in a reversed order.

The localized pulse waves shown in Fig. 2.5**B,D,F** are thus expected to appear when the two travelling fronts have the same speed. These observations are analytically explained in the next section for the piecewise-linear law F_0.

2.5 Construction of travelling fronts for the piecewise-linear friction force

A travelling front solution of (2.8) takes the form:

$$u_n(t) = \varphi(n - c\,t) \tag{2.9}$$

where

$$\varphi(\infty) = U_3 = 0 \quad \text{and} \quad \varphi(-\infty) = U_1 \tag{2.10}$$

with $U_1 \neq 0$ a stable equilibrium. The function φ describes the waveform, and c is the wave speed that has to be determined. Substitution of (2.9) into (2.8) gives the advance-delay differential equation

$$c^2 m\varphi''(\xi) = k(\varphi(\xi+1) + \varphi(\xi-1) - 2\varphi(\xi)) + c\frac{d}{d\xi}F_0(V + \varphi(\xi)) \tag{2.11}$$

where $\xi = n - ct \in \mathbb{R}$ is the travelling wave coordinate. The front solutions described in section 2.4 connect two different stable steady states as $n \to \pm\infty$. In contrast, the travelling pulse tends towards the same stable equilibrium as $n \to \pm\infty$.
We consider here the piecewise linear force F_0 and we assume that each block is in a bistable regime, i.e. we have $V \in (a, a(1+\alpha))$ and $U_1 = -\alpha a$ as in (2.7). We assume that the travelling front solution crosses the threshold (2.6) for only one value of ξ. Translation invariance of travelling waves allows us to fix this value to $\xi = 0$ and we seek for a solution such that

$$\begin{cases} \varphi(\xi) < a - V \text{ for } \xi < 0, \\ \varphi(0) = a - V, \\ \varphi(\xi) > a - V \text{ for } \xi > 0. \end{cases} \tag{2.12}$$

Using (2.12) to simplify the nonlinear term $F(V + \varphi)$, system (2.11) takes the form

$$c^2 m\varphi''(\xi) \;=\; k(\varphi(\xi+1) + \varphi(\xi-1) - 2\varphi(\xi)) + \frac{c}{a}\varphi'(\xi) - \alpha c\delta(\xi), \tag{2.13}$$

where $\delta(\xi)$ is the Dirac delta function.
Equation (2.13) is a linear non-autonomous differential equation so that one may attempt to use the Fourier transform to derive an analytic solution. However a certain

amount of care is needed to correctly handle the Fourier transform of φ due to the nonzero boundary condition at $-\infty$. We look for $\varphi(\xi)$ in the form

$$\begin{cases} \varphi(\xi) = \alpha a \left(\psi(\xi) + H(\xi) - 1\right), \\ \psi(\xi) \in L^2(\mathbb{R}), \quad \lim_{\xi\to\pm\infty} \psi(\xi) = 0, \end{cases} \tag{2.14}$$

where $\psi(\xi)$ needs to be determined. Equation (2.13) is re-expressed in terms of $\psi(\xi)$ and Fourier transform is applied to determine $\psi(\xi)$, and subsequently $\varphi(\xi)$.
Integrating (2.13), gives

$$c^2 m\varphi' \;=\; k \wedge' * \varphi + \frac{c}{a}\varphi + \alpha c(1-H), \tag{2.15}$$

where $\wedge(\xi) = \max(1-|\xi|, 0)$ is the tent function, and where we used for any $f \in L^1_{loc}(\mathbb{R})$,

$$(\wedge' * f)(\xi) = \int_{\xi}^{\xi+1} f(s)ds - \int_{\xi-1}^{\xi} f(s)ds. \tag{2.16}$$

Note that (2.15) together with (2.10) remains equivalent to the original problem (2.13)-(2.10). Injecting (2.14) into (2.15), gives

$$c^2 m\psi' - \frac{c}{a}\psi - k \wedge' * \psi \;=\; k \wedge -c^2 m\delta, \tag{2.17}$$

where we used the property $\wedge' * (H-1) = \wedge$. Taking the Fourier transform as $\widehat{\psi}(\lambda) = \int_{\mathbb{R}} e^{-2\pi i\lambda\xi}\psi(\xi)d\xi$ in (2.17), we obtain

$$\left(2i\pi\lambda c^2 m - \frac{c}{a} - k2i\pi\lambda \mathrm{sinc}^2(\lambda)\right)\widehat{\psi}(\lambda) = k\mathrm{sinc}^2(\lambda) - c^2 m, \tag{2.18}$$

where we used $\widehat{\wedge}(\lambda) = \mathrm{sinc}^2(\lambda)$ with $\mathrm{sinc}(\lambda) = \sin(\pi\lambda)/\pi\lambda$. Let us introduce

$$\widehat{K}(\lambda) = \left(2i\pi\lambda\left[c^2 m - k\mathrm{sinc}^2(\lambda)\right] - \frac{c}{a}\right)^{-1}$$

where one has $\widehat{K}(\lambda), K(\xi) \in L^2(\mathbb{R})$ (K denotes the inverse Fourier transform of $\hat{K}$). From $\frac{d\widehat{K}}{d\lambda} \in L^1(\mathbb{R})$ and using $-2i\pi\xi K = \mathcal{F}^{-1}\left(\frac{d\widehat{K}}{d\lambda}\right) \in L^\infty(\mathbb{R})$, one has $\lim_{\xi\to\pm\infty} K(\xi) = 0$ ($\mathcal{F}^{-1}$ denotes the inverse Fourier transform). From (2.18), we obtain

$$\psi = kK * \wedge - c^2 mK. \tag{2.19}$$

Since $\wedge \in L^1(\mathbb{R})$ we have $K * \wedge \in L^2(\mathbb{R})$, and because $K, \wedge \in L^2(\mathbb{R})$ then $K * \wedge \in C^0(\mathbb{R})$ decays to zero when $\xi \to \pm\infty$. Consequently $\psi(\xi)$ given by (2.19) satisfies the properties assumed in (2.14), and defines a unique solution in $L^2(\mathbb{R})$. Therefore (2.14) is a solution

of (2.13) with boundary conditions (2.10). Regularity properties of $\varphi(\xi)$ can be inferred from the following identity obtained from (2.14) and (2.17)

$$\frac{c^2 m}{\alpha a}\varphi' = \frac{c}{a}\psi + k \wedge' * \psi + k \wedge . \tag{2.20}$$

This implies $\varphi' \in L^1_{loc}(\mathbb{R})$ (since $\wedge' * \psi \in L^2(\mathbb{R})$) and thus ones has $\varphi \in C^0(\mathbb{R})$. We also get from (2.15) that $\varphi' \in C^0(\mathbb{R}^+) \cap C^0(\mathbb{R}^-)$, hence $\varphi \in C^1(\mathbb{R}^+) \cap C^1(\mathbb{R}^-)$, and thus (2.15) gives $\varphi' \in C^1(\mathbb{R}^+) \cap C^1(\mathbb{R}^-)$. We get finally

$$\varphi \in C^2(\mathbb{R}^+) \cap C^2(\mathbb{R}^-) \cap C^0(\mathbb{R}).$$

From the analytical expression of φ, we can determine an equation for the wave speed of the front. Using (2.14), we set

$$\begin{aligned} \frac{\varphi(\xi) + \varphi(-\xi)}{2} &= \frac{\alpha a}{2}\left[\psi(\xi) + \psi(-\xi) - 1\right] \\ &:= \frac{1}{2}G(\xi, c) \end{aligned} \tag{2.21}$$

where ψ is defined by (2.19) (note that we used $H(-\xi) = 1 - H(\xi)$ to eliminate the Heaviside function). Using the threshold condition $\varphi(0) = a - V$ from (2.12) together with (2.21), we obtain that the wave speed satisfies

$$G(0, c) + 2(V - a) = 0. \tag{2.22}$$

This scalar equation allows us to compute c numerically, using a Newton-type method. Computation of K is done using a Gauss-Konrod quadrature formula in a truncated interval $[-10^6, 10^6]$. We restrict to $c > 0$ (the case $c < 0$ can be deduced by symmetry, see section 2.7). A plot of the resulting analytical profile (2.14) is shown in Fig. 2.7**A** and compared with the numerical simulation of (2.8). A perfect matching is realized between the two trajectories. For different sliding velocities, speed curves computed from (2.22) are presented in Fig. 2.7**B**.

2.6 Small coupling limit.

In this section the small coupling limit is explored. We consider the case $c > 0$ (see section 2.7 for the case $c < 0$). From (2.17) and (2.19) with $k \to 0$, we have the leading order equation

$$c^2 m K' - \frac{c}{a}K - k \wedge' * K = \delta, \tag{2.23}$$

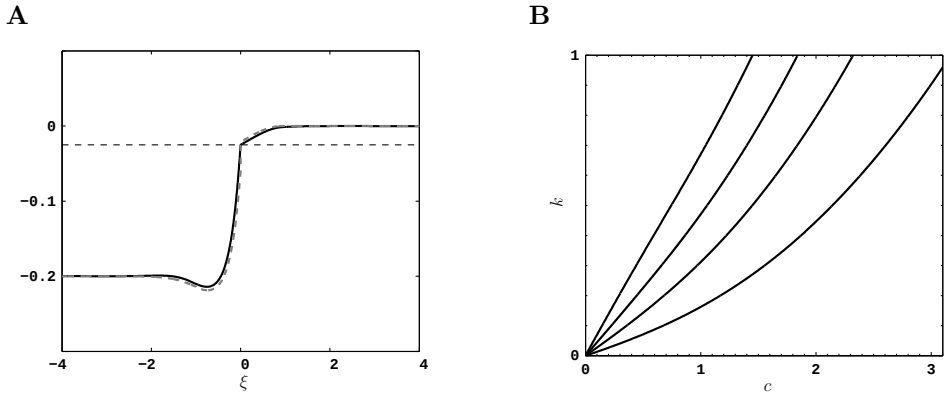

Figure 2.7: **A** Travelling front solution computed from the explicit formula (2.14) where $k = 0.3$, $V = 1.025$, $a = 1$ and $\alpha = 0.2$ (full line). The trajectory is indistinguishable from the ones obtained from the numerical simulation of the chain. The asymptotic approximation (2.29) obtained for $k \ll 1$ is also shown (dashed grey). We have obtained $c = 1.55$ from the threshold condition (2.12) (the dashed line defines the threshold $U_2 = a - V$). **B** Wave speed curves in the (c, k) plane obtained from (2.22) for $V = 1.025$, 1.05, 1.075 and 1.1 (from right to left, respectively).

where we look for a solution of the form

$$K = K_0 + kK_1 + \mathcal{O}(k^2). \tag{2.24}$$

Inserting (2.24) in (2.23), and equating orders of leading terms in k, we obtain

$$\begin{aligned} c^2 m(K_0' - \nu K_0) &= \delta, & (2.25)\\ c^2 m(K_1' - \nu K_1) &= \wedge' * K_0, & (2.26) \end{aligned}$$

where $\nu = (cam)^{-1}$. Observe (2.25) has the unique bounded solution

$$K_0(\xi) = -\frac{1}{c^2 m} e^{\nu\xi} H(-\xi), \tag{2.27}$$

where $K_0 \in L^1(\mathbb{R})$, hence the solution of (2.26) reads

$$\begin{aligned} K_1 &= K_0 * \wedge' * K_0 = \wedge * K_0 * K_0', \\ &= \frac{1}{c^2 m} \wedge * K_0 + \nu \wedge * K_0 * K_0, \end{aligned} \tag{2.28}$$

where we used $K_0' = \frac{1}{c^2 m}\delta + \nu K_0$. Using (2.19) with (2.27) and (2.28), the approximation for φ up to $\mathcal{O}(k^2)$ reads

$$\begin{aligned} \varphi(\xi) &= \alpha a(e^{\nu\xi} - 1)H(-\xi) + \alpha a k\big[- c^2 m K_1(\xi) + \\ &\quad (K_0 * \wedge)(\xi)\big] + \mathcal{O}(k^2) \end{aligned} \tag{2.29}$$

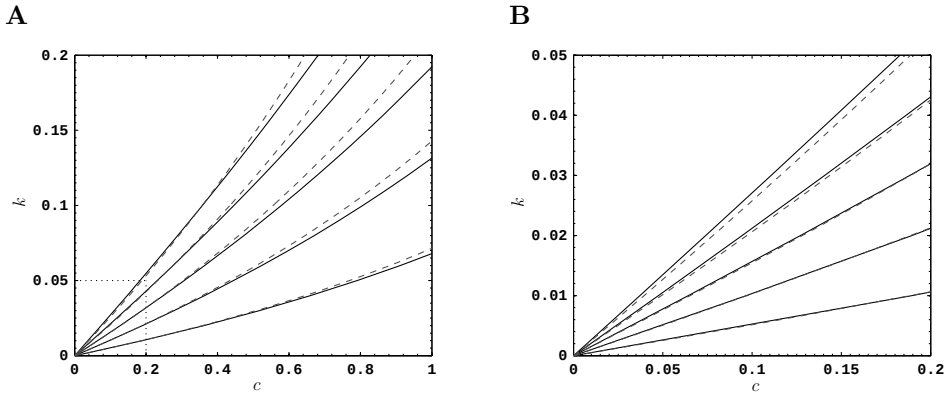

Figure 2.8: **A** Speed curves of the travelling front solution in the (c, k) plane for $V = 1.0025, 1.005, 1.0075$ and 1.01 (from right to left, respectively). Curve solutions (c, k) computed with (2.33) (dashed grey) accurately describes the exact curves (c, k) computed with (2.22) (black continuous) in the limit $c \to 0$. **B** A zoom of the dashed square region in panel **A** is shown. Other parameters include $\alpha = 0.2$, $a = 1$ and $m = 0.15$.

where we used the identity $H(-\xi) = 1 - H(\xi)$. Expression (2.29) allows to obtain an approximation of the wave speed c for small k. From $\varphi(0) = a - V$ and (2.29), we get

$$\begin{aligned} a - V &= \alpha a k \left(-c^2 m K_1(0) + (K_0 * \wedge)(0)\right) + \mathcal{O}(k^2), \\ &= -\alpha k c (\wedge * K_0 * K_0)(0) + \mathcal{O}(k^2), \\ &:= S(c)k + \mathcal{O}(k^2). \end{aligned} \tag{2.30}$$

We obtain after some computations (see appendix A)

$$S(c) = \left[2\alpha m a^3 + \frac{\alpha a^2}{c}\left(g(c) - 1\right)\right] \tag{2.31}$$

where $g(c) = e^{-1/amc}(-2amc - 1)$.

In order to approximate c, we drop $\mathcal{O}(k^2)$ terms in (2.30), fix the value of V, and look for solutions $c \approx 0$ when $k \approx 0$. Observing the exponential decay $g(c) \to 0$ as $c \to 0$, we have, from (2.31) and (2.30) the leading order approximation

$$\left[2\alpha m a^3 - \frac{\alpha a^2}{c}\right] = \frac{a - V}{k} \tag{2.32}$$

for $k, c \to 0$. Therefore we obtain the following approximation for the wave speed

$$c \sim \frac{\alpha a^2}{\frac{V-a}{k} + 2a^3 m \alpha} \tag{2.33}$$

where the leading order approximation reads $c \sim \frac{\alpha a^2 k}{V-a}$.

Formula (2.33) was derived under the assumption that c is small for k small, and

one can easily check that c given by (2.33) satisfies $c \to 0$ as $k \to 0$. To evaluate the accuracy of the asymptotic approximation (2.33), we compare in Fig. 2.8 the (c, k) curves obtained from (2.22) with those computed from (2.33) for different sliding velocities V. The asymptotic approximation (2.29) of the waveform is compared with the solution obtained for $k = 0.3$ in Fig. 2.7**A** and a good agreement is found.

2.7 Reverse travelling fronts and pulses

In the previous section we have constructed travelling fronts connecting the two stable equilibria $U_1 = -\alpha a$ (when $n \to -\infty$) and 0 (when $n \to +\infty$). In this analysis we have restricted our attention to travelling fronts with positive velocity $c(V)$ (for now we consider the dependency of front velocity in V and discard the other parameters). Using symmetry arguments, we show in the sequel the existence of travelling fronts with negative velocity *satisfying the same boundary conditions*. We also deduce the existence of travelling fronts with positive velocity satisfying reverse boundary conditions ($u_n \to -\alpha a$ when $n \to +\infty$ and $u_n \to 0$ when $n \to +\infty$).

Let us start with some symmetry considerations. Consider the advance-delay equation (2.11) with boundary conditions

$$\varphi(-\infty) = U_1, \qquad \varphi(+\infty) = U_3. \tag{2.34}$$

This problem admits the invariance

$$\varphi(\xi) \to \varphi(-\xi), \quad c \to -c, \quad (U_1, U_3) \to (U_3, U_1). \tag{2.35}$$

Moreover, the piecewise-linear friction force F_0 is antisymmetric about $v = a$, i.e. we have

$$F_0(a + h) + F_0(a - h) = 2 - \alpha, \quad \text{for all } h \in \mathbb{R}.$$

As a consequence, one can readily check that (2.11)-(2.34) is invariant by the one-parameter family of transformations

$$\varphi \to -\lambda - \varphi, \quad V \to 2\,a + \lambda - V, \quad (U_1, U_3) \to (-\lambda - U_1, -\lambda - U_3), \tag{2.36}$$

where $\lambda \in \mathbb{R}$ is arbitrary.

Now let us use the above invariances in order to obtain reverse travelling fronts. We define $\tilde{\zeta} = -\alpha\, a - \varphi$, so that $\tilde{\zeta}$ and φ connect stable equilibria in reverse order at infinity. Applying invariance (2.36) for $U_3 = 0$ and $\lambda = \alpha\, a = -U_1$, it follows

that φ is a solution of (2.11) if and only if $\tilde{\zeta}$ is a solution of the same equation with modified sliding velocity $\tilde{V} = a\,(2+\alpha) - V$. From the results of section 2.5, this problem admits for all $\tilde{V} \in (a, a(1+\alpha))$ a front solution $\tilde{\zeta}$ satisfying the boundary conditions $\tilde{\zeta}(-\infty) = -\alpha a$, $\tilde{\zeta}(+\infty) = 0$, with velocity $c(\tilde{V}) > 0$. From invariance (2.35), this equation possesses another front solution $\zeta(\xi) = \tilde{\zeta}(-\xi)$ with velocity $-c(\tilde{V}) < 0$, which satisfies the boundary conditions $\zeta(+\infty) = -\alpha a$, $\zeta(-\infty) = 0$. It follows that for all $V \in (a, a(1+\alpha))$, equation (2.11) with sliding velocity V admits the front solution $\tilde{\varphi} = -\alpha\, a - \zeta$, satisfying the boundary conditions (2.10) and having a negative velocity $-c(a\,(2+\alpha) - V)$. Consequently, the search of front solutions of (2.10)-(2.11) can be reduced to the case $c > 0$ examined in section 2.5, since all fronts with $c < 0$ can be deduced by symmetry.

Furthermore, $\varphi(\xi) = \tilde{\varphi}(-\xi) = -\alpha\, a - \tilde{\zeta}(\xi)$ defines another solution of (2.11) with sliding velocity V. This front has a positive velocity $c(\tilde{V}) = c(a\,(2+\alpha) - V)$ and satisfies the reverse boundary conditions

$$\varphi(-\infty) = 0, \qquad \varphi(+\infty) = -\alpha a. \tag{2.37}$$

The coexistence of this reverse front and the front satisfying (2.10)-(2.11) with the different velocity $c(V)$ can be used to understand the broadening of pulses reported in section 2.4, as well as the existence of steadily propagating pulses observed for particular sliding velocities. Indeed, we can see from Fig. 2.8**B** that the function $V \mapsto c(V)$ is decreasing (this is also clear from the leading order approximation (2.33)). Consequently, gluing the two above fronts to form a pulse decaying to 0 at infinity, the trailing front (at the rear of the propagating pulse) will be slower if $V < \tilde{V}$, resulting in a broadening of the pulse. This regime occurs for $V \in (a, a(1+\frac{\alpha}{2}))$. In the critical case $V = a(1+\frac{\alpha}{2})$, we have $V = \tilde{V}$ and the two fronts have identical velocities, thereby maintaining a steadily propagating pulse (this case is shown in Fig. 2.5**F**). Conversely, for $V \in (a(1+\frac{\alpha}{2}), a(1+\alpha))$, the trailing front is faster and no pulse wave can propagate. Starting from an initial bump condition, an annihilation occurs when the trailing front reaches the leading front. In conclusion, the condition for the existence of broadening pulses reads

$$V < V^* \quad \text{where} \quad V^* = a\left(\frac{\alpha}{2} + 1\right). \tag{2.38}$$

For $V > V^*$, pulse fails to propagate whereas for $V = V^*$ a stable pulse is observed, with a width determined by the initial perturbation. In the small coupling limit, this pulse has a wave speed $c \sim 2ak$ according to approximation (2.33).

2.8 Discussion

We studied localized travelling waves in a nonlinear lattice describing a block-spring chain sliding down a slope. Existence of stable localized travelling waves was illustrated for different spinodal friction laws. For an idealized piecewise-linear friction force, we constructed analytically travelling fronts and analysed their wave speeds. In contrast with discrete Nagumo equations with generic nonlinearities, propagating fronts exist at small coupling values, i.e., propagation failure does not occur for a weak coupling strength. As already observed in a different context [48], the travelling pulses are shaped by the concatenation of two travelling front solutions. We determined analytically the parameter range where pulses of constant width occur, i.e., the leading front and the trailing front have the same velocity. It is worth noting that this analysis does not rely on a time scale separation and differs from the asymptotic construction of pulses done in [16]. In particular, the pulse width is not determined by the equality of the velocity of the two fronts but depends on the initial excitation.

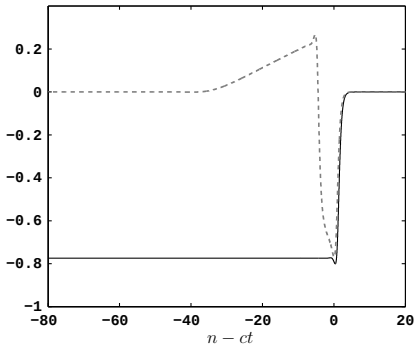

Figure 2.9: Comparison of a front solution of (2.2) (solid line) with a pulse supported by the Burridge-Knopoff model (dotted line). Computations are performed for the cubic friction law $F = F_c$ and the following parameters : $\gamma = 0.05$, $k_c = 10$, $V = 1.025$.

The present study is also of interest for the understanding of the dynamics of the Burridge-Knopoff model where the time evolution of the system is given by

$$\gamma \ddot{y}_n \quad = \quad k_c \Delta_d y_n - F(V + \dot{y}_n) - y_n. \tag{2.39}$$

Let us define $y_n(t) = -F(V) + \gamma z_n(t/\gamma)$ and $k = \gamma k_c$. Assuming $\gamma \ll 1$, then, the Burridge-Knopoff model (2.39) can be rewritten in the fast time scale as

$$\ddot{z}_n \quad = \quad k \Delta_d z_n - F(V + \dot{z}_n) + F(V)$$

that coincides with (2.2). Therefore, for small γ values, the front waves of (2.2) provide useful information on the dynamics of pulse propagation in the Burridge-Knopoff model (2.39). More precisely, fronts approximate the transition region from the ground state to the excited state. This is shown in Fig. 2.9 where the fast time scale of the BK model is accurately reproduced by model (2.2).

2.9 Appendix for chapter 2

We compute here the explicit expression of $S(c) = -\alpha c\,(\wedge * K_0 * K_0)\,(0)$. We reexpress K_0 as $K_0(\xi) = -\frac{G(\xi)}{c^2 m}$ where $G(\xi) = e^{\nu} H(-\xi)$, hence we have

$$S(c) = -\frac{\alpha}{c^3 m^2}\,(\wedge * G * G)\,(0). \tag{2.40}$$

We have

$$(G * G)(-s) = \int_{-s}^{0} G(\tau) G(-s-\tau) d\tau = s e^{-\nu s} H(s)$$

with $s > 0$, therefore

$$\begin{aligned}
(\wedge * G * G)\,(0) &= \int_{\mathbb{R}} \wedge(\tau)(G * G)(-\tau) d\tau \\
&= \int_0^1 (1-\tau)(\tau e^{-\nu\tau}) d\tau \\
&= \frac{\nu + e^{-\nu}\nu - 2 + 2e^{-\nu}}{\nu^3} \\
&= \frac{e^{-\nu}}{\nu^3}(2+\nu) + \frac{-2+\nu}{\nu^3}
\end{aligned}$$

with $\nu = (cam)^{-1}$. We further calculate

$$\frac{e^{-\nu}}{\nu^3}(2+\nu) + \frac{-2+\nu}{\nu^3} = -\nu^{-2}\left[g(\nu) + 2\nu^{-1} - 1\right] \tag{2.41}$$

where $g(\nu) = e^{-\nu}(-2\nu^{-1} - 1)$. Inserting (2.41) into (2.40), gives

$$S(c) = \frac{\alpha \nu^{-2}}{c^3 m^2}\left[g(\nu) + 2\nu^{-1} - 1\right], \tag{2.42}$$

and (2.31) follows.

Chapter 3

Travelling pulses in the Burridge-Knopoff Model

3.1 Introduction

A significant body of work has been devoted to elucidating nonlinear mechanisms of earthquakes [49–51]. Almost fifty years ago, Burridge and Knopoff [46] introduced a nonlinear lattice model to investigate the generation of earthquakes along faults, or more generally the occurrence of dynamical instabilities at frictional interfaces. The Burridge-Knopoff (BK) model formally describes a chain of blocks connected by springs and pulled over a surface, each block being attached to a spring pulled at constant velocity and subject to a friction force with the surface. When considering two plates under friction, the blocks can either correspond to a discretization of a plate or account for an existing microstructure [32]. It has been shown that this simple slider-block model is able to reproduce some statistical features of earthquakes generated by fault dynamics [52].

A key feature of the BK model lies in the friction force between the blocks and the fixed surface, which depends nonlinearly on sliding velocity. Experiments performed with a broad range of materials have revealed that the steady-state kinetic friction coefficient is non-monotone versus sliding velocity (see [53] for a review). Friction is velocity-strengthening (i.e. frictional resistance increases with sliding velocity) for high enough velocities and becomes velocity-weakening in a regime of low velocities, a behaviour intimately linked with the occurrence of stick-slip instabilities and earthquake phenomena. Such velocity-weakening or velocity-strengthening regimes can be

described by different types of friction laws. Rate-and-state friction laws incorporating state variables for the frictional interface are frequently used, see e.g. [54] for a review and a detailed bifurcation analysis in the case of a single block, and [55–57] for dynamical simulations of the BK model. However, the mathematical analysis of such models can be delicate due to the additional degrees of freedom introduced to describe the state of the interface. Another class of widely used friction laws is given by generalized Coulomb laws with velocity-dependent kinetic friction coefficient [58]. In that case, the set-valued character of the friction laws requires an adapted numerical treatment [59–61] and leads to analytical complications in dynamical studies [62]. Alternatively, single-valued laws can be used to approximate set-valued friction laws [52] or account for a velocity-strengthening regime at small enough velocities [27, 28, 46].

The dynamics of the BK model has been extensively studied in the case of steady-state velocity-weakening friction. Depending on the choice of parameters and system size, this regime can lead to chaotic dynamics or to the propagation of nonlinear wave-trains [57, 63, 64]. In particular, periodic travelling waves close to solitary waves (with highly localized slipping events propagating at constant velocity) have been reported in numerical and analytical studies [57, 62, 64–66].

In this chapter, we consider a different situation corresponding to "spinodal" friction laws [46, 54, 67], where steady-state friction is velocity-strengthening both for small and large enough velocities and an intermediate velocity-weakening region exists. This situation has been reported in a number of friction experiments performed with rocks, rubber and hydrogels [26, 28, 68]. In that case, the dynamics of a single block is described by a Van der Pol type equation, a situation frequently encountered in the modelling of excitable media [69–72]. Numerical studies of the BK model with spinodal friction laws (either generalized Coulomb laws or regularizations thereof) have revealed different types of wave patterns, ranging from synchronous oscillations, periodic travelling waves and phase fronts [7, 24] to chimera-like states (see Fig. 8 of reference [73] for an early observation of this phenomenon). These different studies were focused on the oscillatory regime where the pulling velocity lies within the velocity-weakening region.

With regard to spatially localized travelling waves, the existence of fronts has been established in a continuum limit of the BK model [6] (see also [74–76] for numerical studies of rupture fronts in other continuum models based on rate-and-state laws). However, the existence of localized waves was not established so far for the spatially discrete BK model with spinodal friction laws. The analysis of finite amplitude travelling waves in the discrete system is more delicate because it leads to a nonlinear

advance-delay differential equation for the wave profiles. In order to tackle this problem, an interesting inverse approach was described in reference [77], where particular friction laws were computed in order to fit prescribed explicit wave profiles. An analytical moving kink solution (with block displacements given by an odd function of the moving frame coordinate z) was proposed but turns out to be erroneous (the velocity dependent friction force induced by the kink is even in z, and cannot be balanced by the odd inertial and stress terms in the dynamical equation (10) of [77]).

In the present chapter, we analyse in detail the existence of localized waves in the discrete BK model with spinodal friction laws, using both extensive numerical simulations and analytical techniques. We restrict our attention to solitary waves and will treat the case of fronts in a forthcoming publication. We consider the excitable regime where the pulling velocity lies within a velocity-strengthening domain of the spinodal friction laws (above velocity-weakening). In that case, each single block admits a stable state of continuous slip but displays a large response to perturbations above some threshold. When blocks become coupled, our numerical simulations reveal that this response generates a solitary wave for a broad range of friction laws (smooth or nonsmooth) and parameter values. In the case of regularized Coulomb laws, the solitary wave consists of a moving localized region where sticking occurs, in contrast to the propagation of localized slipping events previously reported for velocity-weakening friction [64].

We analyse in detail the influence of parameters on the existence and qualitative properties of solitary waves. For low enough coupling between blocks, we observe a phenomenon of propagation failure corresponding to the rapid extinction of initially propagating pulses. We find that solitary waves develop shock-like profiles in the opposite limit of large coupling, a phenomenon connected with the existence of weak solutions in a formal continuum limit. When the pulling velocity is decreased towards the boundary of the velocity-strengthening domain, the dynamics of the blocks becomes underdamped and we observe solitary waves with oscillatory tails, while propagation failure takes place above some critical pulling velocity. For certain friction laws (near the transition to a velocity-weakening law), we also observe bistability between continuous slip and limit-cycle oscillations and the existence of propagating fronts connecting these two stable states.

In order to obtain analytical expressions for solitary waves and explain some of their qualitative properties, we introduce a simplified piecewise linear friction law with two velocity-strengthening regions separated by a (negative) jump discontinuity. The

discontinuity in the friction force can be interpreted as a rough approximation for the existence of a small intermediate velocity-weakening region. Alternatively, we propose a possible physical realization of this piecewise-linear system as a chain of impulsively forced mechanical oscillators. Such types of nonlinearities have been extensively used for the mathematical study of travelling waves in different types of PDEs [18, 21, 78] and spatially discrete systems [14, 19, 20, 36, 38–40, 44, 45, 79–81]. Following this approach allows us to obtain explicit solitary waves in the form of oscillatory integrals and numerically compute their profiles and wave speed. Moreover, this method provides analytical expansions of the solitary waves at small coupling and for pulling velocities near the jump discontinuity [20]. In this limit, we explain the occurrence of propagation failure below some critical coupling by the existence of a saddle-node bifurcation of solitary waves.

It is worthwhile to stress that we obtain fully localized solitary waves, i.e. blocks lie in the state of stable slip at infinity on both sides of the chain (this constitutes another important difference with the previous works [62, 64]). Similar solutions have been previously obtained for other types of excitable lattice dynamical systems where the coupling is diffusive rather than elastic. These systems correspond to spatially discrete FitzHugh-Nagumo equations with either smooth [15] or piecewise-linear [20] bistable nonlinearities. While our analysis of solitary waves at small coupling closely follows the lines of [20], the properties of solitary waves are quite different at large coupling with the occurrence of shocks in the BK model.

The outline of the chapter is as follows. In section 3.2, we introduce the excitable BK model with different types of spinodal friction laws, summarize several applications of the model (frictional interfaces, mechanical oscillators, nonlinear transmission lines) and illustrate the excitation of solitary waves. In section 3.3, we use numerical simulations to study the existence and shape of solitary waves depending on parameters. We also consider a continuum limit of the model and illustrate the bistable dynamics near the transition to a velocity weakening law. Section 3.4 provides analytical results for the idealized piecewise linear friction law. Section 3.5 summarizes the main findings, describes potential applications of the present work and points out interesting open problems.

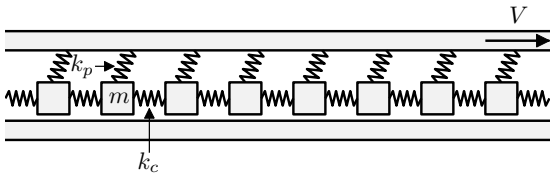

Figure 3.1: The mechanical interpretation of the Burridge-Knopoff model, where V is the pulling velocity or slip rate of the loader plate, m is the mass of a block, k_c and k_p are the stiffness of the Hookean springs.

3.2 The Burridge-Knopoff model and its applications

3.2.1 Dynamical equations and solitary waves

The BK model describes the interaction of two sheared surfaces, one being pulled at a constant speed V and the second is discretized as a chain of N identical blocks with mass m resting over a surface with frictional interaction described by a nonlinear friction function $F(v)$. The blocks are connected to each other through Hookean springs of stiffness k_c, and to the upper plate by springs of stiffness k_p (see Fig. 3.1).

The motion of an isolated block is given by

$$m\frac{d^2x}{dt^2} + k_p x + f_0 F\left(\frac{V + \frac{dx}{dt}}{v_1}\right) = 0, \tag{3.1}$$

where $x(t)$ is the displacement of the block relative to the point of attachment on the moving plate, f_0 and v_1 are two scaling parameters of the friction law. Using the change of variables $y = x/\rho$, $\tau = \rho/v_1$, $\bar{t} = t/\tau$, $\gamma = mv_1^2 k_p/f_0^2$, $\bar{V} = V/v_1$ and $\rho = f_0/k_p$, Eq. (3.1) can be reformulated as the dimensionless dynamical system on the plane:

$$\begin{aligned} \frac{dy}{dt} &= u, \\ \gamma\frac{du}{dt} &= -F(V+u) - y, \end{aligned} \tag{3.2}$$

where the rescaled time $\bar{t}$ and pulling velocity $\bar{V}$ have been rewritten as t and V. The qualitative dynamics of (3.2) highly depends on the shape of the nonlinear function $F(v)$. For a spinodal friction law, similar to the one plotted in Fig. 3.2A, the system shows excitability: a strong enough perturbation of the steady state $(u_s, y_s) = (0, -F(V))$ produces a large trajectory in the phase plane whereas small perturbations monotonically decay to the resting state. In addition, there exists a refractory period where the block is unresponsive to further perturbations. The geometrical illustration of this threshold effect is shown in Fig. 3.2B. This excitability property contrasts with

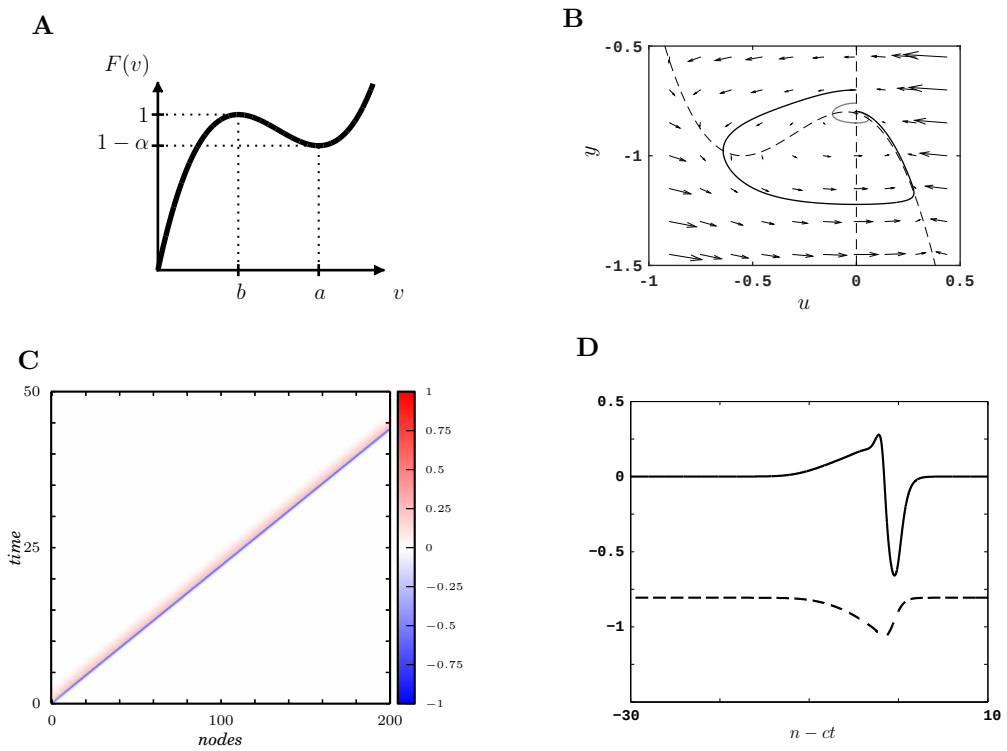

Figure 3.2: **A** The spinodal friction force defined by the cubic polynomial $F_c(v) = 3.2v^3 - 7.2v^2 + 4.8v$ for $v > 0$. In **B**, the responses of an isolated block to perturbations of different magnitudes are shown in the phase plane. The nullclines are represented (dashed lines). For a strong enough perturbation of the resting state, a large trajectory is elicited (solid black), whereas a small perturbation does not produce a significant response (grey line). **C** When the blocks are connected, an initial perturbation of the network elicits the propagation of a stable solitary wave with constant shape and speed. **D** Travelling wave profiles of the velocity (filled line) and the displacement (dashed line) in the moving frame coordinate. Parameters are: $k = 3$, $V = 1.05$, $\gamma = 0.15$. In **B**, the two perturbations are of magnitude 0.11 and 0.05. In **C**, an initial perturbation $(u_0(0), y_0(0)) = (u_s - 1, y_s)$ is imposed on the first block (left edge) of the chain.

the one due to static friction where a critical amount of stress has to be accumulated in order to reach the unstable slipping mode. In our case, for a sufficiently large slip rate V, the slip solution is stable and a temporary incursion in the velocity strengthening creep region is performed following a strong enough perturbation.

When the blocks are interconnected, the resulting network is a discrete excitable medium and the perturbation of one block may propagate to its neighbours producing complex spatiotemporal dynamics, including periodic wave trains, propagating fronts, global oscillations, chaotic dynamics or complex transitions [7, 24]. In the original one-

dimensional BK model, the blocks are connected together by springs and the resulting force on the n-th block is given by $k_c\Delta_d x_n$ where $\Delta_d x_n = x_{n+1} - 2x_n + x_{n-1}$ is the discrete Laplacian and k_c is the linear elastic coupling parameter. Using the dimensionless coupling parameter $k = k_c/k_p$, the governing equations for the n-th block read

$$\begin{aligned} \frac{dy_n}{dt} &= u_n, \\ \gamma\frac{du_n}{dt} &= k\Delta_d y_n - F(V+u_n) - y_n, \end{aligned} \tag{3.3}$$

where $n \in \mathbb{Z}$.

We report here results on the existence of solitary wave solutions where each block returns to the stable state of continuous slip after wave passage (see Fig. 3.2C,D). By a solitary wave solution we mean a solution of (3.3) such that

$$\begin{aligned} u_n(t) &= \varphi(n-ct), \\ y_n(t) &= \psi(n-ct), \end{aligned} \tag{3.4}$$

with $(\varphi(\pm\infty), \psi(\pm\infty)) = (0, -F(V))$. The function (φ, ψ) defines the waveform, and c is the wave speed that has to be determined. Substitution of (3.4) into (3.3) yields the following advance-delay differential equation:

$$\begin{aligned} -c\psi'(\xi) &= \varphi(\xi), \\ -c\gamma\varphi'(\xi) &= k[\psi(\xi+1) - 2\psi(\xi) + \psi(\xi-1)] - F(V+\varphi(\xi)) - \psi(\xi), \end{aligned} \tag{3.5}$$

where $\xi = n - ct \in \mathbb{R}$ represents the travelling wave coordinate.

The spatiotemporal plot of a solitary wave for the cubic friction law is shown in Fig. 3.2C and the corresponding waveforms are depicted in Fig. 3.2D. In the forthcoming sections, we show that the BK model exhibits solitary wave solutions for a large class of nonlinearities F of spinodal type. We also review different physical contexts where such nonlinearities arise.

3.2.2 Friction dynamics

Several non-monotonic friction laws have been proposed in the context of earthquake fault dynamics. Many studies consider generalized Coulomb friction laws with a multivalued part at the origin (see Fig. 3.3A,B). This friction law involves a sticking condition when a block achieves a zero velocity with respect to the lower plate. Single-valued regularized Coulomb laws are also often considered for numerical purpose, or to account for the existence of a velocity-strengthening region for low sliding velocities (this can represent e.g. lubrication effects). In addition, friction laws that switch

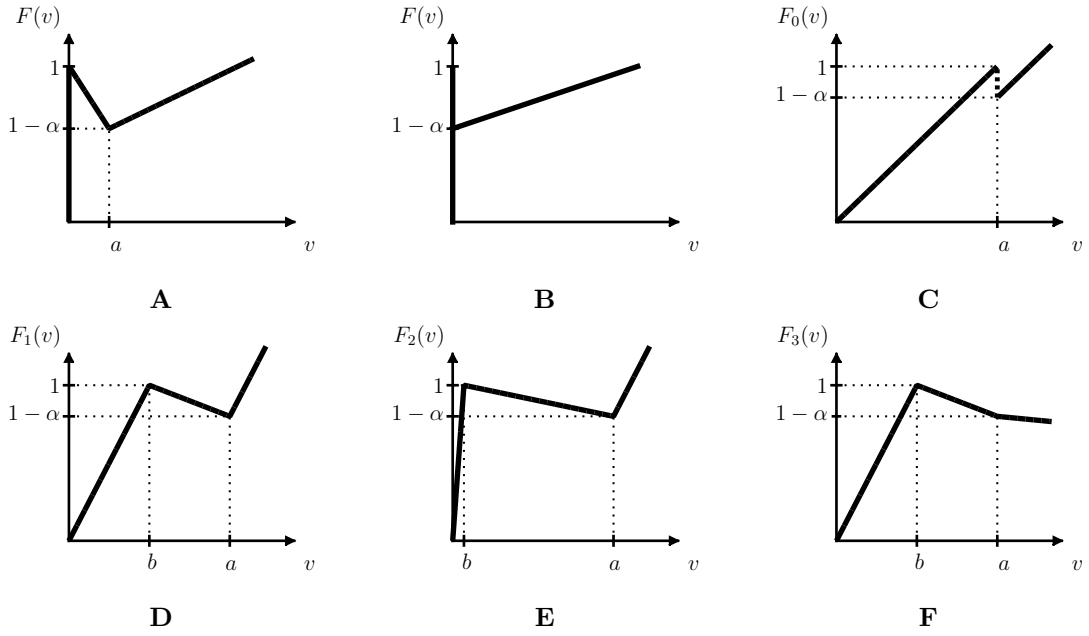

Figure 3.3: Typical piecewise-linear friction laws for the Burridge-Knopoff model. **A**-**E** display different spinodal friction laws (velocity-weakening for an intermediate range of sliding velocities) whereas **F** is velocity-weakening for large enough velocities. **A**, **B** correspond to multivalued laws (generalized Coulomb laws). Velocity-weakening is assumed instantaneous in cases **B**, **C** (the velocity-weakening domains are reduced to a jump discontinuity in the friction force). The single-valued laws **C**-**F** are used in the present work, with $a = 1$ and $\alpha = 0.2$.

from a velocity-weakening to a velocity-strengthening regime for large sliding velocities are also relevant for applications, see [25] and references therein. Combining these different effects results in spinodal friction laws [7, 24] of the type depicted in Fig. 3.2A.

In this chapter, we investigate the dynamics of the BK model using the prototypical smooth spinodal friction law given by the cubic function $F_c(v) = 3.2v^3 - 7.2v^2 + 4.8v$, depicted in Fig. 3.2A. We shall denote by $v = a$ the local minimum of the spinodal friction force, the above cubic friction law corresponding to $a = 1$. In order to analyse the effects of a larger class of spinodal friction laws (in particular with different degrees of smoothness or stiffness), we also introduce the following class of piecewise linear functions

$$F_{PL}(v; a, b, \mu) = \begin{cases} \frac{v}{b}, & 0 \leq v < b \\ \alpha\left(\frac{v-b}{b-a}\right) + 1, & b < v < a \\ \mu(v-a) + 1 - \alpha, & a < v \end{cases} \tag{3.6}$$

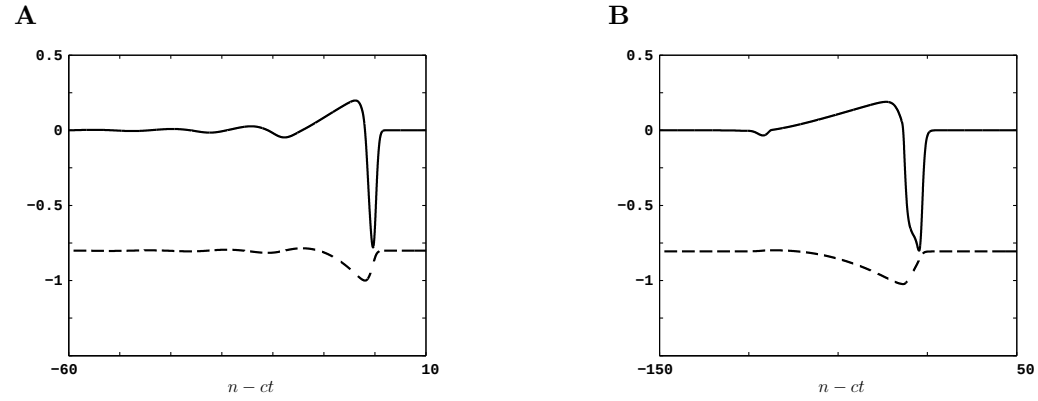

Figure 3.4: Solitary waves profiles $\varphi(n-ct) = u_n(t)$ (solid) and $\psi(n-ct) = y_n(t)$ (dashed) obtained with (**A**) Hertzian and (**B**) linear contact interactions in the Burridge-Knopoff model (cubic friction law). The Hertzian coupling is obtained by replacing the discrete linear Laplacian by $k[(y_{n-1}-y_n)_+^{3/2} - (y_n - y_{n+1})_+^{3/2}]$, and the linear contact law corresponds to $k[(y_{n-1}-y_n)_+ - (y_n - y_{n+1})_+]$, where $(x)_+ = \max(0,x)$. Parameters are: **A**, $k = 20$, $V = 1.025$ and **B**, $k = 150$, $V = 1.05$. The wave speeds are **A**, $c \approx 6.36$ and **B**, $c \approx 32.47$, respectively. The wave is generated from the chain at rest except for the last block, where the initial condition is **A** $(u_s - 2, y_s)$ and **B** $(u_s - 1, y_s)$.

that have been normalized so that $F_{PL}(b) = 1$. For $v < 0$ we set $F_{PL}(v) = -F_{PL}(-v)$. The parameter b is the threshold where the transition from velocity strengthening to velocity weakening occurs. If $\mu \geq 0$, velocity strengthening is recovered above the sliding velocity a and $F(a) = 1 - \alpha$ ($\alpha \in (0,1)$) corresponds to a local minimum of the friction force.

We shall consider more specifically four piecewise linear functions defined as follows and depicted in Fig. 3.3C-F. A crude approximation of spinodal friction laws is given by $F_0(v) = F_{PL}(v; a, a, 1/a)$ (Fig. 3.3C). In that case, the damping ratio in the two velocity-strengthening regimes are identical and the velocity-weakening region is reduced to a jump discontinuity. This friction function can be rewritten as $F_0(v) = v/a - \alpha H(v-a)$ where H is the Heaviside step function. The friction law defined by $F_1 = F_{PL}(v; a, a/2, 2/a)$ is obtained from F_0 with the addition of an intermediate velocity-weakening region with finite thickness (Fig. 3.3D). To regularize a multivalued generalized Coulomb law, we also consider $F_2(v) = F_{PL}(v; a, b, 2/a)$ with $b = 0.01$ (Fig. 3.3E). For this parameter value, the friction law is close to the multivalued case depicted in Fig. 3.3A. It would be also interesting to investigate the limit case of Fig. 3.3B (considered e.g. in [6]), but the numerical simulation of the BK model is more delicate in that case and will be investigated in future work. Finally, to investigate the transition from a velocity-strengthening law to a velocity-weakening

law at large sliding velocities we introduce $F_3(v) = F_{PL}(v; a, a/2, \mu)$ (Fig. 3.3F) where the slope μ may be negative.

Note that the present study examines different types of friction laws but is limited to purely linear nearest-neighbours coupling between blocks. Other types of couplings would be relevant for applications, such as long-range elastic couplings or contact interactions (unilateral springs). We have checked that solitary waves can be generated as well in the case of Hertzian interactions or for a linear contact law (see Fig. 3.4A,B), but a detailed investigation of such systems lies beyond the scope of the present study.

3.2.3 Oscillator chain with impulsive excitations

In this section we describe a possible physical implementation of the BK model with piecewise-linear friction function F_0 (Fig. 3.3-**C**). This system corresponds to a chain of coupled linear oscillators, where each element is subject to an impulsive force (applied e.g. using piezo actuators) when reaching a critical deflection $z = \zeta$. The dynamical equations read

$$m\,\ddot{z}_n + \nu\,\dot{z}_n + k_p\,z_n = k_c\,\Delta_d z_n + \lambda \sum_{\substack{t_k \in \mathbb{R},\\ z_n(t_k) = \zeta}} \operatorname{sign}(\dot{z}_n(t_k^-))\,\delta_{t_k}, \tag{3.7}$$

where $z_n(t)$ is the deflection of the nth oscillator in the chain. In the right side of (3.7), δ_{t_k} denotes the Dirac distribution at $t = t_k$, *sign* the usual sign function (odd and equal to unity on $(0, +\infty)$), and we use the notation $\dot{z}_n(t_k^-)$ (resp. $\dot{z}_n(t_k^+)$) for the left (resp. right) limit of $\dot{z}_n$ at $t = t_k$. For the series of impulses to be well defined as a distribution, it is assumed that each component $z_n(t)$ crosses the critical value $z = \zeta$ for a countable set of times t_k (generally depending on n) without finite accumulation point (i.e. Zeno behaviour does not occur). The external (state-dependent) impulsion has a fixed magnitude $\lambda > 0$ and is always applied in the direction of motion. Each oscillator is damped ($\nu > 0$ denotes the associated damping constant) and the other physical parameters in (3.7) are the same as in section 3.2.1.

The components z_n correspond to continuous piecewise-differentiable functions, displaying jumps of derivatives at $t = t_k$. One obtains from (3.7)

$$[\dot{z}_n]_{t_k} = \frac{\lambda}{m} \operatorname{sign}(\dot{z}_n(t_k^-)), \tag{3.8}$$

with $[f]_{t_0} = f(t_0^+) - f(t_0^-)$ denoting the jump discontinuity of a function f at t_0. In order to map (3.7) to the piecewise-linear BK model, we need the following technical lemma.

Lemma 1. *Let u denote a continuous piecewise-differentiable function such that $u(0) = 0$, $\dot{u}(0^-) \neq 0$. The following properties are equivalent :*

$$\begin{aligned} &i) \qquad \operatorname{sign}([\dot{u}]_0) = \operatorname{sign}(\dot{u}(0^-)), \\ &ii) \qquad \operatorname{sign}([\dot{u}]_0) = [H(u)]_0. \end{aligned}$$

Proof. Let us first assume *i)* and show that *ii)* holds true. Since $\dot{u}(0^+) = \dot{u}(0^-) + [\dot{u}]_0$, *i)* implies $\operatorname{sign}(\dot{u}(0^+)) = \operatorname{sign}(\dot{u}(0^-))$. This equality implies $[H(u)]_0 = \operatorname{sign}(\dot{u}(0^\pm))$ (since $\dot{u}(0^\pm) \neq 0$), which leads to *ii)* using *i)*.

Now let us show that *ii)* implies *i)*. We prove this statement for $\dot{u}(0^-) > 0$, the proof for $\dot{u}(0^-) < 0$ being similar. The above assumptions imply $\operatorname{sign}([\dot{u}]_0) = [H(u)]_0 \geq 0$, hence $\dot{u}(0^+) \geq \dot{u}(0^-) > 0$, leading to $[H(u)]_0 = 1$. From *ii)* we then get $\operatorname{sign}([\dot{u}]_0) = 1$ and thus *i)* holds true. ■

In the sequel we restrict our attention to solutions of (3.7) satisfying the following transversality condition for all n and all crossing times t_k :

$$\dot{z}_n(t_k^-) \neq 0. \tag{3.9}$$

Applying lemma 1 to $u(t) = z_n(t + t_k) - \zeta$, property *i)* is satisfied thanks to (3.8) (with $\lambda, m > 0$) and thus $\operatorname{sign}(\dot{u}(0^-)) = [H(u)]_0$, meaning that

$$\operatorname{sign}(\dot{z}_n(t_k^-)) = [H(z_n - \zeta)]_{t_k}. \tag{3.10}$$

Consequently, equation (3.7) and the transversality condition (3.9) lead to

$$m\,\ddot{z}_n + \nu\,\dot{z}_n + k_p\,z_n = k_c\,\Delta_d z_n + \lambda\,\frac{d}{dt}\,H(z_n - \zeta). \tag{3.11}$$

Similarly, applying lemma 1-*ii)* to any solution of (3.11) satisfying (3.9), one establishes the equivalence between equations (3.7) and (3.11) under the above transversality condition.

Assuming further $z_n(0) \neq \zeta$ for all n and integrating (3.11) on $[0, t]$, one obtains the equivalent formulation

$$m\,\dot{z}_n + \nu\,(z_n - \zeta - \frac{\lambda}{\nu}\,H(z_n - \zeta)) = (k_c\,\Delta_d - k_p)\,\int_0^t z_n(s)\,ds + p_n \tag{3.12}$$

with

$$p_n = m\,\dot{z}_n(0) + \nu(z_n(0) - \zeta) - \lambda\,H(z_n(0) - \zeta).$$

Let us either consider an infinite lattice with periodic or free end boundary conditions, or bounded sequences $(z_n, \dot{z}_n)$ on an infinite lattice. In each case the linear map $k_c\,\Delta_d - k_p$ is invertible $(k_c, k_p > 0)$ and one can introduce the new variable

$$x_n(t) = \int_0^t z_n(s)\,ds + (k_c\,\Delta_d - k_p)^{-1} p_n - \frac{f_0}{k_p},$$

where f_0 denotes an arbitrary constant. Substitution in (3.12) leads to the piecewise-linear BK model

$$m\,\ddot{x}_n + F(\dot{x}_n) + k_p\,x_n = k_c\,\Delta_d x_n, \tag{3.13}$$

where

$$F(u) = \nu\,(u - \zeta) - \lambda\,H(u - \zeta) + f_0. \tag{3.14}$$

This family of piecewise-linear functions is parametrized by the slope ν, position ζ and magnitude λ of the jump discontinuity and local maximum f_0.

3.2.4 Nonlinear transmission lines

The mechanical BK system (3.3) has an electrical equivalent as an active transmission line made of electronic L-C circuits coupled to a diode. The corresponding two-node

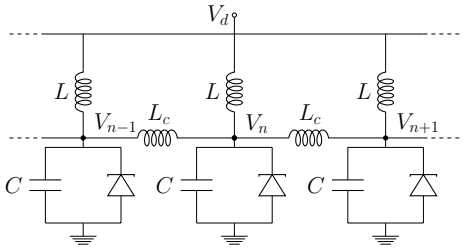

Figure 3.5: Electrical analogue of the excitable Burridge-Knopoff model as a nonlinear transmission line.

circuit has been already introduced and studied [82].
Application of Kirchoff's current law at the node n (see Fig. 3.5) gives

$$C\frac{d^2Y_n}{dt^2} + \left(\frac{1}{L} + \frac{1}{L_c}\right) Y_n - \frac{1}{L_c}\,(Y_{n+1} + Y_{n-1}) + F\left(V_d + \frac{dY_n}{dt}\right) = 0, \tag{3.15}$$

where $Y_n = \int (V_n - V_d)$, V_n is the voltage at node n, V_d is the driving voltage, C is the capacitance, L and L_c are inductances, and the function F defines the current-voltage

relationship of the nonlinear component. For $L = L_c/(1 + L_c)$, $C = \gamma$, $k = 1/L_c$, $y_n(t) = Y_n(t)$ we recover the BK system (3.3). The tunnel diode has a spinodal current-voltage characteristic as the one depicted in Fig. 3.2A (in the I-V plane) where a negative resistance occurs at intermediate voltage values. A sufficiently strong voltage perturbation may initiate the propagation of a solitary wave along the transmission line. Potential applications of nonlinear electrical wave propagation in electronic devices include broadband circuits, microwaves, instrumentation and the electronic generation of optical signals [10].

3.3 Qualitative properties of solitary waves

3.3.1 Regimes of solitary wave generation

Unless stated otherwise, simulations are done with a network size and for a time duration such that a stationary solution is reached. The network is initialized at its resting state $(u_s, y_s)_n$ and free boundary conditions are taken. For the numerical integration, the adaptive scheme Lsoda is employed with a minimal error tolerance set at $1.5e{-}8$. A time step $\Delta t = 0.001$ is used to follow the numerical solution. All the numerical results are illustrated with the fixed parameter $\gamma = 0.15$, which leads to an overdamped regime for the piecewise-linear friction laws considered herein (the underdamped case will be briefly discussed at the end of this section). The existence of solitary waves is explored in the excitable regime, i.e. for a pulling velocity such that $a < V < V_{max}$, where $V_{\max} > a$ is defined through $F(V_{\max}) = 1$. The two limiting regimes, $V \to a^+$ and $V \to V_{max}^-$, will be referred to as the small pulling velocity regime and the maximal pulling velocity regime, respectively. To explore intermediate velocity regimes, we also consider a medium pulling velocity $V_{med} > a$ defined through $F(V_{med}) = 1 - \alpha/2$. For ensuring a stable localized wave propagation, typical network size is of order one hundred for small pulling velocities, whereas medium velocities require around ten thousands blocks. Such large network simulations have to be performed because the increase of V also requires increasing k in order to excite solitary waves (see below). This parameter regime results in higher wave speed, convergence time towards steady state, and pulse width (simulations for these network sizes can be efficiently addressed using Python programming language).

Propagating waves are initiated using a shock-like initial condition: a strong perturbation is applied on the resting state of a subset of blocks in the network, possibly

reduced to a single block perturbation near the left edge of the network. The shock excitation is applied to the position or to the velocity. The magnitude of the excitation required to generate a propagation depends on V. In the regime of small pulling velocity, a velocity perturbation of magnitude in the interval $[0.125, 2.5]$ is sufficient to excite a solitary wave for all friction forces. An excitation of the position is more efficient to produce trains of solitary waves and a perturbation magnitude in the interval $[0.01, 0.5]$ is used (this higher sensitivity to perturbations of positions is clearly illustrated for a single block by Fig. 3.2-B). For a medium pulling velocity ($V \sim V_{med}$), a stronger perturbation on the velocity is needed, up to 10, whereas perturbations in the position remain similar. In the maximal velocity regime, excitations of the network fail to produce travelling waves.

Localized solutions can propagate stably along the network in the excitable regime for a sufficiently large coupling value. The wave speed and width increase with the coupling value when the other parameters are fixed, while increasing γ decreases the wave speed. For a given pulling velocity, there exists a critical coupling value k^* below which no propagation occurs. This phenomenon has been coined propagation failure and is well documented for excitable lattices of diffusive type [13]. As V increases, the critical value k^* increases and a vertical asymptote is observed near $V = V_{max}$. This is shown in Fig. 3.6B where the regime of existence and stability of solitary waves is indicated in the $V - k$ plane for the cubic friction law. Qualitatively similar results are obtained for the other spinodal friction functions (results not shown). Table 3.1 presents computations of k^* values for different friction laws and pulling velocities.

Friction function	Small pulling velocity $V = 1.025$	Medium pulling velocity V_{med}
$F_c(v)$	$k^* \approx 1.4$	$k^* \approx 360.8$
$F_0(v)$	$k^* \approx 0.43$	$k^* \approx 1915.3$
$F_1(v)$	$k^* \approx 4.5$	$k^* \approx 99$
$F_2(v)$	$k^* \approx 48$	$k^* \approx 602$

Table 3.1: Critical coupling k^* for different friction functions and different pulling velocities. Parameter values for a, b and α are as in Fig. 3.3.

The increase of k^* versus V can be intuitively explained by the geometry of excitability of a single block: for small pulling velocities, the initial state of the network is near the right knee of the spinodal friction function and a small perturbation is sufficient to reach the threshold of excitability. As V increases, the steady state gets

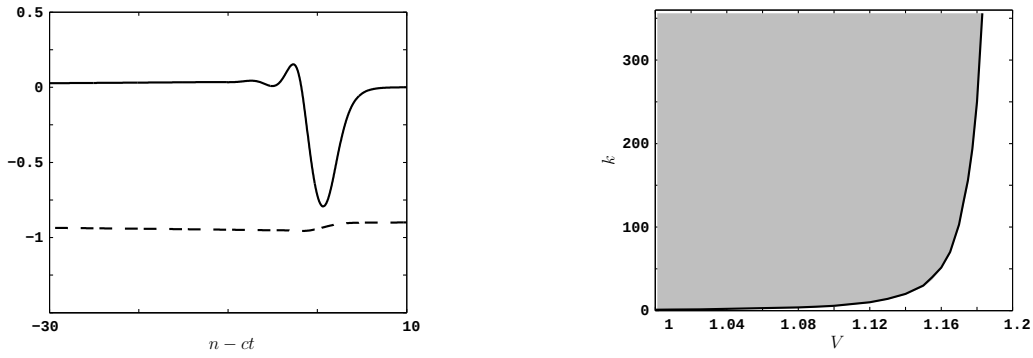

Figure 3.6: **A** Wave profiles of the velocity $\varphi(n-ct)$ (solid) and the displacement $\psi(n-ct)$ (dashed) for the cubic friction law $F_c(v)$, $V = 1.183$ and $k = 400$. The wave speed of the localized travelling wave is $c \approx 50.05$. **B** Regimes of existence and stability of solitary waves in the $V - k$ plane (grey shading) for the cubic friction law. The solid line indicates the critical coupling values k^* below which propagation failure occurs. Regimes are computed from numerical simulations in which the wave is initiated by imprinting a velocity u_p to the first block in the chain (magnitude up to $u_p = -10$). Note that here $V_{\max} = 1.25$.

away from the threshold separatrix and the perturbation has to be stronger in order to initiate a large response of the block. Above V_{max} the excitability property of the block disappears.

The waveforms obtained for different friction laws, pulling velocities V and coupling strengths k share common features. The displacement profile presents a hump whereas the velocity profile shows a rapid downstroke followed by an upstroke reminiscent to the action potential of spiking neurons. This is illustrated in Fig. 3.7A-D using the different friction laws. Note that $\int_{\mathbb{R}} \varphi \, d\xi = c\,(\psi(+\infty) - \psi(-\infty)) = 0$. The discontinuous law defined by F_0 produces a rather symmetric velocity profile where the positive and negative peaks are quasi-equidistant from the resting state. This property is more pronounced in the small pulling velocity regime and tends to break down as V increases. The symmetry is broken for the other friction laws (F_c, F_1, F_2 and F_3) with the existence of a velocity-weakening region. The positive peak of the velocity profile is less marked and the magnitude of the negative spike is determined by the distance between the stable steady state and the left branch of the velocity-nullcline (see Fig. 3.2B). When the velocity weakening range increases, the amplitude of the negative peak of the velocity profile becomes larger while the wave speed decreases.

The tail of the velocity profile presents either a monotonic or an oscillatory return to

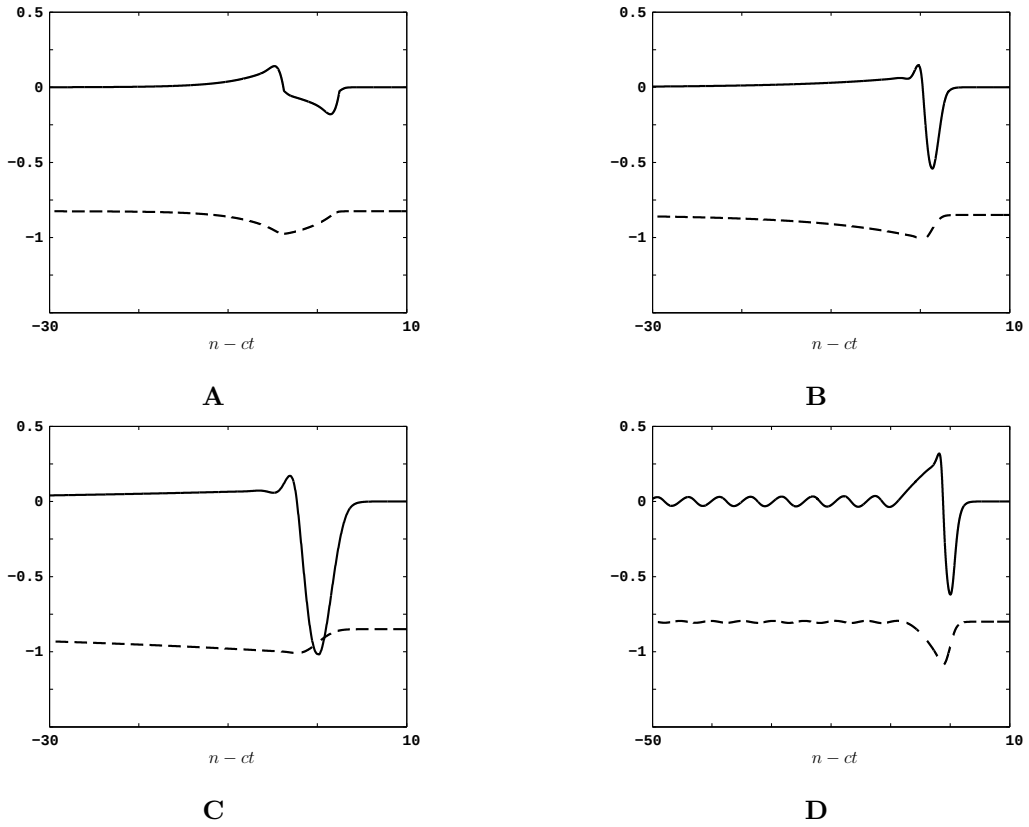

Figure 3.7: Plot of the waveforms $\varphi(n-ct)$ (solid) and $\psi(n-ct)$ (dashed) for, **A** $F_0(v)$, $V = 1.025$, $k = 2$, **B** $F_1(v)$, $V = 1.025$, $k = 5$, **C** $F_2(v)$, $V = 1.025$, $k = 70$ and, **D** $F_c(v)$, $V = 1$, $k = 2$. The local minimum of each spinodal friction force is located at $a = 1$. The computed wave speed values are $c = 4.39$, $c = 5.36$, $c = 21.23$, $c = 4.04$ for **A-D**, respectively. Simulations are done for a strong perturbation ($u_p = -10$) of the velocity of the first block.

the resting state. This feature is determined by the modes around the resting state. Linearisation of (3.3) around the steady state $(u_n, y_n) = (0, -F(V))$ reads

$$\gamma \ddot{y}_n = k\Delta y_n - y_n - F'(V)\dot{y}_n. \tag{3.16}$$

In order to analyse the relaxation towards the rest state, we look for normal modes $y_n(t) = Ae^{iqn+\sigma(q)t} + c.c.$ where $A \neq 0$ and $\sigma(q)$ are two complex numbers, $q \in [0, \pi]$ and c.c. stands for complex conjugate. This leads to

$$\sigma(q) = \left[-F'(V) \pm \sqrt{\Delta(q)}\right] \frac{1}{2\gamma}, \tag{3.17}$$

where $\Delta(q) = F'(V)^2 - 4\gamma\left[1 + 4k\sin^2(q/2)\right]$ is a decreasing function of q on $[0, \pi]$. The asymptotic decay rate is controlled by the slowest decaying mode (obtained for $q = 0$),

which also describes the relaxation of the uncoupled system. When V approaches the local minimum of the cubic friction force F_c, the value of $F_c'(V)$ tends towards 0 and all modes become underdamped (σ being imaginary). The resulting feature is an oscillatory tail of the wave as shown in Fig. 3.7D where the envelope of the oscillations becomes larger as V decreases. Due to the constant derivative of the piecewise linear friction forces F_0, F_1, F_2 for sliding velocities above a, the modes do not depends on V. In that case the occurrence of oscillatory behaviour can be analysed as above and only depends on γ, k and the slope μ in (3.6).
In the following two subsections we explore two limiting regimes of particular interest: the continuum limit and a bistability regime.

3.3.2 Continuum limit

We are interested in the study of solitary waves when the discrete BK model approaches a continuum limit, i.e. for $k \gg 1$. Near the continuum limit, system (3.3) takes the form:

$$\gamma \frac{\partial^2 y}{\partial t^2} + F\left(V + \frac{\partial y}{\partial t}\right) + y = \frac{\partial^2 y}{\partial x^2} + \frac{h^2}{12}\frac{\partial^4 y}{\partial x^4} + \mathcal{O}(h^4) \tag{3.18}$$

where we have set $y_n(t) = y(x,t)$, $x = n/\sqrt{k}$ and $h = 1/\sqrt{k} \ll 1$. The equation obtained by neglecting $\mathcal{O}(h^4)$ terms in (3.18) is known as a Boussinesq-type approximation. We look for solitary wave solutions of (3.18) and set $y(x,t) = Y(s)$ with $s = x/\tilde{c} - t$ (for system (3.3), this corresponds to solitary waves with large velocity $c = \tilde{c}\sqrt{k}$). The above Ansatz leads to the ODE

$$\Lambda Y'' - F\left(V - Y'\right) - Y = -\frac{h^2}{12\tilde{c}^4} Y^{(4)} + \mathcal{O}(h^4) \tag{3.19}$$

where $\Lambda = 1/\tilde{c}^2 - \gamma$.

The fourth derivative at the right side of (3.19) may be useful to account for the appearance of high frequency oscillations (see below), but this problem will not be analysed in the present study. In this work we restrict to the second order model obtained by neglecting $\mathcal{O}(h^2)$ terms, which reads

$$\Lambda Y''(s) - F\left(V - Y'(s)\right) - Y = 0. \tag{3.20}$$

This equation admits the unique equilibrium $(Y, Y') = (-F(V), 0)$. In what follows we study the case of the cubic friction law $F = F_c$. The equilibrium point is a saddle point for $\Lambda > 0$, an unstable point (source) for $\Lambda < 0$ and $\Delta \geq 0$, an unstable focus for $\Lambda < 0$ and $\Delta < 0$, where $\Delta = F'(V)^2 + 4\Lambda$. The existence of a smooth solitary

wave corresponds to the existence of an homoclinic orbit for equation (3.20). In the unstable configuration ($\Lambda < 0$) it is clear that such an orbit cannot exist. In the saddle case ($\Lambda > 0$), an additional equilibrium inside the homoclinic orbit has to be present because the phase space is two-dimensional. Since there is only one single equilibrium point, smooth solitary waves cannot exist in the continuum model (3.20).

However for large k values, numerical simulations of the discrete BK model reveal the existence of solitary waves. Typical profiles of these waves are shown in Fig. 3.8. The velocity component displays two shocks (resulting in two slope discontinuities for the displacement component), and we observe long-lived (i.e. metastable) oscillations in the vicinity of the rear shock. An interesting open question concerns the existence of exact travelling wave solutions of this type (i.e. with an oscillatory shock) in the BK model (3.3) or in the higher order continuum model obtained by neglecting $\mathcal{O}(h^4)$ terms in (3.19). These problems will be addressed in future works using numerical continuation techniques. After a very long transient, the fast oscillations near the rear shock disappear, which leads to the shock-wave profiles displayed in the right column of Fig. 3.8. Given the long time scale of simulations, it is not clear whether this slow drift towards a non-oscillatory shock is a dynamical property of the BK model or is due to numerical integration errors.

The profile of the asymptotic non-oscillatory pulse can be analytically captured by considering equation (3.20) with $\Lambda = 0$, which corresponds to fixing $\tilde{c} = \sqrt{1/\gamma}$. In that case, the solitary wave of (3.3) propagates at the sound velocity $c = \sqrt{k/\gamma}$. This case leads to the differential-algebraic equation

$$Y = -F(V - Y'). \tag{3.21}$$

Solutions of (3.21) are plotted in Fig. 3.8 (blue lines). They correspond to weak solutions $y(x,t) = Y\left(x/\tilde{c} - t\right)$ of the nonlinear PDE obtained by setting $h = 0$ in (3.18). In particular, the solution of (3.21) shown the right column of Fig. 3.8 perfectly matches the stationary profiles shown in Fig. 3.8C,E. For the parameter values provided in Fig. 3.8, the wave speed of the numerically observed solitary wave is $c \approx 2587$ and the analytical approximation $c = \sqrt{k/\gamma} = 2582$ is quite accurate (relative error $< 2{\cdot}10^{-3}$). In the case of oscillatory shocks, solutions of (3.21) provide reasonably accurate approximations of block displacements (see Fig. 3.8D), but they only approximate velocity oscillations on average near the rear shock (Fig. 3.8B).

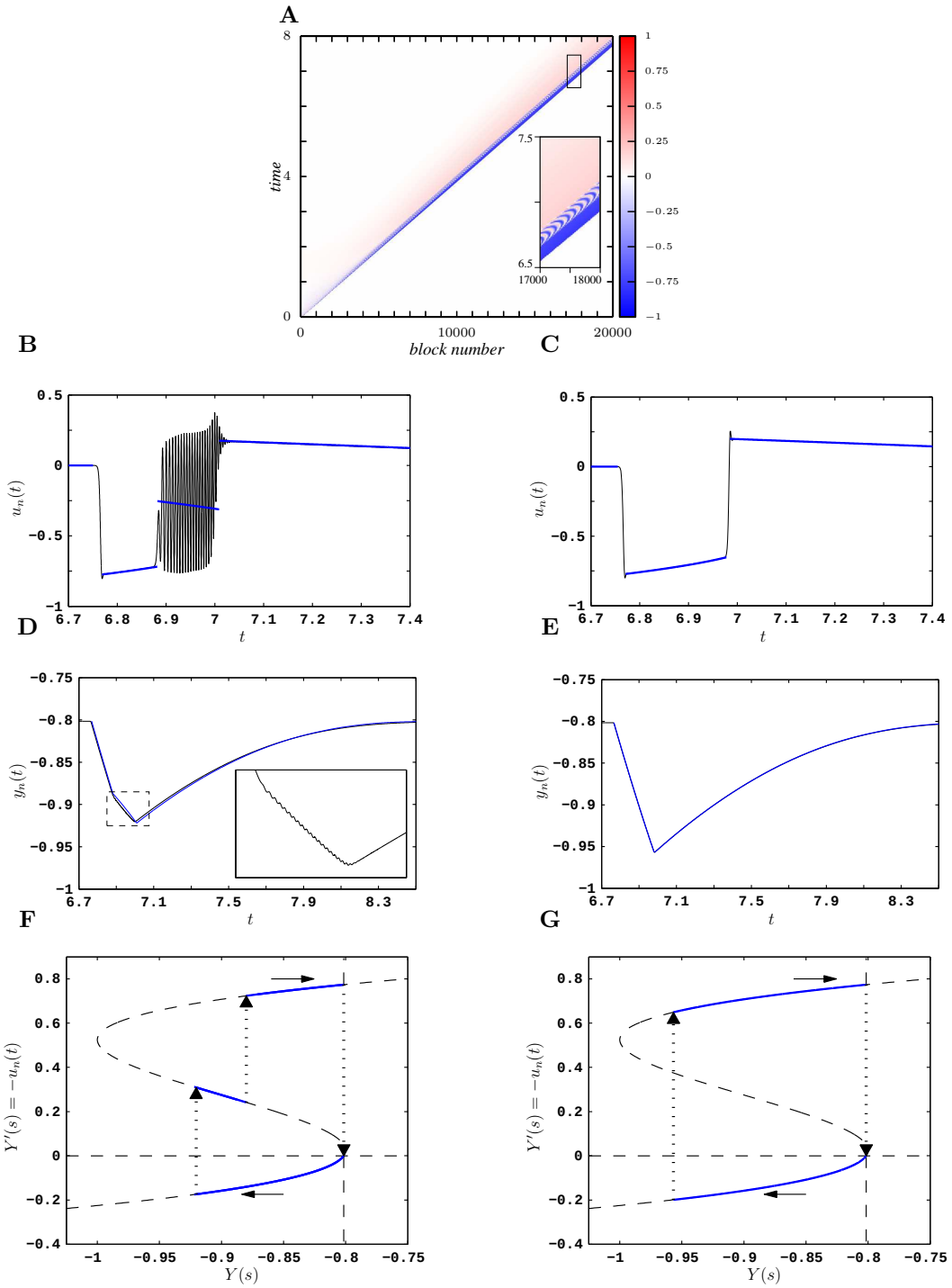

Figure 3.8: Simulation of the BK model (3.3) in the high coupling limit ($k = 10^6$), for $V = 1.025$ and friction law $F_c(v)$. **A** Spatiotemporal plot of $u_n(t)$. When the pulse reaches $n > 15000$, a quasi-stationary state is reached. **B** Plot of $u_n(t)$ (black line) for $n = 17500$ and **D**, plot of $y_n(t)$ (black line) where the inset is an enlargement that shows the small fluctuations of $y_n(t)$ in the highly oscillatory region of $u_n(t)$. In **C** and **E**, we plot the asymptotic solitary wave profiles for $n > 95000$ (time has been shifted for convenience). In **F** and **G**, the blue lines are different solutions of (3.21) that match the quasi-stationary waveforms shown in **B,C** and **D,E**, respectively. Nullclines of (3.20) are represented in the (Y, Y') plane as dashed lines. Solid arrows indicate the time trajectory. Dotted arrows represent the fast transition between the blue lines of plots **B** and **C**. Initial excitation: $(u_0(0), y_0(0)) = (u_s - 10, y_s)$.

3.3.3 Bistability regime

The excitable nature of system (3.3) can give rise to an oscillatory behaviour, similar to the self-sustained oscillations produced by excitable membranes in biology [1]. The state of continuous slip loses its stability when the friction law operates a transition from a velocity-strengthening regime to a velocity-weakening regime. For the friction law F_3 defined in section 3.2.2, this case occurs when $V > a$ and the slope parameter μ switches from positive to negative. The dynamics of a single block is illustrated in the top panels of Fig. 3.9. In the velocity-weakening regime $\mu < 0$, there exists a large-amplitude stable limit cycle, which persists in the range $\mu > 0$ provided μ is not too large (see the bifurcation diagram in Fig. 3.9A). For the state of continuous slip, a subcritical Hopf bifurcation occurs at $\mu = 0$, leading to the existence of an unstable periodic orbit when μ is positive and not too large. If μ further increases, the two periodic orbits disappear through a saddle-node bifurcation. Consequently, there exists a narrow interval of positive values of μ where the model exhibits bistability between the state of continuous slip and a limit cycle (a typical phase portrait is shown in Fig. 3.9B). The two attractors are separated by an unstable periodic orbit, and a change of position (or velocity) can switch the system from rest to oscillation and vice versa.

In this parameter regime, it is an interesting problem to examine the possible spatiotemporal patterns which can be generated by coupling the bistable units. The stability of steady sliding can be analysed through the linear system (3.16), with eigenvalues given by (3.17) for $F'(V) = \mu$. For $\mu > 0$, the equilibrium state (u_s, y_s) is locally asymptotically stable, while for $\mu < 0$ it becomes unstable. For $\mu > 0$, different types of dynamics can be observed depending on the initial perturbation, as exemplified by Fig. 3.9C-D. In this example, velocity perturbations of one block with large magnitudes produce a front wave with oscillations in the back (periodic travelling waves are clearly visible), while much smaller perturbations produce complex oscillatory patterns. The dynamics of the BK model in the bistable regime is likely to be very rich and needs to be explored in more detail in future works.

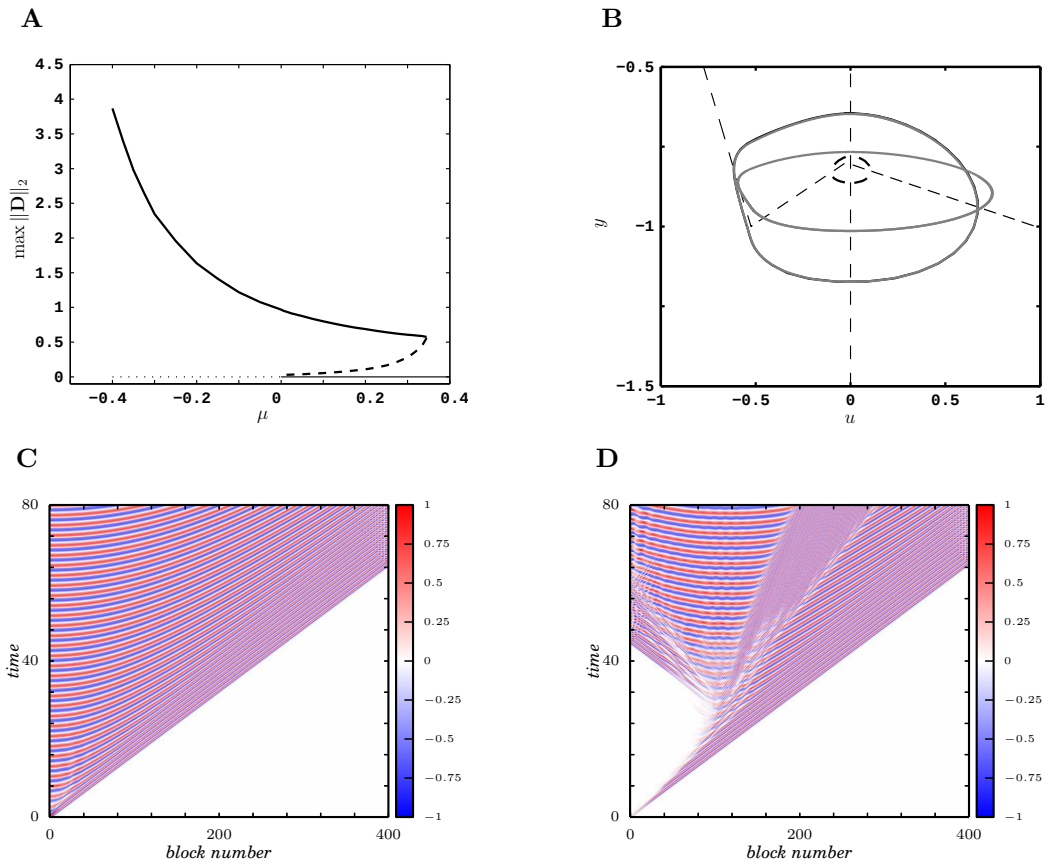

Figure 3.9: Simulations of the BK model with friction law $F_3(v)$ in a bistable regime, with $\mu = 0.2$, $V = 1.025$ and $k = 5$. **A** Bifurcation diagram of a single block that shows the amplitudes of the stable (solid line) and unstable (dashed line) periodic orbits. The amplitude is defined by $\max_{t>0} \|(u(t) - u_s, y(t) - y_s)\|_2$, where (u_s, y_s) is the equilibrium state. The latter is stable (solid straight line) or unstable (dotted straight line) depending on μ. **B** Phase plane of a single block. The nullclines (dashed lines), the stable limit cycle (bold solid circle) and unstable limit cycle (dashed line) are represented. **C,D** Wave patterns generated in the chain of blocks. A perturbation $(u_0(0), y_0(0)) = (u_s + u_p, y_s)$ with $u_p = -10$ is used in **C**, whereas $u_p = -0.25$ is used in **D**. For the simulation shown in **C**, the asymptotic states of two blocks ($n = 0$, $n = 380$) are also plotted in figure **B**, where the trajectory of the first block converges towards the limit cycle.

3.4 Construction of solitary waves for the discontinuous piecewise-linear friction force

In this section we study analytically and numerically the solutions of the following travelling wave equation derived from (3.5):

$$c^2\gamma \frac{d^2\varphi}{d\xi^2} = k\Delta_d\varphi + c\frac{d}{d\xi}F(V+\varphi) - \varphi, \tag{3.22}$$

with $\varphi(\xi) \to 0$ as $\xi \to \pm\infty$. We consider the friction force given by the piecewise linear function:

$$F_0(v) \;=\; \frac{v}{a} - \alpha H(v-a), \quad v > 0,$$

where the velocity weakening regime is assumed to be instantaneous. A strict velocity threshold occurs at the discontinuity $\varphi = -\beta = a - V < 0$ unlike the smooth velocity threshold induced by the cubic friction law. Numerical simulations suggest that this piecewise linear model captures the qualitative features of the localized solitary waves observed for a broader class of friction forces.

The strict velocity threshold makes it possible to classify travelling waves based on the threshold hitting. Let us define the decreasing (finite or infinite) sequence $(\xi_k)_k$ through

$$\varphi(\xi_k) \;=\; -\beta.$$

Translation invariance of the solution allows us to fix $\xi_0 = 0$. Different wave types can be obtained according to their signature $(\sigma_j)_j$ defined as (see Fig. 3.10)

$$\sigma_j \;=\; [H(\varphi+\beta)]_{\xi_j}.$$

We distinguish between threshold crossing from above, threshold crossing from below, and threshold reaching without crossing that read $\sigma_j = -1$, $\sigma_j = 1$, and $\sigma_j = 0$, respectively. The solitary wave solutions are classified according to the changes of sign of $\varphi + \beta$ that is given by the sequence $(\sigma_j)_j$. It is worth nothing that travelling sliding solutions are excluded, i.e. the solution is not allowed to remain on the discontinuity line of the friction force.

Fixing $(\sigma_j)_j$, we have:

$$\begin{aligned}
\frac{d}{d\xi}F_0(V+\varphi) &= \left\{\frac{d}{d\xi}F_0(a+\varphi+\beta)\right\} + \sum_i \left[\, F_0(a+\varphi+\beta)\,\right]_{\xi_i}\delta_{\xi_i}, \\
&= \left\{F_0'(a+\varphi+\beta)\right\}\left\{\varphi'\right\} + [F_0]_a \sum_i \sigma_i\,\delta_{\xi_i}, \\
&= \frac{\varphi'}{a} - \alpha\sum_i \sigma_i\,\delta_{\xi_i},
\end{aligned}$$

where δ_{ξ_i} is the Dirac distribution at ξ_i. Travelling waves in the class $(\sigma_j)_j$ satisfy the linear non-homogeneous differential equation:

$$c^2\,\gamma\,\varphi'' - \frac{c}{a}\,\varphi' + \varphi \;=\; k\,\Delta_d\varphi - c\,\alpha\sum_i \sigma_i\,\delta_{\xi_i}. \tag{3.23}$$

A solution of (3.23) is a travelling wave solution of (3.22) if the crossing conditions at $(\xi_j)_j$ are satisfied together with the sign conditions given by the signature $(\sigma_j)_j$. This leads to the following admissibility conditions:

$$\begin{cases} \varphi(\xi_{2j}) = \varphi(\xi_{2j+1}) = -\beta \\ \varphi(\xi) < -\beta \ \text{ if } \ \xi \in]\xi_{2j+1}, \xi_{2j}[\\ \varphi(\xi) > -\beta \quad \text{otherwise,} \end{cases} \tag{3.24}$$

where we assume for clarity that there is no threshold reaching without crossing (no i such that $\sigma_i = 0$).

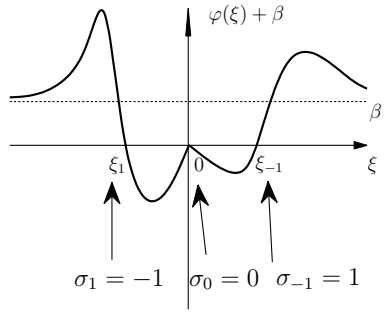

Figure 3.10: Signature $(\sigma_j)_j$ for the different threshold crossings.

By Fourier transform, we construct a localized solution $\varphi(\xi)$ of system (3.23). A travelling wave solution can be expressed as

$$\varphi(\xi) \quad = \quad \sum_p \int_{\mathbb{R}} e^{i2\pi\lambda\xi} g_{c,\xi_p}(\lambda) d\lambda \tag{3.25}$$

where

$$g_{c,\xi_p}(\lambda) \quad = \quad \alpha c \sigma_p e^{-2\pi i \lambda \xi_p} \left[4\pi^2 c^2 \lambda^2 \gamma - 4k \sin^2(\pi\lambda) + \frac{2\pi i c \lambda}{a} - 1 \right]^{-1}.$$

The analytical expression (3.25) only provides trial solutions. Indeed, the admissibility conditions (3.24) have to be fulfilled in order to define a solution of (3.22).
The simplest solitary waves cross the threshold only two times, at $\xi_0 = 0$ and at $\xi_1 < 0$, which gives two nonlinear equations

$$\begin{cases} \varphi(0) = -\beta, \\ \varphi(\xi_1) = -\beta. \end{cases} \tag{3.26}$$

The crossing points of the two level curves (3.26) in the plane (c, ξ_1) determine the speed and the width of trial solutions. We numerically compute the two level curves

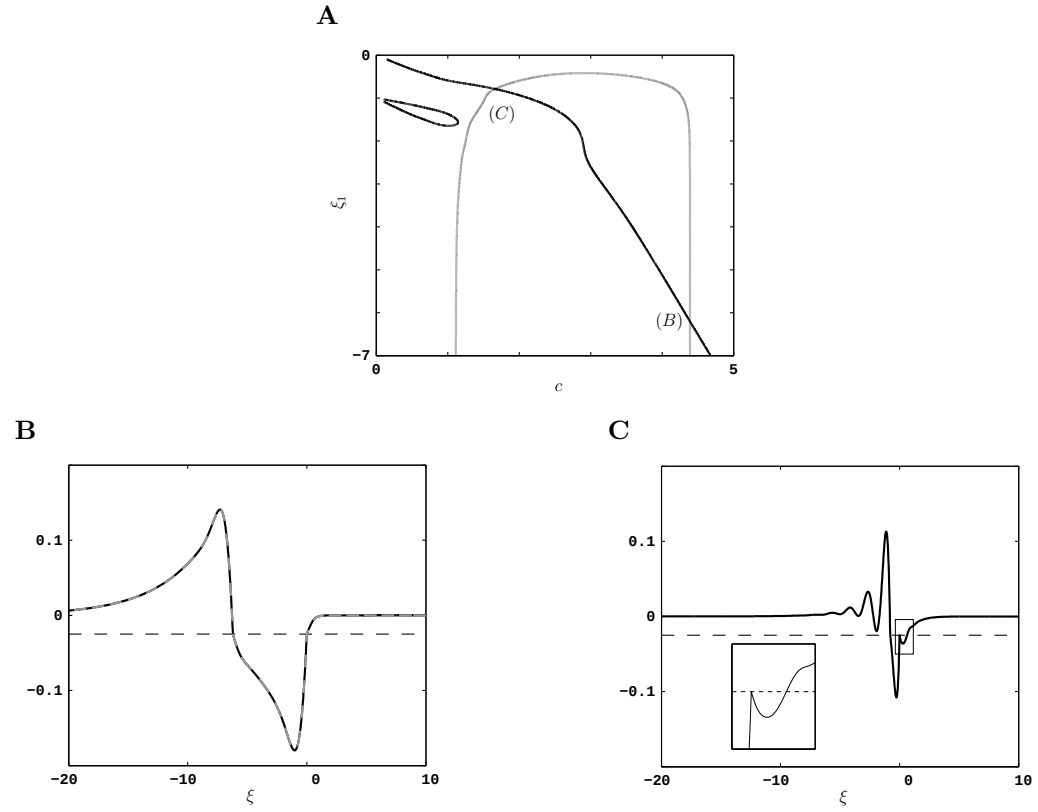

Figure 3.11: In **A** plot of the two level curves $\varphi(\xi_1) = -\beta$ (black) and $\varphi(0) = -\beta$ (grey) in the (c, ξ_1) parameter plane. Crossing points define trial solutions for solitary waves of the Burridge-Knopoff model. The crossing point $(B) \approx (4.39, -6.21)$ is associated with the waveform shown in **B** (black line). We also plot the solution obtained by the numerical simulation of the network (grey dashed). A perfect match is realized with the analytical solution. The crossing point $(C) \approx (1.65, -0.8)$ defines a spurious solution as shown in **C** where the enlargement (inset) reveals the violation of the inequality constraints. Parameters are $k = 2$, $V = 1.025$.

using a grid with mesh size 0.001. A Gauss-Konrod quadrature formula in a truncated interval $[-10^6, 10^6]$ is used to evaluate (3.25). Approximate solutions for (3.26) are found with a trust-region dogleg algorithm. As shown in Fig. 3.11A different crossing points exist.

The inequality constraints of the admissibility conditions have to be checked in order to exclude spurious solutions. Plot of the waveform (3.25) allows to determine if the sign conditions are fulfilled (see Fig. 3.11B,C). It can be seen that one of the two crossing points is not associated to a travelling wave solution (see the enlargement in Fig. 3.11C).

In Fig. 3.12, we plot the (c, k) curve of the travelling wave solutions. The speed curve is U-shaped with a fold at (c^*, k^*). For $c > c^*$ stable solitary wave solutions are

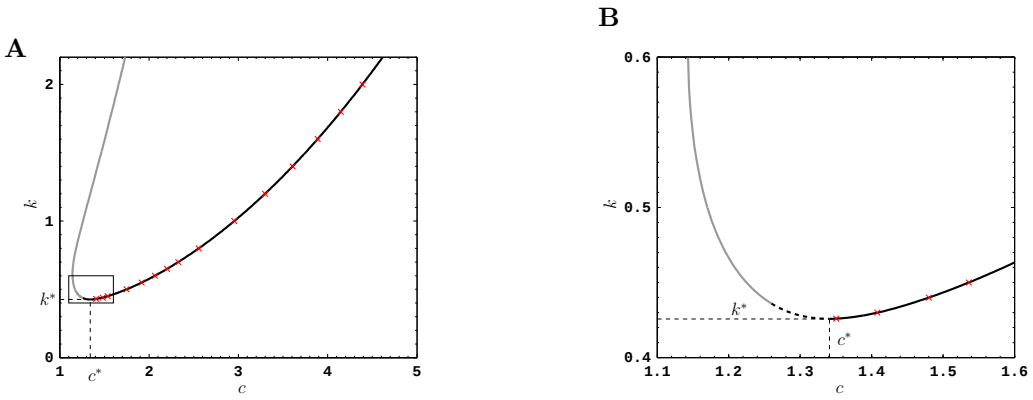

Figure 3.12: **A** and **B** (zoom), curves of the coupling strength k with respect to the wave speed c obtained by solving the non linear system (3.26). k^* is the critical coupling where propagation failure occurs and c^* is the related wave speed. The full line corresponds to stable solitary wave solutions. The dotted line represents solitary waves that are conjectured to be unstable (not observed in dynamical simulations). The grey line denotes spurious solutions. The red crosses are obtained from network simulations. The fold of the speed curve is located at $c^* \approx 1.34135$, $k^* \approx 0.42585$. As k increases, the solitary waves with $c < c^*$ disappear through a border collision bifurcation at $(c_s, k_s) \approx (1.2598, 0.4360)$. Parameter $V = 1.025$.

obtained. For $c < c^*$ solitary wave solutions are conjectured to be unstable (they are not observed in dynamical simulations) and become spurious solutions as k increases. A border collision bifurcation is reached below which no solution to (3.22) can be found with exactly two threshold crossings. We suspect that a travelling sliding solution appears or an additional threshold crossing occurs (both situations are not captured by the present analysis).

3.5 Discussion

In this chapter, we have reported the existence of solitary waves and oscillatory patterns in the excitable Burridge-Knopoff model. We have studied the influence of the friction law and parameters on the robustness and qualitative properties of solitary waves. Wave profiles have been obtained analytically for a piecewise-linear caricature of the friction law. In that case, we have shown that two branches of solitary waves coexist: one corresponding to stable waves whereas the other consists of presumably unstable waves or spurious solutions.

Despite the very different nature of the coupling, the waves observed in the excitable BK model share many similarities with the "taxis waves" recently reported in excitable systems with cross-diffusion [3, 8, 83]. In particular, reflection from boundaries and

penetration of solitary waves through each other are observed in both cases, and annihilation of two solitary waves can be also observed in the discrete BK model (results not shown).

A key problem left open in this chapter concerns the theoretical justification of the trial solutions (3.25)-(3.26), which requires to check the inequality constraints in (3.24). This problem will be addressed in the next chapter in the small coupling limit.

Chapter 4

Existence theorem for solitary waves in the Burridge-Knopoff model

4.1 Introduction

As in chapter 3, we consider the Burridge-Knopoff model

$$\gamma \ddot{y}_n = k(y_{n+1} - 2y_n + y_{n-1}) - F(V + \dot{y}_n) - y_n, \qquad n \in \mathbb{Z} \tag{4.1}$$

where y_n denotes the displacement of the n^{th} block in the moving frame (of velocity V), k is a rescaled linear coupling strength, and γ denotes a mass parameter. In this chapter we consider the piecewise linear and discontinuous friction force (already introduced in the two previous chapters)

$$F(v) = \frac{v}{a} - \alpha H(v - a), \quad v > 0, \tag{4.2}$$

and prove an existence theorem for solitary wave solutions. Piecewise linear functions have been introduced by several authors for the construction of travelling wave solutions in lattice models. Examples of this approach include the work of Truskinovsky and Vainchtein for martensitic phase transitions models [40] (see also [41]) and for the Fermi-Pasta-Ulam model [42]. Other studies include the work of Rosakis and Vainchtein for the analysis of the Frenkel-Kontorova model [43], Tonnelier [20] for the discrete FitzHugh-Nagumo model and Cahn et al. [19] for the Nagumo equation on a two-dimensional lattice.

As we have seen in the previous chapter, trial solutions can be constructed explicitly in the form of oscillatory integrals (using Fourier transform) once the spatiotemporal structure of the solitary wave has been prescribed (admissibility conditions thereafter). The pulse width and velocity are determined by two equality constraints (threshold conditions), and the trial solutions must fulfil certain inequality constraints in order to correspond to solutions of (4.1). In particular, it can happen that trial solutions satisfy the threshold conditions but not the inequality constraints, so that they do not satisfy (4.1). In that case, we shall refer to them as spurious solutions. The validity of trial solutions is usually asserted by checking the inequality constraints numerically (this is what was done in the previous chapters). In most cases, analytic proofs that the inequality constraints are satisfied are quite technical [23, 44, 84] (see also [85] for further extensions).

In order to show that the admissibility conditions are fulfilled by trial solutions, we work in the weak coupling regime where perturbation and ODE techniques can be used to estimate the solution. Although this limit introduces many simplifications, the existence proof for solitary waves is not straightforward and requires to match different estimates of the solution (inner and outer approximations) near and far from threshold crossings.

The outline of this chapter is as follows. Section 4.2 presents the equivalent form of (4.4) under the admissibility conditions and states the main result on the existence of solitary waves (Theorem 1). Thereafter the key points supporting Theorem 1 are summarized. In section 4.3, we construct trial solitary wave solutions for small k, providing asymptotic expansions and error bounds. In particular, we derive the wave speed and width of the solitary wave for small coupling k. We also show that a critical coupling value k^* exists below which solitary waves with exactly two threshold crossings do not exist. Section 4.4 contains technical results on the monotonicity of trial solutions in suitable neighbourhoods of threshold crossings (Theorem 2). These results are used to check the inequality constraints in section 4.5 (Theorem 3), from which Theorem 1 follows.

4.2 Statement of the main results

We look for a travelling wave solution of (4.1) in the form $y_n(t) = \psi(n - ct)$ with wave speed $c > 0$. Substitution of ψ in (4.1) gives

$$c^2\gamma\psi'' = k\Delta_d\psi - F\left(V - c\psi'\right) - \psi, \tag{4.3}$$

where $\Delta_d\psi(\xi) = \psi(\xi + 1) - 2\psi(\xi) + \psi(\xi - 1)$ is the discrete Laplacian operator and $\xi = n - ct$. Differentiating (4.3) with respect to ξ gives:

$$c^2\gamma\varphi'' = k\Delta_d\varphi + c\frac{d}{d\xi}F(V + \varphi) - \varphi, \tag{4.4}$$

where $\varphi = -c\psi'$ and derivatives are meant in the sense of distributions. We fix the boundary conditions

$$\varphi(-\infty) = \varphi(\infty) = 0. \tag{4.5}$$

We seek solutions $\varphi \in C^0(\mathbb{R}) \cap L^1(\mathbb{R})$ of (4.4) and (4.5) that are piecewise smooth and satisfy the admissibility conditions:

$$\text{(AC):} \begin{cases} \varphi(0) = \varphi(\xi_1) = -\beta & (4.6) \\ \varphi(\xi) < -\beta \qquad \text{if } \ \xi \in (\xi_1, 0) & (4.7) \\ \varphi(\xi) > -\beta \qquad \text{otherwise} & (4.8) \end{cases}$$

where $\beta = V - a > 0$ and $-\beta$ is referred to as the *threshold*. For values of ξ such that $\varphi(\xi) = -\beta$, the friction force $F(V+\varphi(\xi))$ reaches a discontinuity. We assume that $\varphi(\xi)$ crosses the velocity threshold $-\beta$ at exactly two different points on the ξ axis (note that jumps in φ' will occur at these points). The parameter $\xi_1 < 0$ has to be determined and defines the width of the solitary wave (studied in subsection 4.3.4). The admissibility conditions (AC) presented here characterize the simplest form of solitary wave solution. Using (AC) we obtain:

$$c^2\gamma\varphi'' - \frac{c}{a}\varphi' + \varphi = k\Delta_d\varphi + \alpha c\left(\delta_{\xi_1} - \delta_0\right), \tag{4.9}$$

where δ_x is the Dirac distribution located at $\xi = x$.

Integrating (4.9) over $\mathbb{R}$ yields $\int_{\mathbb{R}} \varphi\, d\xi = 0$, hence $\psi(\xi) = -\frac{1}{c}\int_{-\infty}^{\xi} \varphi(s)\, ds$ corresponds to a solitary wave solution of (4.3). We shall prove the following existence theorem:

Theorem 1 (Existence of solitary waves)**.** *Assume $\gamma < \frac{1}{4a^2}$. Fix $c > \frac{b}{a\gamma \ln\left(\frac{1+b}{1-b}\right)}$ with $b = \sqrt{1 - 4a^2\gamma}$. Then there exist functions $\bar{V}(k)$ and $\xi_1(k)$ such that the following*

result holds. For all k small enough, for $V = \bar{V}(k) = a + \mathcal{O}(k)$, there exists a solution of (4.2)-(4.4)-*(AC) such that* $\lim_{\xi\to\pm\infty}\varphi(\xi) = 0$. *This solution takes the following form when $k \to 0$:*

$$\varphi(\xi) = \alpha c\,[K(\xi - \xi_1) - K(\xi)] + \mathcal{O}(k) \tag{4.10}$$

where K denotes the fundamental solution of the operator $c^2\gamma\frac{d^2K}{d\xi^2} - \frac{c}{a}\frac{dK}{d\xi} + K$. We have in addition when $k \to 0$

$$\xi_1 = \mathcal{O}(\ln k). \tag{4.11}$$

Comments on the proof of Theorem 1

We consider the trial solution of (4.2)-(4.4)-(AC) obtained in chapter 3. Expressed as a Fourier transform, it takes the form

$$\varphi(\xi) = \int_{\mathbb{R}} e^{i2\pi\lambda\xi} G(\lambda, c, \xi_1) d\lambda, \tag{4.12}$$

where

$$G(\lambda, c, \xi_1) = \alpha c(1 - e^{-2\pi i\lambda\xi_1})\left[4\pi^2c^2\lambda^2\gamma - 4k\sin^2(\pi\lambda) + \frac{2\pi ic\lambda}{a} - 1\right]^{-1}.$$

Expression (4.12) is useful for exact numerical integration (as shown in the previous chapter) but is difficult to handle mathematically. In section 4.3.1, we derive a more tractable expansion of φ for $k \approx 0$ which is complemented by some error bounds.

In a second step, we take into account the two equality constraints, whose number equals the number of unknown parameters of the solitary wave (velocity c and width ξ_1). To prove the existence theorem, we work at fixed velocity c and consider ξ_1 and the pulling velocity V as two unknowns. The two equality constraints form a nonlinear system of equations for (V, ξ_1) which is solved in the small coupling regime by a fixed point argument, in a domain where ξ_1 is large and V close to a (with $V > a$). This provides us with an asymptotic expansion for the width of the solitary wave $\xi_1(k)$ at small k. We show a slow (logarithmic) divergence of the width of the solitary wave when $k \to 0$ (see (4.11)). In that sense, the limit of vanishing coupling is singular for solitary waves (a situation different from the case of periodic travelling waves [62]). We also obtain in this way a pulling velocity $V = a + \mathcal{O}(k)$ and derive expansion (4.10).

The next step is the main difficulty of the proof. It concerns the verification of the inequality constraints in (AC) for the trial solution obtained with the above (implicitly defined) values of ξ_1 and V. The assumption $\gamma < \frac{1}{4a^2}$ in Theorem 1 sets the analysis in

the overdamped regime. As shown in the leading order approximation (4.10), the shape of the solitary wave solution φ for small k is determined by the fundamental solution K defined in (4.14) and shown in Fig. 4.1A. The form of K has a fundamental role for the verification of the inequality constraints carried out through Theorems 2 and 3. The absence of oscillations in $K(\xi)$ in the overdamped regime makes the proofs much more tractable (see Lemmas 2 and 3). We remark that a study of the underdamped regime $\gamma > \frac{1}{4a^2}$ would require a more delicate analysis because the oscillations of the solitary wave solution may lead to several crossings of the velocity threshold.

To check the inequality constraints, a first step consists in establishing the monotonicity of φ in suitable neighbourhoods of the threshold crossings. This task (hereafter denoted as local analysis) is carried out in Theorem 2. The proof of this result is composed of four Lemmas which define monotonicity conditions for the trial solution $\varphi(\xi)$ in two local regions, an interval $[\xi_1 + x_{\min}, \xi_1 + x_{\max}]$ around $\xi = \xi_1$ and an interval $[x_{\min}, x^+_{\max}]$ around the origin, see Fig. 4.1B. It is shown that $\varphi(\xi)$ crosses the threshold $\varphi = -\beta$ only once in each enclosed region. The analysis of monotonicity in these regions is done through a $\mathcal{O}(k^2)$ approximation of the trial solution and its derivative.

In Theorem 3, the admissibility constraints are checked using expansion (4.10), the above local analysis and Proposition 1, which extends the monotonicity regions derived previously. This step is achieved under the sufficient condition

$$\sigma_2 e^{-\sigma_2} > \sigma_1 e^{-\sigma_1}, \tag{4.13}$$

where σ_1 and σ_2 are two positive eigenvalues controlling the spatial decay of K (see Lemmas 2 and 3). From the definitions of σ_1 and σ_2, condition (4.13) reads

$$c > \frac{b}{a\gamma \ln\left(\frac{1+b}{1-b}\right)},$$

which is the wave speed condition given in Theorem 1.

Connection with propagation failure

As illustrated in the previous chapter, propagation failure occurs at low enough coupling k (when the pulling velocity V is fixed), a phenomenon related to a saddle-node bifurcation of solitary waves occurring at some critical value $k = k^*$ (see Fig. 3.12). In section 4.3.4, we are able to partially analyse this bifurcation by working at the level of the trial solutions satisfying the equality constraints. This is done using the expansions of ξ_1 and V obtained in Theorem 1. The corresponding family of trial

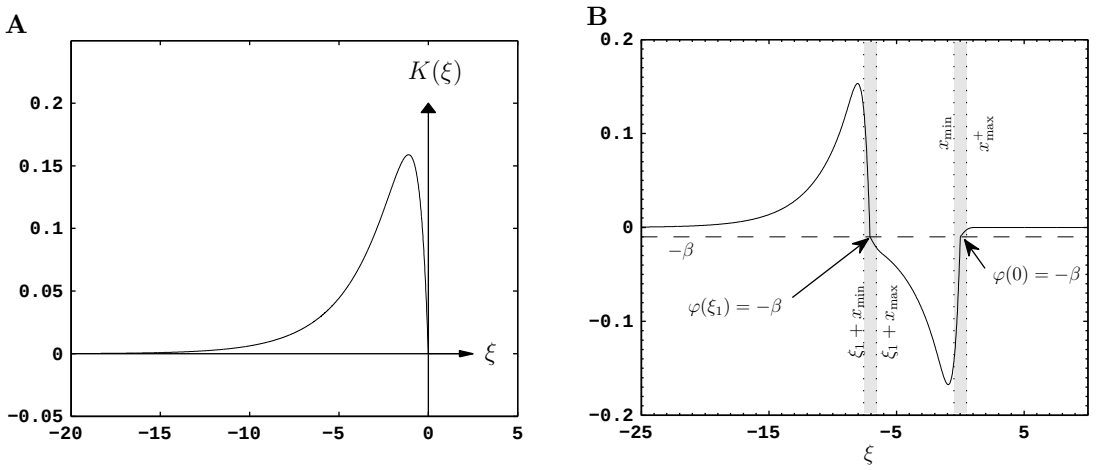

Figure 4.1: **A** Typical graph of the function K defined in Lemma 3. **B** Solitary wave solution φ of the BK model (4.9) with $c > \frac{b}{a\gamma \ln\left(\frac{1+b}{1-b}\right)}$. We shall establish the monotonicity of $\varphi(\xi)$ close to threshold in the intervals $[\xi_1 + x_{\min}, \xi_1 + x_{\max}]$ and $[x_{\min}, x^+_{\max}]$ (grey strips). A global analysis will be performed outside these local regions to check the constraints (4.7) and (4.8) in (AC). The function K and the solitary wave solution φ shown here correspond to $\alpha = 0.2$, $k = 0.5$, $\gamma = 0.15$, $a = 1$, $V = 1.01$, $\xi_1 = 7.07$, $c = 3.12$.

solutions is reparameterized by $V \approx a$ (instead of k), and ξ_1, k are expressed as functions of V. Using leading order expansions valid for $V \approx a$, we study how the coupling k depends on the wave velocity c (a typical wave speed curve in the (c, k) plane is shown in Fig. 4.2). We obtain a lower bound for the coupling (corresponding to a leading order approximation of k^*) below which solitary waves satisfying (AC) do not exist. This minimum of k is obtained for a certain velocity $c^* > 0$.

In the same Fig. 4.2, the minimal wave velocity available from Theorem 1 is plotted as a vertical line and labelled as $\tilde{c}$. The corresponding solitary wave solutions are only known to exist for $c > \tilde{c} > c^*$, so the above analysis does not provide a bifurcation result for exact solitary wave solutions. However, the nonexistence of trial solutions satisfying the equality constraints is sufficient to conclude on the non-existence of solutions of (4.2)-(4.4)-(AC) at low coupling.

4.3 Approximation of trial solutions at low coupling

4.3.1 Asymptotic expansions

To analyse the small coupling limit, we shall use the following properties of the differential operator at the left side of (4.9) (these results are elementary and stated without

proof).

Lemma 2. *For* $0 < \gamma < \frac{1}{4a^2}$*, the solutions of* $c\gamma\bar{y}''(\xi) - \frac{c}{a}\bar{y}'(\xi) + \bar{y}(\xi) = 0$ *are spanned by* $\bar{y}_i(\xi) = e^{\sigma_1\xi}$*,* $i = 1, 2$ *where* $\sigma_1 = \frac{1}{2c^2\gamma}\left(\frac{c}{a} - \sqrt{\Delta}\right) > 0$*,* $\sigma_2 = \frac{1}{2c^2\gamma}\left(\frac{c}{a} + \sqrt{\Delta}\right) > \sigma_1$ *and* $\Delta = 4c^2\left(\frac{1}{4a^2} - \gamma\right)$*.*

Lemma 3. *For* $0 < \gamma < \frac{1}{4a^2}$*, the unique bounded solution of* $c^2\gamma y'' - \frac{c}{a}y' + y = \delta_{\xi_0}$ *is* $y(\xi) = K(\xi - \xi_0)$ *with*

$$K(\xi) = \frac{H(-\xi)}{\sqrt{\Delta}}\left(e^{\sigma_1\xi} - e^{\sigma_2\xi}\right), \tag{4.14}$$

where H *denotes the Heaviside function.*

In what follows, we denote by $C_b^m(\mathbb{R})$ the Banach space of m times differentiable functions with bounded derivatives up to order m, equipped with the norm $\|f\|_{C_b^m} = \sum_{i=0}^m \|\partial^i f\|_\infty$. We note $W^{m,p}(\mathbb{R})$ the usual Sobolev space with the norm $\|f\|_{W^{m,p}} = \sum_{i=0}^m \|\partial^i f\|_p$, and where $H^m(\mathbb{R}) = W^{m,2}(\mathbb{R})$ correspond to a Hilbert space. We set

$$\varphi(\xi) = \alpha c R_{\xi_1}\Psi(\xi) \tag{4.15}$$

where $\Psi(\xi) \in L^1(\mathbb{R})$ is a function to be determined, and $R_{\xi_1}(.)$ is the linear operator $R_{\xi_1}f(\xi) = f(\xi - \xi_1) - f(\xi)$. Inserting (4.15) in (4.9) yields,

$$\mathcal{L}\Psi = k\Delta_d\Psi + \delta_0 \tag{4.16}$$

where $\mathcal{L}$ is the differential operator $\mathcal{L} \equiv c^2\gamma\partial_\xi^2 - \frac{c}{a}\partial_\xi + 1$. Equation (4.16) does not depend on parameter ξ_1 that will be determined in subsection 4.3.4. The issue here is to construct $\Psi(\xi)$ for small k. Setting $k = 0$ in (4.16), we define $\mathcal{L}\Psi_0 = \delta_0$, the fundamental solution given by

$$\Psi_0 = K \in H^1(\mathbb{R}), \tag{4.17}$$

as shown in Lemma 3. Having (4.17) as the fundamental solution associated with the operator $\mathcal{L}$, the unique bounded solution of

$$\mathcal{L}\Psi = f, \tag{4.18}$$

then reads $\Psi = \Psi_0 * f$ for all $f \in L^1(\mathbb{R})$. Using this relation in (4.16) gives

$$\Psi = \Psi_0 + k\Psi_0 * \Delta_d\Psi. \tag{4.19}$$

Observing that $\Psi_0 * \Delta_d f = \Delta_d\Psi_0 * f$, for all $f \in L^1(\mathbb{R})$, we thus have

$$\Psi = K + kG * \Psi, \tag{4.20}$$

where we define

$$G = \Delta_d \Psi_0. \tag{4.21}$$

From (4.18) with $\Psi = \Psi_0 * f$ we observe that $G * f = \Delta_d \mathcal{L}^{-1} f$ where the operator $\mathcal{L}^{-1}$ maps $C_b^k \to C_b^{k+2}$, so we observe that higher order terms in the expansion of Ψ are more regular. Using this property, we consider the Ansatz

$$\Psi = K + kG * K + k^2 \Psi_2, \tag{4.22}$$

where Ψ_2 is a unknown function. Using (4.20) and (4.22), we obtain

$$\begin{aligned} \Psi_2 - kG * \Psi &= G * G * K \\ &= \Delta_d^2 \mathcal{L}^{-2} K. \end{aligned}$$

Since $K \in H^1(\mathbb{R})$ and $\mathcal{L}^{-1} \in \mathscr{L}\left(H^m(\mathbb{R}), H^{m+2}(\mathbb{R})\right)$ we have $G * G * K \in H^5(\mathbb{R})$. Because $\|G * \|_{\mathscr{L}(H^m)} \leq \|G\|_1$ hence we get for $k < \|G\|_1^{-1}$

$$\Psi_2 = (I - kG*)^{-1} (G * G * K) \quad \text{in} \quad H^5(\mathbb{R}), \tag{4.23}$$

with Ψ_2 being analytic in $k \in (-\|G\|_1^{-1}, \|G\|_1^{-1})$. Therefore, we have

$$\varphi = \alpha c R_{\xi_1} K + \mathcal{O}(k) \quad \text{in} \quad H^1(\mathbb{R}),$$

$$\varphi - \alpha c R_{\xi_1} K = \alpha c k R_{\xi_1} (G * K) + \mathcal{O}(k^2) \quad \text{in} \quad H^3(\mathbb{R}), \tag{4.24}$$

$$\varphi - \alpha c R_{\xi_1} [K + kG * K] = \alpha c k^2 R_{\xi_1} \Psi_2 \quad \text{in} \quad H^5(\mathbb{R}). \tag{4.25}$$

Setting

$$\varphi_0 = \alpha c R_{\xi_1} K, \tag{4.26}$$

and using (4.24), we define

$$\tilde{\varphi} = \varphi_0 + kG * \varphi_0, \tag{4.27}$$

which defines the $\mathcal{O}(k^2)$ expansion of the formal solitary wave solution. Expression (4.27) takes a central part in the analysis of (AC).

4.3.2 Error bounds for the trial solutions

The elimination of the $\mathcal{O}(k^2)$ terms in $\bar{\varphi}(\xi)$ induce a certain error magnitude in the approximation of our trial solution $\varphi(\xi)$. We shall introduce a bound for this error magnitude which will be useful for the analysis of the (AC) using (4.27). From (4.20), we set

$$\begin{aligned} G * \Psi - G * K &= kG * G * \Psi, \\ &= kG * [G * \Psi - G * K] + kG * G * K, \end{aligned} \tag{4.28}$$

estimating (4.28) gives

$$\|G*\Psi - G*K\|_{C_b^1} \leq k\|G\|_1\|G*\Psi - G*K\|_{C_b^1} + k\|G*G*K\|_{C_b^1}. \quad (4.29)$$

For the last term in the right hand side of (4.29), we get

$$\|G*G*\partial^i K\|_\infty \leq \|\partial^i K\|_1\|G*G\|_\infty < \|\partial^i K\|_1\|G\|_2^2 \quad (4.30)$$

for $i = 0, 1$. Using (4.29) and (4.30), we obtain

$$\|G*\Psi - G*K\|_{C_b^1} \leq \frac{k\|G\|_2^2\|K\|_{W^{1,1}}}{1-k\|G\|_1}, \quad (4.31)$$

this gives with (4.20)

$$\|\Psi - K - kG*K\|_{C_b^1} \leq \frac{k^2\|G\|_2^2\|K\|_{W^{1,1}}}{1-k\|G\|_1} < \frac{16k^2\|K\|_2^2\|K\|_{W^{1,1}}}{1-4k\|K\|_1}, \quad (4.32)$$

where we used $\|G\|_p \leq 4\|K\|p$ for $p = 1, 2$. Therefore we have $k^2\Psi_2(\xi)$ bounded by (4.32). Using (4.32), an error estimate for (4.25) is then

$$\|\varphi - \alpha c R_{\xi_1}\left[K + k(G*K)\right]\|_{C_b^1} < \frac{32\alpha c k^2\|K\|_2^2\|K\|_{W^{1,1}}}{1-4k\|K\|_1}. \quad (4.33)$$

The bounds (4.32) and (4.33) are recalled in the following sections.

4.3.3 Qualitative properties of the fundamental solution K

For the monotonicity analysis, we provide analytical computations of the functions $K'(\xi)$, $(K*K)(\xi)$ and $(K*K')(\xi)$. Their properties relevant to the analysis are presented. We start with the following Lemma that describes the sign of $K'(\xi)$,

Lemma 4. *For $\gamma < \frac{1}{4a^2}$, there exists*

$$x_c = \frac{\ln(\sigma_1) - \ln(\sigma_2)}{\sigma_2 - \sigma_1} < 0, \quad (4.34)$$

such that for

$$K'(x) = \frac{1}{\sqrt{\Delta}}(\sigma_1 e^{\sigma_1 x} - \sigma_2 e^{\sigma_2 x})H(-x), \quad (4.35)$$

we have that

$$K'(x) > 0 \quad for \quad x \in (-\infty, x_c), \quad K'(x_c) = 0, \quad K'(x) < 0 \quad for \quad x \in (x_c, 0^-], \quad (4.36)$$

and where $K'(0^-) = -\frac{1}{c^2\gamma}$.

Proof. We get (4.35) by deriving (4.14). Setting $K'(x_c) = 0$, we get (4.34) where $x_c < 0$ assuming $\sigma_2 > \sigma_1 > 0$, i.e., $\gamma < \frac{1}{4a^2}$. In the same way, we get (4.36) for $\sigma_2 > \sigma_1 > 0$. ■

We now focus on the expressions of $(K * K)(\xi)$ and $(K * K')(\xi)$ given by

$$(K * K)(\xi) = \frac{H(-\xi)}{\Delta}\left[-\left(\xi + \frac{2}{\sigma_2 - \sigma_1}\right)e^{\sigma_1\xi} + \left(\frac{2}{\sigma_2 - \sigma_1} - \xi\right)e^{\sigma_2\xi}\right], \tag{4.37}$$

$$\left(K * K'\right)(\xi) = \frac{H(-\xi)}{\Delta}\left[-\left(\sigma_1\xi + \frac{\sigma_1 + \sigma_2}{\sigma_2 - \sigma_1}\right)e^{\sigma_1\xi} + \left(\frac{\sigma_1 + \sigma_2}{\sigma_2 - \sigma_1} - \sigma_2\xi\right)e^{\sigma_2\xi}\right]. \tag{4.38}$$

Assuming $\gamma < \frac{1}{4a^2}$, so $\sigma_2 > \sigma_1 > 0$, we have

$$\lim_{\xi\to-\infty}(K * K)(\xi) = 0, \qquad \text{and} \qquad \lim_{\xi\to-\infty}\left(K * K'\right)(\xi) = 0. \tag{4.39}$$

Observe from (4.21) and (4.17) that $G * K = \Delta_d K * K$ and $G * K' = \Delta_d K * K'$, where

$$(\Delta_d K * K)(\xi) = (K * K)(\xi + 1) - 2(K * K)(\xi) + (K * K)(\xi - 1), \tag{4.40}$$

$$(\Delta_d K * K')(\xi) = (K * K')(\xi + 1) - 2(K * K')(\xi) + (K * K')(\xi - 1), \tag{4.41}$$

and where, using (4.39), we have that

$$\lim_{\xi\to-\infty}(G * K)(\xi) = 0, \qquad \text{and} \qquad \lim_{\xi\to-\infty}(G * K)'(\xi) = 0. \tag{4.42}$$

Let us now introduce the following Lemma that is related to expression (4.41),

Lemma 5. *For all $\xi_{\max}(k)$ such that $\xi_{\max}(k) \to -\infty$ as $k \to 0$ then*

$$\lim_{k\to 0}\|\Delta_d K * K'\|_{L^\infty(-\infty,\xi_{\max}(k))} = 0.$$

Proof. For $\Delta_d K, K' \in L^2(\mathbb{R})$ then $\lim_{\xi\to\pm\infty}(\Delta_d K * K')(\xi) = 0$ holds. Therefore for $\varepsilon > 0$ there exists A, where $\xi \le A$, such that $\|(\Delta_d K * K')(\xi)\| < \varepsilon$. Equivalently, there exists k_0, where $k \ge k_0$, such that $\xi_{\max}(k) \le A$. Therefore $\|(\Delta_d K * K')(\xi)\| < \varepsilon$ for any $\xi \le \xi_{\max}(k)$. ■

We also have from (4.40) and (4.41) the following values at $\xi = 0$

$$(G * K)(0) = (\Delta_d K * K)(0) = (K * K)(-1) := p, \tag{4.43}$$

$$(G * K)'(0) = (\Delta_d K * K')(0) = (K * K')(-1) := -\mu. \tag{4.44}$$

where parameters p and μ will be used later (in the local and global analysis). We can simplify the expressions for p and μ using the auxiliary parameter

$$s = \frac{\sqrt{\Delta}}{2c^2\gamma}, \tag{4.45}$$

such that $\sigma_1 = \frac{1}{2c\gamma a} - s$, $\sigma_2 = \frac{1}{2c\gamma a} + s$, and $\sigma_2 - \sigma_1 = 2s$. Using those identities, we can easily calculate that

$$(K * K)(-1) = \frac{2}{\Delta}\left[\cosh(s) - \frac{\sinh(s)}{s}\right] e^{-\frac{1}{2c\gamma a}} = p, \tag{4.46}$$

$$(K * K')(-1) = \frac{1}{\Delta}\left[\frac{1}{\gamma ac}\left(\cosh(s) - \frac{\sinh(s)}{s}\right) - 2s\sinh(s)\right] e^{-\frac{1}{2c\gamma a}} = -\mu. \tag{4.47}$$

For convenience we will use in the sequel the parameter

$$d = -p \tag{4.48}$$

and notice that $d < 0$ if $s > 0$.

4.3.4 Estimation of width and speed of the solitary wave

To determine ξ_1 as a function of k, we first treat ξ_1 as a parameter and obtain k as a function of ξ_1. For this purpose, we use a fixed point argument on a nonlinear equation $k = \mathcal{M}(k, \xi_1)$ for the coupling k, which is obtained from (4.6) in (AC). We show that the function $\mathcal{M}$ is a contraction on an interval around $k = 0$ for large negative ξ_1. Moreover, we show that to each small k given by $k = \mathcal{M}(k, \xi_1)$ corresponds a unique ξ_1.

Using (4.15) in the equality condition $\varphi(0) = \varphi(\xi_1)$ of (AC), we obtain:

$$2\Psi(0) - \Psi(\xi_1) - \Psi(-\xi_1) = 0.$$

Using (4.22) this yields,

$$2kp - K(\xi_1) - k\,(G * K)\,(\xi_1) + k^2\,(2\Psi_2(0,k) - \Psi_2(\xi_1,k) - \Psi_2(-\xi_1,k)) = 0, \tag{4.49}$$

where $p > 0$ (see (4.46)) and where we assumed $\xi_1 \leq -1$. Hence using (4.49), we define the fixed point problem

$$\begin{aligned} k &= \frac{1}{2p}\left[K(\xi_1) + k\,(G * K)\,(\xi_1) - k^2\,(2\Psi_2(0,k) - \Psi_2(\xi_1,k), -\Psi_2(-\xi_1,k))\right] \\ &:= \mathcal{M}(k, \xi_1). \end{aligned} \tag{4.50}$$

The next Lemma shows that the map $k \mapsto \mathcal{M}(k, \xi_1)$ is a contraction mapping.

Lemma 6. *There exists a constant η small enough, such that $0 < \eta < \|G\|_1^{-1}$ and the following properties hold for $k \in \mathcal{E} = [-\eta, \eta]$. For all large enough negative $\xi_1 < -1$, the map $k \mapsto \mathcal{M}(k, \xi_1)$ is a contraction on $\mathcal{E}$ and (4.50) admits a unique solution $k = \kappa(\xi_1) \in \mathcal{E}$ depending smoothly on ξ_1. The function κ is increasing on an interval $(-\infty, \xi_1^{\max}]$ and satisfies $\lim_{\xi_1 \to -\infty} \kappa(\xi_1) = 0$. Moreover, each small k given as a fixed point of (4.50) in $\mathcal{E}$ is positive and provided by a unique ξ_1.*

Proof. Let us first estimate the term $D(k,\xi_1) = \Psi_2(\xi_1,k) + \Psi_2(-\xi_1,k) - 2\Psi_2(0,k)$. Using the bound (4.32), we have for any $|k| \leq \eta$

$$\sup_{k<\eta} |D| < \frac{48\|K\|_2^2\|K\|_{W^{1,1}}}{1-4\eta\|K\|_1} = B_\Psi. \tag{4.51}$$

From this estimate and the decay of $K(\xi_1)$ when $\xi_1 \to -\infty$, it follows that $\mathcal{E}$ is invariant by $\mathcal{M}(.,\xi_1)$ for all large enough negative ξ_1. Now for $|k|, |\bar{k}| \leq \eta$, we have

$$\begin{aligned} & |\mathcal{M}(k,\xi_1) - \mathcal{M}(\bar{k},\xi_1)| \\ = \; & \frac{1}{2p}\left|(k-\bar{k})\,(G*K)\,(\xi_1) + \left(k^2-\bar{k}^2\right) D(k,\xi_1) + \bar{k}^2\left(D(k,\xi_1) - D(\bar{k},\xi_1)\right)\right|. \end{aligned} \tag{4.52}$$

We know from (4.23) that $k \mapsto \Psi_2(.,k)$ is analytic from $(-\|G\|_1^{-1}, \|G\|_1^{-1})$ into $H^5(\mathbb{R})$. Using this property in the above identity, we obtain

$$\begin{aligned} & |\mathcal{M}(k,\xi_1) - \mathcal{M}(\bar{k},\xi_1)| \\ \leq \; & \frac{1}{2p}\left(|(G*K)(\xi_1)| + 2\eta\,|B_\Psi| + \|\partial_k D\|_{C_b^1(\mathcal{E},L^\infty(\mathbb{R}))}\eta^2\right)|k-\bar{k}|. \end{aligned} \tag{4.53}$$

To have a contraction in $\mathcal{E} = [-\eta,\eta]$, it is necessary to have a Lipschitz constant < 1 in the right side of inequality (4.53). This is the case provided ξ_1 is sufficiently large negative and η sufficiently small, due to the fact that $|(G*K)(\xi_1)| \to 0$ as $\xi_1 \to -\infty$. Then from the contraction mapping theorem, (4.50) admits a unique solution $k = \kappa(\xi_1) \in \mathcal{E}$. The function κ is smooth with respect to ξ_1 as a result of the uniform contraction principle. The property $\lim_{\xi_1\to-\infty}\kappa(\xi_1) = 0$ simply follows from letting $\xi_1 \to -\infty$ in (4.50).

Now we address the monotonicity of $\xi_1 \mapsto \kappa(\xi_1)$ in the domain of large negative ξ_1. For notational simplicity we shall use the same symbol for the variable k and the function $k(\xi_1) = \kappa(\xi_1)$. From (4.50), we get $k(\xi_1) = \mathcal{M}(k(\xi_1),\xi_1)$ and obtain by differentiating with respect to ξ_1

$$k'(\xi_1)\left(1 - \frac{\partial\mathcal{M}(\xi_1,k)}{\partial k}\right) = \frac{\partial\mathcal{M}(\xi_1,k)}{\partial\xi_1}. \tag{4.54}$$

Returning to the definition of $\mathcal{M}$, we always have $1 - \frac{\partial\mathcal{M}(\xi_1,k)}{\partial k} > 0$ if ξ_1 is sufficiently large negative and η sufficiently small. This means that the sign of $k'(\xi_1)$ is given by the sign of the right hand side of (4.54). We have

$$\frac{\partial\mathcal{M}(\xi_1,k)}{\partial\xi_1} = \frac{1}{2p}\left[K'(\xi_1) + k(G*K')(\xi_1) + \text{h.o.t.}\right], \tag{4.55}$$

for small k, where $p > 0$ and h.o.t. stands for higher order terms. In the regime of k small and large negative ξ_1, the sign of (4.55) is determined by the sign of $K'(\xi_1)$. From Lemma 4, we have $K'(\xi_1) > 0$ for any $\xi_1 < x_c$ (and hence for any large negative ξ_1). Therefore in the regime of k small, $k(\xi_1)$ is monotone increasing for all large negative $\xi_1 < x_c$. In this domain, it follows that the map $\xi_1 \mapsto k(\xi_1)$ is invertible, and k is positive because $\lim_{\xi_1 \to -\infty} k(\xi_1) = 0$. ■

Identity (4.50) takes the form

$$k = \frac{1}{2p} \left[K(\xi_1) + \text{h.o.t.} \right], \tag{4.56}$$

for small k and large negative ξ_1. From Lemma 6, the function $\xi_1 \mapsto k$ is invertible in this regime (we shall denote this inverse function by $\xi_1(k)$ for notational simplicity). At leading order, we obtain from (4.56) with (4.14),

$$\xi_1(k) = \frac{1}{\sigma_1} \ln \left[-2kd\sqrt{\Delta} \right] + o(1), \tag{4.57}$$

where we recall that $-d = p$ with p defined in (4.46). As previously stated in Theorem 1, we have from (4.57)

$$\xi_1 = \mathcal{O}\left(\ln k \right) \tag{4.58}$$

for $k \to 0$.

To complete the proof of the expansions announced in Theorem 1, it remains to evaluate $\beta = V - a$ for $k \approx 0$. For this purpose we consider the remaining equality constraint in (AC) given by $\varphi(0) = -\beta$. Using (4.24) yields

$$\begin{aligned} \varphi(0) &= \alpha c k R_{\xi_1} (G * K)(0) + \mathcal{O}(k^2) \\ &= -\alpha c p k + \mathcal{O}(k^2) = -\beta. \end{aligned} \tag{4.59}$$

Since p and c are positive, we obtain for $k \to 0^+$

$$\beta = \mathcal{O}(k) > 0, \tag{4.60}$$

$$V = a + \mathcal{O}(k) > a, \tag{4.61}$$

as stated in Theorem 1.

Using (4.57) and (4.35), we now prove the following technical Lemma which will be needed in the proof of Theorem 2.

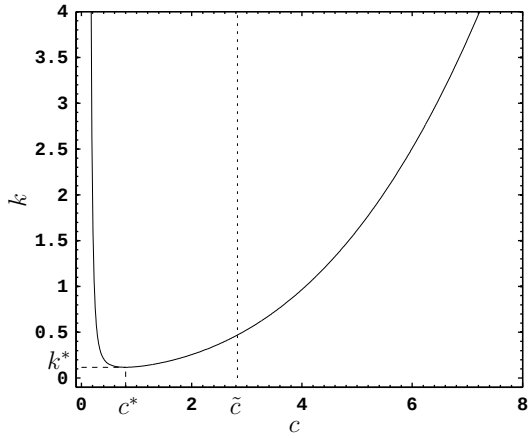

Figure 4.2: Graph of coupling strength k with respect to the wave speed c obtained from (4.62) for certain parameter values. Note that k^* is the critical coupling where propagation failure occurs and c^* the related wave speed. The vertical dashed line at $\tilde{c} = \frac{b}{a\gamma \ln\left(\frac{1+b}{1-b}\right)}$ corresponds to the wave speed given in the existence theorem (Theorem 1). Parameters are $\alpha = 0.2$, $\gamma = 0.15$, $a = 1$, $V = 1.01$, and we get $\tilde{c} = 2.72$.

Lemma 7. *Fix $\delta = \frac{\sigma_2}{\sigma_1} > 1$ and assume $x \in [x_{\min}, x_{\max}]$. Then for $k \to 0$, we have*

$$K'(\xi_1 + x) = -2\sigma_1 k d e^{\sigma_1 x} + kR_k(x),$$

where $\|R_k\|_{L^\infty(x_{\min},x_{\max})} \leq e^{\sigma_2 x_{\max}}\varepsilon(k)$ with $\varepsilon(k) \to 0$ independently of x.

Proof. Using (4.57), we have $\sigma_1\xi_1 = \ln\left(-2kd\sqrt{\Delta}\right) + o(1)$ for $k \to 0$. This gives with $K'(\xi)$ defined in (4.35)

$$\begin{aligned} K'(\xi_1 + x) &= \frac{1}{\sqrt{\Delta}}\left[\sigma_1 e^{\sigma_1\xi_1}e^{\sigma_1 x} - \sigma_2 e^{\sigma_2\xi_1}e^{\sigma_2 x}\right] \\ &= \frac{1}{\sqrt{\Delta}}\sigma_1\left(-2\sqrt{\Delta}kd\right)e^{\sigma_1 x} + o(k)\mathcal{O}(e^{\sigma_1 x_{max}}) + \mathcal{O}(k^\delta e^{\sigma_2 x_{max}}). \end{aligned}$$

■

We are now interested in deriving a lower bound on the coupling k for the existence of trial solutions when β is fixed and small. Hence, it remains to study the velocity c of the trial solution for small k and β. We show that a critical value k^* exists, such that if $k < k^*$, no wave speed c exists satisfying (AC). Using (4.59) and the implicit function theorem, we have

$$\begin{aligned} k(c) &= \frac{\beta}{\alpha c p(c)} + \mathcal{O}(\beta^2), \\ &= \beta\nu N(s(c)) + \mathcal{O}(\beta^2), \end{aligned} \tag{4.62}$$

where we reexpress $p(c) = (\alpha c \nu N(s(c)))^{-1}$ with $\nu = \frac{b^3}{4\alpha a^3 \gamma}$, $b = \sqrt{1-4a^2\gamma}$,

$$N(s(c)) = \frac{e^{s(c)/b}}{s(c)\cosh(s(c)) - \sinh(s(c))},$$

and $s(c) = \frac{\sqrt{\Delta}}{2c^2\gamma}$. The existence of a global minimum $k^* > 0$ in (4.62) is proved in the following Lemma.

Lemma 8. *Assume $\gamma < \frac{1}{4a^2}$. Then for $k(c)$ defined in (4.62), there exists $c^* > 0$ such that $k(c) \geq k(c^*) > 0$ for all $c \in (0, \infty)$.*

Proof. From (4.62) we have to study the variations of $N(s(c))$. We observe that $N(s)_{s\to 0^+} \sim \frac{3}{s^3}$ (case $c \to +\infty$) and $N(s)_{s\to+\infty} \sim \frac{2}{s} e^{s(1/b-1)}$ (case $c \to 0^+$). We have also $N(s) > 0$ since $s > \tanh(s)$ for any $s \in (0, \infty)$, and consequently for any $c \in (0, \infty)$. So $N(s(c))$ diverges at both limits of the interval $(0, \infty)$ and is always positive, hence $N(s(c))$ has a lower bound for a certain c^*, such that $\min N(s(c)) = N(s(c^*))$. Consequently we have that $\min k(c) = \frac{\beta\nu}{2} N(s(c^*)) + \mathcal{O}(\beta^2)$. ■

The function $k(c)$ is plotted in Fig. 4.2 for certain parameter values. In the same figure, as established by Theorem 1, the values $c > \tilde{c}$ correspond to wave speeds of exact solitary wave solutions of the BK model (i.e. trial solutions that satisfy (AC)).

4.4 Local monotonicity of the solution

4.4.1 Statement of the main results

The Local Monotonicity Theorem given below identifies a neighbourhood of $\xi = \xi_1$ where $\varphi(\xi)$ is decreasing, and a second local region enclosing $\xi = 0$ where $\varphi(\xi)$ is increasing (see Fig 4.1B). This result is valid under some conditions on parameters (condition $\mu > 0$ assumed below).

Theorem 2 (Local Monotonicity Theorem)**.** *Assume $\mu > 0$ defined at (4.47). Let $\lambda < 0$ be defined by (4.70), $x_{\min} \in (x_c, 0)$ with $x_c < 0$ defined by eq. (4.34), $x_{\max} > 0$ defined by eq. (4.73) and $x^+_{\max} > 0$ defined by (4.74). Then for all k small enough, $\tilde{\varphi}(\xi) = \varphi_0(\xi) + k(G * \varphi_0)(\xi)$ satisfies*

$$\tilde{\varphi}'(\xi) \leq \frac{\alpha c}{2} K'(x_{\min}) < 0 \quad \textit{for} \quad \xi \in [\xi_1 + x_{\min}, \xi_1]\,, \tag{4.63}$$

$$\tilde{\varphi}'(\xi) \leq \frac{\alpha c}{2} \lambda k < 0 \quad \textit{for} \quad \xi \in [\xi_1, \xi_1 + x_{\max}]\,, \tag{4.64}$$

$$\tilde{\varphi}'(\xi) \geq \frac{\alpha c}{2} \left|K'(x_{\min})\right| > 0 \quad \textit{for} \quad \xi \in [x_{\min}, 0]\,, \tag{4.65}$$

$$\tilde{\varphi}'(\xi) \geq \frac{\alpha c}{2} \mu k > 0 \quad \textit{for} \quad \xi \in \left[0, x^+_{\max}\right]. \tag{4.66}$$

Moreover, for all k small enough, $\varphi(\xi)$ is decreasing in $[\xi_1 + x_{\min}, \xi_1 + x_{\max}]$ and increasing in $[x_{\min}, x^+_{\max}]$.

Corollary 1. *For $\mu > 0$, then $\varphi(\xi) = -\beta$ has the the unique solutions $\xi = \xi_1$ and $\xi = 0$ in the intervals $[\xi_1 + x_{\min}, \xi_1 + x_{\max}]$ and $[x_{\min}, x^+_{\max}]$ respectively.*

The monotonicity of φ in Theorem 2 simply follows from the results stated for its approximation $\tilde{\varphi}$ and the error bound (4.33). The main difficulty in the proof of Theorem 2 concerns the estimates of $\tilde{\varphi}'$. These results are proved in four Lemmas (9,10,11,12). Lemmas 9 and 10, correspond to the statements (4.63) and (4.65) (Left neighbourhood for $\xi = \xi_1$ and $\xi = 0$). Because the proofs of statements (4.63) and (4.65) are brief, those are presented first. Lemmas 11 and 12 correspond to the statements (4.64) and (4.66) (Right neighbourhood for $\xi = \xi_1$ and $\xi = 0$). Because their proofs are more elaborated we present them afterwards. For the analysis around $\xi = 0$, we consider the definition of $\tilde{\varphi}'(\xi)$ given by

$$\tilde{\varphi}'(\xi) = \alpha c \left[K'(\xi - \xi_1) - K'(\xi) - k\left(\Delta_d K * K'\right)(\xi) + k\left(\Delta_d K * K'\right)(\xi - \xi_1)\right] \quad (4.67)$$

obtained by deriving (4.27). By setting $\xi = \xi_1 + x$, we can reexpress (4.67) as

$$\tilde{\varphi}'(\xi_1 + x) = \alpha c \left[K'(x) - K'(\xi_1 + x) + k\left(\Delta_d K * K'\right)(x) - k\left(\Delta_d K * K'\right)(\xi_1 + x)\right], \quad (4.68)$$

which is useful to simplify the analysis around $\xi = \xi_1$. Note that (4.67) and (4.68) significantly involve the function $K'(\xi)$. The statements (4.63) and (4.65) (Lemmas 9 and 10) are mainly deduced from the study of the sign of $K'(\xi)$ which is characterized in Lemma 4.

The statements (4.64) and (4.66) (Lemmas 11 and 12) are associated with the sign of parameters

$$\mu = -(K * K')(-1), \quad (4.69)$$

$$\lambda = -\mu + 2\sigma_1 d, \quad (4.70)$$

where μ was previously defined in (4.47). A main sign property for μ will be proved to be

$$\mu > 0 \quad \text{if} \quad \gamma a c > \frac{1}{6}. \quad (4.71)$$

Parameter λ is derived in the local analysis. Its construction relies on μ and d. Note that $d < 0$ and $\sigma_1 > 0$, hence

$$\mu > 0 \quad \text{implies} \quad \lambda < 0, \quad (4.72)$$

which allows to set Corollary 1. Using the sign conditions in μ and λ, the values $x_{\max}$ and $x_{\max}^{+}$ will be derived in the local analysis. The value for $x_{\max}$ is defined implicitly by

$$x_{\max}\left[\tilde{M} + M_1\sigma_1 e^{\sigma_1 x_{\max}}\right] = \frac{|\lambda|}{3} \tag{4.73}$$

where $M_1 = 2\sigma_1|d| > 0$ and $\tilde{M} = \|K'\|_2^2 > 0$. Note that $x_{\max} \to 0^+$ when $|\lambda| \to 0$. For the case of $x_{\max}^{+}$, we will derive that

$$x_{\max}^{+} = \min\left(1, \frac{\mu}{2\tilde{M}}\right). \tag{4.74}$$

In what follows, we present the development of the local analysis.

4.4.2 Proof of Theorem 2

Lemma 9. *Assume $x \in [x_{\min}, 0]$ with $x_{\min} \in (x_c, 0)$ and x_c given by (4.34). Then for k small enough*

$$\varphi_0'(\xi) + k\left(G * \varphi_0'\right)(\xi) \leq \frac{\alpha c}{2}K'(x_{\min}) < 0 \quad \textit{for} \quad \xi \in [x_{\min} + \xi_1, \xi_1].$$

Proof. Fix $x_{\min} \in (x_c, 0)$ and assume $x \in [x_{\min}, 0]$, then by Lemma 7

$$K'(\xi_1 + x) = \mathcal{O}(k)$$

uniformly in $x \in [x_{\min}, 0]$. Set $\xi = \xi_1 + x$ in $\tilde{\varphi}'(\xi)$, then (4.68) and Lemma 5 yield

$$\frac{1}{\alpha c}\left[\varphi_0'(\xi) + k\left(G * \varphi_0'\right)(\xi)\right] = K'(x) + \mathcal{O}(k) \leq K'(x_{\min}) + \mathcal{O}(k)$$

uniformly for $x \in [x_{\min}, 0]$. So considering (4.36) in Lemma 4, we get for k small enough

$$\varphi_0'(\xi) + k\left(G * \varphi_0'\right)(\xi) \leq \frac{\alpha c}{2}K'(x_{\min}) < 0 \qquad \text{for} \quad \xi \in [x_{\min} + \xi_1, \xi_1]. \tag{4.75}$$

■

Lemma 10. *Assume $\xi_1 + 1 \leq \xi \leq 0$, then for k small enough*

$$\varphi_0'(\xi) + k\left(G * \varphi_0'\right)(\xi) \geq \left|\frac{\alpha c}{2}K'(x_{\min})\right| > 0 \quad \textit{for} \quad \xi \in [x_{\min}, 0].$$

Proof. Assume $\xi_1 + 1 \leq \xi \leq 0$, therefore

$$K'(\xi - \xi_1) = 0, \quad \left(K * K'\right)(\xi - \xi_1 - 1) = 0 \quad \text{and} \quad \left(\Delta_d K * K'\right)(\xi - \xi_1) = 0$$

hence we have for (4.67)

$$\frac{1}{\alpha c}\left[\varphi_0'(\xi)+k(G*\varphi_0')(\xi)\right]=-K'(\xi)-k\left(\Delta_d K*K'\right)(\xi).$$

So considering (4.36) in Lemma 4, for k small enough:

$$\varphi_0'(\xi)+k\left(G*\varphi_0'\right)(\xi)\geq\frac{\alpha c}{2}\left|K'(x_{\min})\right|>0\quad\text{for}\quad\xi\in[x_{\min},0]. \tag{4.76}$$

■

Lemma 11. *Assume $\lambda\neq 0$ and $x\in[0,x_{\max}]$ with $x_{\max}$ defined by (4.73). Then there exists k_0 such that for all $k\leq k_0$, we have*

$$\left|\varphi_0'(\xi)+k\left(G*\varphi_0'\right)(\xi)\right|\geq\alpha ck\frac{|\lambda|}{2}\quad\textit{for}\quad\xi\in[\xi_1,\xi_1+x_{\max}]. \tag{4.77}$$

Proof. From definition (4.35), we have $K'(x)=0$ for any $x\geq 0$ and $\left(\Delta_d K*K'\right)(x)=0$ for any $x\geq 1$ by definition (4.41). Therefore for any $x\geq 0$:

$$\begin{aligned}\left(\Delta_d K*K'\right)(x)&=\left(K*K'\right)(x-1)\\&=\left(K*K'\right)(-1)+xR(x)=-\mu+xR(x)\end{aligned} \tag{4.78}$$

with

$$\|R\|_\infty\leq\|K'*K'\|_\infty\leq\|K'\|_2^2=\tilde{M}. \tag{4.79}$$

Assume $x\leq x_{\max}(k)$ with $\lim_{k\to 0}(\xi_1+x_{\max})=-\infty$, and set $\xi=\xi_1+x$ in $\varphi'(\xi)$. Therefore (4.68) with Lemma 5 and (4.78) yield

$$\frac{1}{\alpha c}\left[\varphi_0'(\xi)+k\left(G*\varphi_0'\right)(\xi)\right]=-K'(\xi_1+x)-k\mu+kxR(x)+o(k),$$

uniformly in $x\in[0,x_{\max}]$. Let us assume x_{max} independent of k, then with $-\mu$ given in (4.47), d given in (4.48), and using Lemma 7, we get

$$\begin{aligned}&\frac{1}{\alpha c}\left[\varphi_0'(\xi)+k\left(G*\varphi_0'\right)(\xi)\right]\\&=2\sigma_1 kde^{\sigma_1 x}+\frac{k}{\Delta}\left[\frac{1}{\gamma ac}\left(\cosh(s)-\frac{\sinh(s)}{s}\right)-2s\sinh(s)\right]e^{-\frac{1}{2c\gamma a}}+kxR(x)+o(k)\\&=2\sigma_1 kde^{\sigma_1 x}-\frac{k}{2\gamma ac}d-\frac{2k}{\Delta}s\sinh(s)e^{-\frac{1}{2c\gamma a}}+kxR(x)+o(k)\\&=\frac{kd}{c^2\gamma}\left[e^{\sigma_1 x}\left(\frac{c}{a}-\sqrt{\Delta}\right)-\frac{c}{2a}\right]-\frac{2k}{\Delta}s\sinh(s)e^{-\frac{1}{2\gamma ac}}+kxR(x)+o(k)\end{aligned} \tag{4.80}$$

uniformly in $x \in [0, x_{\max}]$, where $s = \frac{\sqrt{\Delta}}{c^2\gamma}$. We define now,

$$\lambda = \frac{2}{\Delta} e^{-\frac{1}{2\gamma ac}} s \sinh(s) \Lambda \tag{4.81}$$

$$\Lambda = \frac{f(s)}{c^2\gamma} \left[\left(\sqrt{\Delta} - \frac{c}{a} \right) + \frac{c}{2a} \right] - 1 \tag{4.82}$$

$$f(s) = \left(\cosh(s) - \frac{\sinh(s)}{s} \right) [s \sinh(s)]^{-1}, \tag{4.83}$$

where we note that $f(s)$ is even, decreasing in $s \in [0, \infty]$ and $\|f\|_\infty = f(0) = 1/3$. We then have for (4.80) with (4.81), (4.82) and (4.83),

$$\frac{1}{\alpha c} \left[\varphi_0'(\xi) + k \left(G * \varphi_0' \right)(\xi) \right] = k \left[\lambda + \tilde{\varepsilon}(k) + x \left(R(x) + \frac{d}{c^2\gamma} \left(\frac{c}{a} - \sqrt{\Delta} \right) \frac{e^{\sigma_1 x} - 1}{x} \right) \right] \tag{4.84}$$

uniformly in $x \in [0, x_{max}]$, where $\tilde{\varepsilon}(k) \to 0$ as $k \to 0$. To study the sign behaviour of (4.84), we need to know the sign behaviour of λ. We have $\sqrt{\Delta} < \frac{c}{a}$ so $\Lambda < \frac{f(s)}{2a\gamma c} - 1 \leq \frac{1}{6a\gamma c} - 1$ and therefore

$$\lambda < 0 \quad \text{for} \quad \gamma ac \geq \frac{1}{6}. \tag{4.85}$$

To find when $\lambda > 0$, we fix $c = \frac{\theta}{\gamma a}$ with $\theta = \frac{1}{6}$, so $\gamma ac < \frac{1}{6}$ (i.e., we have $2\gamma ac < \|f\|_\infty$). Let $s_{\max} > 0$ such that $f(s_{\max}) = 2\theta$ and assume $s \in [0, s_{\max}]$, so $f(s) > 2\gamma ac$. This gives with (4.81) and (4.82)

$$\lambda > 0 \quad \text{for} \quad f(s) \left[2\sqrt{1 - 4a^2\gamma} - 1 \right] > 2a\gamma c, \tag{4.86}$$

where $\left[2\sqrt{1 - 4a^2\gamma} - 1 \right] \in (-1, 2)$ for $\gamma < \frac{1}{4a^2}$. Therefore if $f(s) > 2\gamma ac$ for $s \in [0, s_{\max}]$, then (4.86) holds true provided γ is small enough.
Now we can study the sign of (4.84). Assume $\lambda \neq 0$ and set $\frac{|d|}{c^2\gamma} \left(\frac{c}{a} - \sqrt{\Delta} \right) = M_1$. Then for all $x \in [0, x_{\max}]$

$$\left| \lambda + x \left(R(x) - M_1 \frac{e^{\sigma_1 x} - 1}{x} \right) \right| \geq |\lambda| - x \left(\tilde{M} + M_1 \sigma_1 e^{\sigma_1 x_{\max}} \right) \geq \frac{2}{3} |\lambda| > 0 \tag{4.87}$$

for $x_{\max}$ implicitly defined by:

$$x_{\max} \left(\tilde{M} + M_1 \sigma_1 e^{\sigma_1 x_{\max}} \right) = \frac{|\lambda|}{3}. \tag{4.88}$$

We have clearly $x_{\max} > 0$ for $|\lambda| > 0$. Knowing (4.87) and assuming $\lambda \neq 0$ and $x \in [0, x_{\max}]$, then letting $k \to 0$ yields in (4.84):

$$\left| \varphi_0'(\xi) + k \left(G * \varphi_0' \right)(\xi) \right| \geq \alpha ck \frac{|\lambda|}{2} \quad \text{for} \quad \xi \in [\xi_1, \xi_1 + x_{\max}]$$

with $x_{\max}$ defined implicitly by (4.88). This ends the proof of Lemma 11. ■

Lemma 12. *Set* $x^+_{\max} = \min\left(1, \frac{\mu}{2\tilde{M}}\right)$, *with* μ *defined by* (4.69) *and* $\tilde{M}$ *by* (4.79). *Assume* $f(s) \neq 2\gamma ac$ *and* $\xi \in [0, x^+_{\max}]$. *Then* $\varphi_0'(\xi) + k\left(G * \varphi_0'\right)(\xi)$ *has the same sign as* μ *and*

$$\left|\varphi_0'(\xi) + k(G * \varphi_0')(\xi)\right| \geq k\alpha c\frac{|\mu|}{2} \quad \textit{for} \quad \xi \in [0, x^+_{\max}].$$

In addition, the critical coefficient λ *defined in eq.* (4.81) *satisfies*

$$\lambda = -\mu + 2\sigma_1 d < -\mu. \tag{4.89}$$

In particular, $\mu > 0$ *implies* $\lambda < 0$ *and* $\lambda > 0$ *implies* $\mu < 0$.

Proof. Note that for $\xi \geq 0$ we have $K'(\xi) = 0$, while for $\xi \geq 1$ we get $\left(\Delta K * K'\right)(\xi) = 0$ and so $\varphi_0(\xi) + k\left(G * \varphi_0'\right)(\xi) = 0$. Hence we only consider the interval $\xi \in [0, 1]$ in (4.67), which gives

$$\begin{aligned}\varphi_0'(\xi) + k\left(G * \varphi_0'\right)(\xi) =& - k\alpha c\left(K * K'\right)(\xi - 1)\\ =& - k\alpha c\left[(K * K')(-1) + \xi R(\xi)\right] = k\alpha c[\mu - \xi R(\xi)].\end{aligned} \tag{4.90}$$

Using (4.47) and (4.83), we reexpress μ as

$$\mu = \frac{2}{\Delta}e^{-\frac{1}{2\gamma ac}}s\sinh(s)\left(1 - \frac{f(s)}{2\gamma ac}\right), \tag{4.91}$$

in order to study its sign. Recall that $\|f\|_\infty = 1/3$, therefore we get from (4.91) that

$$\mu > 0 \quad \text{for} \quad \gamma ac > 1/6. \tag{4.92}$$

If $\gamma ac < 1/6$, then there exists $s_{\max} > 0$ such that $2\gamma ac = f(s_{\max})$, and we have $\mu > 0$ for $s \in (s_{max}, \infty)$ and $\mu < 0$ for $s \in (0, s_{\max})$. Assuming $\mu \neq 0$, and then considering $R(\xi)$ and its estimate (4.79), we have

$$|\mu - \xi R(\xi)| \geq |\mu| - \xi\tilde{M} \geq \frac{|\mu|}{2} \quad \text{if} \quad \xi \leq \frac{|\mu|}{2\tilde{M}}. \tag{4.93}$$

Then from (4.93), we obtain from (4.90)

$$\varphi_0'(\xi) + k\left(G * \varphi_0'\right)(\xi) \geq k\alpha c\frac{|\mu|}{2} \quad \text{for} \quad \xi \in [0, x^+_{\max}]$$

where $x^+_{\max} = \min\left(1, \frac{\mu}{2\tilde{M}}\right)$. This proves the first claim of the Lemma.
For the second claim, observe that λ in (4.81) is equal to

$$\lambda = -\mu + \left(\frac{c}{a} - \sqrt{\Delta}\right)\frac{d}{c^2\gamma} = -\mu + 2\sigma_1 d \tag{4.94}$$

by using (4.91). Because $\sigma_1 > 0$ and $d < 0$ as shown in Lemma 2 and (4.48), we have then

$$\lambda = -\mu + 2\sigma_1 d < -\mu,$$

and we conclude that $\mu < 0$ implies $\lambda > 0$ and $\lambda < 0$ implies $\mu > 0$. ■

4.5 Global analysis

This section completes the analysis of the trial solution φ in order to check (AC) on the whole interval $\xi \in (-\infty, \infty)$. The main result corresponds to Theorem 3 below.

Theorem 3 (Global verification of (AC))**.** *Assume $\sigma_2 e^{-\sigma_2} > \sigma_1 e^{-\sigma_1}$ and consider $x^+_{\max}$ defined by* (4.74)*. Then for all k small enough:*

$$\varphi(\xi) \text{ is increasing on } \left[-1, x^+_{\max}\right], \tag{4.95}$$

$$\varphi(\xi) \text{ is decreasing on } \left[\xi_1 - 1, \frac{\xi_1}{2}\right], \tag{4.96}$$

$$\varphi(\xi) > -\beta \text{ for } \xi \leq \xi_1 - 1 \text{ and } \xi \geq x^+_{\max}, \tag{4.97}$$

$$\varphi(\xi) < -\beta \text{ for } \xi \in \left[\frac{\xi_1}{2}, -1\right]. \tag{4.98}$$

Corollary 2. *Assume $c > \frac{b}{a\gamma \ln\left(\frac{1+b}{1-b}\right)}$ with $b = \sqrt{1-4a^2\gamma} \in \mathbb{R}$. Then for all k small enough, there exists a solitary wave solution of the BK model* (4.9) *satisfying (AC) and given by (4.10).*

The proof of Theorem (3) is based on Theorem 2 and Proposition 1 (to be shown below). In particular, we derive in Proposition 1 the condition $\sigma_2 e^{-\sigma_2} > \sigma_1 e^{-\sigma_1}$ appearing in Theorem 3. From this inequality we obtain the wave speed condition $c > \frac{b}{a\gamma \ln\left(\frac{1+b}{1-b}\right)}$ of Corollary 2, which is also assumed in the main existence theorem (Theorem 1).

Proposition 1. *Assume $\sigma_2 e^{-\sigma_2} > \sigma_1 e^{-\sigma_1}$. Then one has $\mu > 0$ and $\tilde{\varphi}'(\xi) \geq \alpha c k u(\xi) > 0$ for $\xi \in [0, 1)$, where*

$$u(\xi) = \frac{1}{\Delta}\left[\sigma_2 e^{-\sigma_2} - \sigma_1 e^{-\sigma_1}\right]\left[\frac{1 - e^{\sigma_1(\xi-1)}}{\sigma_1} - \frac{1 - e^{\sigma_2(\xi-1)}}{\sigma_2}\right]. \tag{4.99}$$

We also have $\tilde{\varphi}'(1) = 0$ and $\tilde{\varphi}(\xi) = 0$ for $\xi \in [1, \infty)$. Moreover, let $x_{\max}(k)$ satisfying $\lim_{k\to 0}(\xi_1 + x_{\max}(k)) = -\infty$. Then if k is small enough, one has $\tilde{\varphi}'(\xi) \leq k\sigma_1 d\alpha c < 0$ for $\xi \in [\xi_1, \xi_1 + x_{\max}(k)]$.

We first present the proof of Proposition 1 and then continue with the proof of Theorem 3 in section 4.5.2.

4.5.1 Proof of Proposition 1

Proof. From (4.27) we have $\tilde{\varphi}(\xi) = 0$ for $\xi \geq 1$ and $\tilde{\varphi}(\xi) = -k\alpha c\,(K * K)(\xi - 1)$ for $\xi \in [0, 1]$. Set

$$y(\xi) = (K * K)(\xi) \qquad \text{and} \qquad \mathfrak{J}(\xi) = y'(\xi) = (K * K')(\xi).$$

We want to find conditions ensuring $\tilde{\varphi}'(\xi) \geq 0$ for $\xi \in [0,1]$, which is equivalent to $\mathfrak{J}(\xi) \leq 0$ for $\xi \in [-1,0]$. We infer from (4.69) that

$$\text{if} \quad \mu > 0 \quad \text{then} \quad \mathfrak{J}(-1) < 0. \tag{4.100}$$

We also have $\mathfrak{J}(0) = \mathfrak{J}'(0) = 0$. Hence having $\mathfrak{J}(x) = \int_x^0 K(x-s)K'(s)ds$, where $K(x) > 0$ for $x \in (-\infty, 0)$, we have

$$\mathfrak{J}(x) < 0 \quad \text{for} \quad x \in [-1,0) \quad \text{if} \quad K'(x) \leq 0 \quad \text{for} \quad x \in [-1,0], \tag{4.101}$$

and $K'(x) \leq 0$ for $x \in [-1,0]$ if $x_c \leq -1$ (see Lemma 4). Hence setting $x_c \leq -1$ and using (4.34), we find the main condition

$$\sigma_2 e^{-\sigma_2} \geq \sigma_1 e^{-\sigma_1}. \tag{4.102}$$

Inequality (4.102) holds if $1 \geq \sigma_2$. Note from Lemma 2 that $\sigma_2 > \frac{1}{2\gamma ac}$, hence if $1 \geq \sigma_2$ we have $\gamma ac > 1/2$. So by (4.92), we have $\mu > 0$ and therefore $\mathfrak{J}(-1) < 0$ by (4.100), and we conclude that a sufficient condition for (4.102) is $1 \geq \sigma_2$.
If $x_c < -1$ then $K'(x) \leq K'(-1) < 0$ for $x \in [-1,0]$, and therefore

$$\begin{aligned} |\mathfrak{J}(x)| &\geq \left|K'(-1)\right| \left(\int_x^0 K(t)dt\right) \\ &= \frac{|K'(-1)|}{\sqrt{\Delta}} \left[\frac{1-e^{\sigma_1 x}}{\sigma_1} - \frac{1-e^{\sigma_2 x}}{\sigma_2}\right] \\ &\geq \frac{1}{\Delta}\left[\sigma_2 e^{-\sigma_2} - \sigma_1 e^{-\sigma_1}\right] \left[\frac{1-e^{\sigma_1 x}}{\sigma_1} - \frac{1-e^{\sigma_2 x}}{\sigma_2}\right] := u(x). \end{aligned} \tag{4.103}$$

Note that when (4.102) holds true we have

$$\tilde{\varphi}'(\xi) = -k\alpha c(K * K')(\xi - 1) = -k\alpha c\mathfrak{J}(\xi - 1) > 0 \quad \text{for} \quad \xi \in [0,1)$$

because (4.101) holds when (4.102) holds. Then using (4.103), we have

$$\tilde{\varphi}'(\xi) \geq k\alpha c u(\xi - 1) > 0 \quad \text{for} \quad \xi \in [0,1)$$

when (4.102) holds. This ends the proof of the first claim.

We address the second claim. Set $\xi = \xi_1 + x$ in $\tilde{\varphi}'(\xi)$ and assume (4.102) holds. Using (4.68), we find for $x \geq 0$

$$\begin{aligned} \frac{1}{\alpha c}\tilde{\varphi}'(\xi_1 + x) &= -K'(\xi_1 + x) + k\left(K * K'\right)(x-1) - k\left(\Delta_d K * K'\right)(\xi_1 + x) \\ &\leq -K'(\xi_1 + x) - k\Delta_d\left(K * K'\right)(\xi_1 + x), \end{aligned} \tag{4.104}$$

because $(K * K')(x-1) = \mathfrak{J}(x-1) \leq 0$ for $x \in [0,1]$ (by (4.101)) and $(K * K')(x-1)$ vanishes for $x \geq 1$. Note that $K'(x)$ defined in (4.35) has a unique global maximum at $x^* = 2x_c$, where $K''(x^*) = 0$ and $x* < x_c < 0$, and so $K'(x^*) > 0$. From Lemma 7, we have

$$K'(\xi_1) = -2\sigma_1 dk + o(k) \tag{4.105}$$

as $k \to 0$, and therefore we have $0 < K'(\xi_1) < K'(x^*)$ and $\xi_1 < x^*$ for k small enough. So by the intermediate value theorem, there exists $\xi_2(k) \in (x^*, x_c)$ such that $K'(\xi_1) = K'(\xi_2)$. Because $\lim_{k\to 0} \xi_1(k) = -\infty$ then $\lim_{k\to 0} K'(\xi_1(k)) = 0^+$, and thus $\lim_{k\to 0} \xi_2(k) = x_c$. If $\xi_1 + x \in [\xi_1, \xi_2]$ then $K'(\xi_1 + x) \geq K'(\xi_1)$ for $x \in [0, \xi_2 - \xi_1]$. This property gives in (4.104)

$$\frac{1}{\alpha c}\tilde{\varphi}'(\xi_1 + x) \leq -K'(\xi_1) - k\Delta_d \left(K * K'\right)(\xi_1 + x). \tag{4.106}$$

Now let us assume $x \in [0, x_{\max}(k)]$ with $\lim_{k\to 0} (\xi_1 + x_{\max}(k)) = -\infty$. Then by (4.105) and Lemma 5, we obtain from (4.106)

$$\begin{aligned}\frac{1}{\alpha c}\tilde{\varphi}'(\xi_1 + x) \leq& 2\sigma_1 dk + o(k) \leq \sigma_1 dk\end{aligned}$$

uniformly in $x \in [0, x_{\max}]$, for all k small enough. This completes the proof of Proposition 1. ■

4.5.2 Proof of Theorem 3

Let $x^+_{\max} = \min\left(1, \frac{\mu}{2\tilde{M}}\right)$ as in Lemma 12. Then with Theorem 2 we have

$$\begin{aligned}\tilde{\varphi}(x^+_{\max}) &= \tilde{\varphi}(0) + x^+_{\max}\tilde{\varphi}'(\theta), \qquad \theta \in (0, x^+_{\max}) \\ &\geq x^+_{\max}\frac{\alpha c}{2}\mu k - \beta + \mathcal{O}(k^2),\end{aligned}$$

where the last inequality holds from the error estimate (4.33). From Proposition 1, $\tilde{\varphi}(\xi)$ is increasing for $\xi \geq x^+_{\max}$, so

$$\tilde{\varphi}(\xi) \geq x^+_{\max}\frac{\alpha c}{2}\mu k - \beta + \mathcal{O}(k^2), \quad \text{for} \quad \xi \geq x^+_{\max}.$$

Then using the error estimate (4.33), we have

$$\varphi(\xi) \geq x^+_{\max}\frac{\alpha c}{2}\mu k + \mathcal{O}(k^2) - \beta > -\beta \quad \text{for} \quad \xi \geq x^+_{\max}. \tag{4.107}$$

Let us now estimate $\varphi(\xi)$ for $\xi < x_{\min} + \xi_1$. Set $\xi = \xi_1 + x$ and assume $x \leq x_{\min} < 0$. Then we get using (4.27),

$$\frac{1}{\alpha c}\tilde{\varphi}(\xi) = K(x) - K(x + \xi_1) + k\left(\Delta_d K * K\right)(x) - k\left(\Delta_d K * K\right)(x + \xi_1). \tag{4.108}$$

Then by setting $K(\xi) = e^{\sigma_1 \xi}\eta(\xi)$, where we define

$$\eta(\xi) = H(-\xi)\frac{1}{\sqrt{\Delta}}\left[1 - e^{(\sigma_1-\sigma_2)\xi}\right],$$

we obtain from (4.108),

$$\begin{aligned}\frac{1}{\alpha c}e^{-\sigma_1 x}\left[\tilde{\varphi}(\xi) - \alpha c K(x)\right] &= -e^{\sigma_1\xi_1}\eta(x+\xi_1) + 2k[\cosh(\sigma_1)-1]\left(\Delta_d\eta * \eta\right)(x) \\ &\quad -2ke^{\sigma_1\xi_1}[\cosh(\sigma_1)-1]\left(\Delta_d\eta*\eta\right)(x+\xi_1) \\ &= -e^{\sigma_1\xi_1}\tau_{\xi_1}\eta(x) \\ &\quad +2k\left[\cosh(\sigma_1)-1\right]\left(1 - e^{\sigma_1\xi_1}\tau_{\xi_1}\right)\left(\delta^+\eta * \delta^-\eta\right)(x) \quad (4.109)\end{aligned}$$

where we denote $\tau_{\xi_1}\eta(x) = \eta(x+\xi_1)$, $\delta^+ = \tau_1 - 1$, $\delta^- = 1 - \tau_{-1}$, and $\Delta_d = \delta^+\delta^-$. From (4.57), we have $e^{\sigma_1\xi_1} = -2kd\sqrt{\Delta} + o(k)$ for $k \approx 0$, and we get from (4.109),

$$\frac{1}{\alpha c}\|e^{-\sigma_1 x}\left(\tau_{\xi_1}\tilde{\varphi} - \alpha c K\right)\|_\infty \le 3k|d|\sqrt{\Delta}\|\eta\|_\infty + 4k\left(\cosh(\sigma_1)-1\right)\|\delta^+\eta\|_2^2 := \frac{b}{\alpha c}k, \quad (4.110)$$

where $b = \alpha c\left[3|d|\sqrt{\Delta}\|\eta\|_\infty + 4\left(\cosh(\sigma_1)-1\right)\|\delta^+\eta\|_2^2\right]$. Using estimate (4.110) in (4.109), we get

$$\begin{aligned}\tilde{\varphi}(\xi_1 + x) &\ge -bke^{\sigma_1 x} + \alpha c K(x) \\ &= e^{\sigma_1 x}\left[\alpha c\eta(x) - bk\right] \\ &\ge e^{\sigma_1 x}\left[\alpha c\eta(x_{\min}) - bk\right] > 0 \quad \text{for} \quad k \le \frac{\alpha c}{b}\eta(x_{\min}),\end{aligned}$$

uniformly in $x \in \mathbb{R}$. Therefore with the error estimate (4.33) it follows that

$$\varphi(\xi) \ge \tilde{\varphi}(\xi) + \mathcal{O}(k^2) \ge \mathcal{O}(k^2) > -\beta \quad \text{for} \quad \xi \le x_{\min} + \xi_1 \quad (4.111)$$

for all k small enough.

Let us now estimate $\varphi(\xi)$ for $\xi \in [\xi_1/2, x_{\min}]$. Using (4.57), we have

$$K\left(\frac{\xi_1}{2}\right) = \frac{1}{\sqrt{\Delta}}\left(e^{\sigma_1\xi_1/2} - e^{\sigma_2\xi_1/2}\right) \approx \sqrt{2k|d|}\Delta^{-1/4} \quad (4.112)$$

for $k \to 0$. Then, assuming k small enough in order to have $\xi_1 \le -2$ (so that $\frac{\xi_1}{2} - \xi_1 - 1 \ge 0$), one has for all $\xi \in \left[\frac{\xi_1}{2}, x_{\min}\right]$ (where $x_{\min} < 0$), using (4.27) and (4.112),

$$\begin{aligned}\tilde{\varphi}(\xi) &= -\alpha c K(\xi) - \alpha c k\left(\Delta_d K * K\right)(\xi) \\ &\le -\alpha c K\left(\frac{\xi_1}{2}\right) + \alpha c k\|\Delta_d K * K\|_\infty \\ &= -\alpha c\sqrt{2|d|}\Delta^{-1/4}\sqrt{k} + o(k).\end{aligned}$$

By using the error estimate (4.33), we have then

$$\varphi(\xi) \leq \tilde{\varphi}(\xi) + \mathcal{O}(k^2) \leq -\alpha c\sqrt{2|d|}\Delta^{-1/4}\sqrt{k} + o(\sqrt{k}) < -\beta \quad \text{for} \quad \xi \in \left[\frac{\xi_1}{2}, x_{\min}\right]. \tag{4.113}$$

Let us now set $x_{\max}(k) = \frac{|\xi_1|}{2}$, so that we have $\xi_1 + x_{\max}(k) = \frac{\xi_1}{2} \to -\infty$ as $k \to 0$. Then Proposition 1 ensures that for all k small enough

$$\tilde{\varphi}'(\xi) \leq k\sigma_1 d\alpha c < 0 \quad \text{for} \quad \xi \in \left[\xi_1, \frac{\xi_1}{2}\right].$$

Then using the error estimate (4.33) yields

$$\varphi'(\xi) \leq k\sigma_1 d\alpha c + \mathcal{O}(k^2) < 0 \quad \text{for} \quad \xi \in \left[\xi_1, \frac{\xi_1}{2}\right], \tag{4.114}$$

which means $\varphi(\xi)$ is decreasing on $\left[\xi_1, \frac{\xi_1}{2}\right]$. Fixing $x_{\min} = -1$, it follows that (4.95) holds by Theorem 2, (4.96) holds by (4.114), (4.97) holds by (4.107) and (4.111), (4.98) holds by (4.113). This completes the proof of Theorem 3. ■

Chapter 5

Conclusions and perspectives

The main goal of this thesis was the understanding of propagation phenomena in elastic discrete excitable systems. We have considered two mechanical models. The first one describes the displacement of an infinite spring-block chain subjected to gravity and sliding down a slope. The second corresponds to the Burridge-Knopoff model that has been previously introduced to describe the dynamics of two elastic media under frictional contact. Both models involve a nonlinear friction law of spinodal type (with velocity-strengthening regions at both low and high sliding velocities) which induces excitable properties. We have studied the consequences of such friction laws on the dynamics of travelling fronts and pulses.

The analysis of the chain sliding down a slope was done in chapter 2. We have shown the existence of propagation phenomena that have not been previously reported in the discrete diffusive counterpart (discrete Nagumo-type equations). A first example is the existence of pulses made out of two front solutions (a leading front and a trailing front). This property has been observed in a totally different context corresponding to feedforward neural networks with excitatory and inhibitory connections [48]. A second difference with respect to previous works [14–16, 20, 30] is that front propagation failure does not occur at weak coupling strengths. In discrete Nagumo equations, this situation occurs only for special nonlinearities [81, 86]. The propagation failure of pulses occurs through the collision and annihilation of two travelling fronts propagating in the same direction, with the trailing front faster than the leading front. Such phenomenon occurs when the pulling velocity is greater than a critical value. At the end of chapter 2, we have drawn a link between the above front solutions and solitary waves of the Burridge-Knopoff model, showing that the fronts can approximate small transition re-

gions of solitary waves. This suggest the possibility of an asymptotic construction of pulses in the BK model based on the solutions of the falling chain model. Similar ideas have been previously exploited in FitzHugh-Nagumo systems to construct travelling pulses [30].

In chapters 3 and 4, several spinodal friction laws were considered for the analysis of solitary waves in the BK model, including a piecewise-linear discontinuous function of the sliding velocity. The use of this piecewise linear function allowed us to construct solitary waves explicitly in the form of oscillatory integrals and prove an existence theorem at low coupling. Flytzanis et al. [38] considered a similar approach based on piecewise-linear nonlinearities to study a lattice model of dislocation. Using the same idea, Vainchtein et al. [40–43] have obtained travelling fronts and solitary waves in Frenkel-Kontorova and Fermi-Pasta-Ulam chains. Herrmann et al. [87] have shown the robustness of this approach when nonlinear terms are regularized by adding of a small spinodal layer. It would be very interesting to adapt the approach of [87] in order to establish the existence of solitary waves in the BK model with smooth spinodal friction laws close to the idealized piecewise-linear law considered in this thesis. On another aspect, it would be interesting to extend our theoretical results to more general friction laws. Different analytical techniques could be applied to bilinear laws regularized by a small spinodal layer, discontinuous laws with two different slopes or the trilinear law, see e.g. [38, 41, 42, 85, 88–91] and references therein.

Another important extension of this work would be to treat the case of multivalued friction laws, i.e. generalized Coulomb laws of spinodal type. Such friction force will require a careful treatment in the numerical and in the analytical study, since differential inclusions should be considered if sliding solutions occur. In the present work, we have numerically observed solitary wave propagation in the BK model with regularized spinodal Coulomb laws, hence we conjecture the persistence of such waves for multivalued friction laws. In the case of the piecewise-linear discontinuous friction law, the jump discontinuity did not require special attention since we considered solutions that cross the discontinuity transversally, discarding any sliding solutions.

It would be also interesting to compute the travelling waves numerically using Newton-type methods and path following (in particular to study the transition from low coupling to the continuum limit) and to analyse the linear stability of solitary

waves and fronts. The linear stability problems may be also addressed analytically in the case of the piecewise-linear friction law. Such analysis may clarify the similarities with reaction-diffusion systems of FitzHugh-Nagumo type where two travelling pulse solutions have been found: a stable fast pulse and an unstable slow pulse [18]. Other studies on the stability of travelling waves in lattices which could be useful in the present context include the works of Hupkes et al. [92] and Carpio et. al [93].

The models studied here are one-dimensional. The generalization to two-dimensional networks is a challenging problem with, in particular, the following issues: understanding propagation failure, derivation of the wave speed, shape of the travelling wave profiles, influence of the propagation angle. The investigation of spiral waves in 2-dimensional excitable elastic media remains to be done. Spiral waves are well-known patterns in two-dimensional reaction-diffusion systems [8, 83, 94], hence we can wonder if those patterns may exist in elastic excitable systems [95]. Another aspect not explored in the BK model was the reflection of pulses at the boundaries and the penetration of waves with and without annihilation. Those properties are reported in excitable systems with linear-cross diffusion and are also found in the BK model [83].

Finally, we have proposed in chapters 3 a possible mechanical implementation of the BK model with piecewise-linear discontinuous nonlinearity. This system corresponds to a chain of linear oscillators subjected to impulsive forces applied in the direction of motion when their deflection crosses a specific threshold. It would be interesting to realize such an experimental setup (for example using MEMS) in order to investigate the excitation of solitary waves. Along the same line, the experimental observation of solitary waves along regular patterned interfaces displaying spinodal frictional resistance constitutes a challenging open problem.

Bibliography

[1] G. B. Ermentrout, D. H. Terman, Mathematical foundations of neuroscience, Springer, 2010.

[2] J. P. Françoise, Oscillations en biologie, Biomathematics, Springer-Verlag Berlin Heidelberg, 2005.

[3] V. N. Biktashev, M. A. Tsyganov, Solitary waves in excitable systems with cross-diffusion, Proc. R. Soc. A 461 (2005) 3711–3730.

[4] A. V. Holden, M. Markus, H. G. Othmer, Nonlinear wave processes in excitable media, Springer Sciences + Business Media, 1989.

[5] J. D. Murray, Mathematical biology II: Spatial modes and biomedical applications, Springer, 2003.

[6] C. B. Muratov, Traveling wave solutions in the Burridge-Knopoff model, Phys. Rev. E 59 (1999) 3847–3857.

[7] J. H. E. Cartwright, E. Hernández-García, O. Piro, Burridge-Knopoff models as elastic excitable media, Phys. Rev. Lett. 79 (1997) 527–530.

[8] M. A. Tsyganov, V. N. Biktashev, J. Brindley, A. V. Holden, G. R. Ivanitsky, Waves in systems with cross-diffusion as a new class of nonlinear waves, Physics-Uspekhi 50 (2007) 263–286.

[9] M. Locher, G. A. Johnson, E. R. Hunt, Spatiotemporal stochastic resonance in a system of coupled diode resonators, Phys. Rev. Lett. 77 (1996) 4698.

[10] M. Remoissenet, Waves called solitons - Concepts and experiments, Springer Verlag Berlin, 1999.

[11] J. P. Laplante, T. Erneux, Propagation failure in arrays of coupled bistable chemical reactors, J. Phys. Chem. 96 (1992) 4931.

[12] T. H. Keit, M. A. Lewis, R. D. Holt, Alle effects, invasion pinning, and species borders, Am. Nat. 157 (2001) 203 – 216.

[13] J. P. Keener, Propagation and its failure in coupled systems of discrete excitable cells, SIAM J. Appl. Math. 47 (1987) 556–572.

[14] C. E. Elmer, E. S. Van Vleck, Spatially discrete FitzHugh-Nagumo equations, SIAM J. Appl. Math. 65 (2005) 1153–1174.

[15] H. J. Hupkes, B. Sandstede, Travelling pulses for the discrete FitzHugh-Nagumo system, SIAM J. Appl. Dyn. Syst. 9 (2010) 827–882.

[16] A. Carpio, L. Bonilla, Pulse propagation in discrete systems of coupled excitable cells, SIAM J. Appl. Math. 63 (2002) 619–635.

[17] A. Carpio, L. Bonilla, Wave front depinning transition in discrete one-dimensional reaction-diffusion systems, Phys. Rev. Lett. 86 (2001) 26.

[18] J. Rinzel, J. B. Keller, Traveling wave solutions of a nerve conduction equation, Biophys. J. 13 (1973) 1313–1337.

[19] J. W. Cahn, J. Mallet-Paret, E. S. Van Vleck, Traveling wave solutions for systems of ODEs on a two-dimensional spatial lattice, SIAM J. Appl. Math. 59 (1999) 455–493.

[20] A. Tonnelier, McKean caricature of the FitzHugh-Nagumo model: traveling pulses in a discrete diffusive medium, Phys. Rev. E 67 (2003) 036105.

[21] E. P. Zemskov, E. P. Zykov, V. S. Kassner, S. C. Muller, Stability of travelling fronts in a piecewise-linear reaction-diffusion system, Nonlinearity 13 (2000) 2063–2076.

[22] T. Erneux, G. Nicolis, Propagating waves in discrete bistable reaction-diffusion systems, Physica D 67 (1993) 237–244.

[23] B. Zinner, Existence of traveling wavefront solutions for the discrete Nagumo equation, J. of Diff. Eqs. 96 (1992) 1–27.

[24] J. H. E. Cartwright, V. M. Eguíluz, E. Hernández-García, O. Piro, Dynamics of elastic excitable media, Int J. Bif. Chaos 9 (1999) 2197–2202.

[25] F. Heslot, T. Baumberger, B. Perrin, C. Caroli, B. Caroli, Creep, stick-slip, and dry friction dynamics: Experiments and a heuristic model, Phys. Rev. E 49 (1994) 4973–4988.

[26] F. Wu-Bavouzet, J. Clain-Burckbuchler, A. Buguin, P.-G. De Gennes, F. Brochard-Wyart, Stick-Slip: wet versus dry, The Journal of Adhesion 83 (2007) 761–784.

[27] K. Vorvolakos, M. K. Chaudhury, The effects of molecular weight and temperature on the kinetic friction of silicone rubbers, Langmuir 19 (2003) 6778–6787.

[28] J. P. Gong, Friction and lubrication of hydrogels - its richness and complexity., The Royal Society of Chemistry 2006 2 (2006) 544–552.

[29] B. N. J. Persson, E. Tosatti, Physics of Sliding Friction, Springer Science, 2007.

[30] A. Carpio, L. Bonilla, Depinning transitions in discrete reaction-diffusion equations, SIAM J. Appl. Math. 63 (2002) 1056–1082.

[31] M. Varenberg, S. N. Gorb, Hexagonal surface micropattern for dry and wet friction, Advanced Materials 21 (2009) 483–486.

[32] W. Huang, X. Wang, Biomimetic design of elastomer surface pattern for friction control under wet conditions, Bioinspiration and Biomimetics 8 (2013) 046001.

[33] Y. S. Kivshar, F. Zhang, S. Takeno, Nonlinear surface modes in monoatomic and diatomic lattices, Physica D 113 (1998) 248–260.

[34] P. Maniadis, S. Flach, Mechanism of discrete breather excitation in driven micromechanical cantilever arrays, Europhys. Lett. 74 (2006) 452–458.

[35] J. Rhoads, S. W. Shaw, K. L. Turner, Nonlinear dynamics and its applications in micro-and nanoresonators, Proceedings of DSCC2008 158 (2008) 1–30.

[36] A. Vainchtein, E. S. V. Vleck, Nucleation and propagation of phase mixtures in a bistable chain, Phys. Rev. B 79 (2009) 144123.

[37] J. D. Murray, Mathematical biology I. An introduction, Interdisciplinary applied mathematics 17, Springer-Verlag Berlin Heidelberg, 2002.

[38] N. Flytzanis, S. Crowley, V. Celli, High velocity dislocation motion and interatomic force law, J. Phys. Chem. Solids 38 (1977) 539–552.

[39] W. Atkinson, N. Cabrera, Motion of a Frenkel-Kontorova dislocation in a one-dimensional crystal, Phys. Rev. A 138 (1965) 763–766.

[40] L. Truskinovsky, A. Vainchtein, Kinetics of martensitic phase transitions: Lattice model, SIAM J. Appl. Math. 66 (2005) 533–553.

[41] A. Vainchtein, The role of spinodal region in the kinetics of lattice phase transitions, Journal of Mechanics and Physics of Solids 58 (2010) 227–240.

[42] L. Truskinovsky, A. Vainchtein, Solitary waves in a nonintegrable Fermi-Pasta-Ulam chain, Physical Review E 90 (2014) 42903.

[43] P. Rosakis, A. Vainchtein, New solutions for slow moving kinks in a forced Frenkel-Kontorova chain, Journal of Nonlinear Science 23 (2013) 1089–1110.

[44] H. Schwetlick, J. Zimmer, Existence of dynamic phase transitions in a one-dimensional lattice model with piecewise quadratic interaction potential, SIAM J. Math. Anal. 41 (2009) 1231–1271.

[45] A. Vainchtein, E. S. V. Vleck, A. Zhang, Propagation of periodic patterns in a discrete system with competing interactions, SIAM J. Appl. Dyn. Systems 14 (2015) 523–555.

[46] R. Burridge, L. Knopoff, Model and theoretical seismicity, Bull. Seismol. Soc. Am. 57 (1967) 341–371.

[47] M. Duanmu, N. Whitaker, P. Kevrekidis, A. Vainchtein, J. Rubin, Traveling wave solutions in a chain of periodically forced coupled nonlinear oscillators, Physica D 325 (2016) 25–40.

[48] A. Tonnelier, Stabilization of pulse waves through inhibition in a feedforward neural network, Physica D 210 (2005) 118–137.

[49] Y. Y. Kagan, Observational evidence for earthquakes as a nonlinear dynamic process, Physica D 77 (1994) 160–192.

[50] C. Scholz, The Mechanics of Earthquakes and Faulting, Cambridge University Press, 2002.

[51] B. Kaproth, C. Marone, Slow earthquakes, preseismic velocity changes, and the origin of slow frictional stick-slip, Science 341 (2013) 1229–1232.

[52] J. M. Carlson, J. S. Langer, Properties of earthquakes generated by fault dynamics, Phys. Rev. Lett. 62 (1989) 2632.

[53] Y. Bar-Sinai, R. Spatschek, E. A. Brener, E. Bouchbinder, On the velocity-strengthening behaviour of dry friction, J. Geophys. Res. Solid Earth 119 (2014) 1738–1748.

[54] T. Putelat, J. Dawes, J. Willis, Regimes of frictional sliding of a spring-block system, J. Mech. Phys. Sol. 58 (2010) 27–53.

[55] J. Wang, R. Hwang, One-dimensional dynamic simulations of slip complexity of earthquake faults, Earth Planets Space 53 (2001) 91–100.

[56] A. Ohmura, H. Kawamura, Rate- and state-dependent friction law and statistical properties of earthquakes, EPL (Europhysics Letters) 77 (2007) 69001.

[57] B. Erickson, B. Birnir, D. Lavallée, Periodicity, chaos and localization in a Burridge–Knopoff model of an earthquake with rate-and-state friction, Geophys. J. Int. 187 (2011) 178–198.

[58] J. Wang, One-dimensional dynamical modelling of earthquakes: a review, Terr. Atmos. Ocean. Sci 19 (2008) 183–203.

[59] V. Acary, B. Brogliato, Numerical methods for nonsmooth dynamical systems. Applications in mechanics and electronics, Springer, 2008.

[60] J. Bastien, C. Lamarque, Theoretical study of a chain sliding on a fixed support, Mathematical Problems in Engineering 2009 (2009) 19 pages. doi:10.1155/2009/361296.

[61] X. Xiong, R. Kikuuwe, M. Yamamoto, Implicit Euler simulation of one-dimensional Burridge-Knopoff model of earthquakes with set-valued friction laws, Advances in Computational Mathematics 41 (2015) 1039–1057.

[62] M. Lebellego, Phénomènes ondulatoires dans un modèle discret de faille sismique, Ph.D. thesis, Université de Toulouse (2011).

[63] J. M. Carlson, J. S. Langer, Mechanical model of an earthquake fault, Phys. Rev. A 40 (1989) 6470–6484.

[64] J. Schmittbuhl, J. P. Vilotte, S. Roux, Propagative macrodislocation modes in an earthquake fault model, Europhys. Lett. 21 (1993) 375–380.

[65] P. Español, Propagative slipping modes in a spring-block model, Phys. Rev. E 50 (1994) 227–235.

[66] J. Schmittbuhl, J. P. Vilotte, S. Roux, A dissipation-based analysis of an earthquake fault model, J. Geophys. Res. 101 (1996) 27741–27764.

[67] Y. Estrin, Y. Bréchet, On a model of frictional sliding, Pure Appl. Geophys. 147 (1996) 745–762.

[68] T. Shimamoto, Transition between frictional slip and ductile flow for halite shear zones at room temperature, Science 231 (1986) 711–714.

[69] R. FitzHugh, Impulses and physiological states in theoretical models of nerve membrane, Biophysical Journal 1 (1961) 445 – 466.

[70] E. C. Zeeman, Differential equations for the heartbeat and nerve impulse, in: Towards a theoretical biology, Vol. 4, Edinburgh University Press Edinburgh, 1972, pp. 8–67.

[71] M. Feingold, D. L. Gonzalez, O. Piro, H. Viturro, Phase locking, period doubling, and chaotic phenomena in externally driven excitable systems, Phys. Rev. A 37 (1988) 4060–4063.

[72] E. M. Izhikevich, Dynamical systems in neuroscience: The geometry of excitability and bursting, The MIT Press, 2007.

[73] H. J. Xu, L. Knopoff, Periodicity and chaos in a one-dimensional dynamical model of earthquakes, Phys. Rev. E 50 (1994) 3577–3581.

[74] E. Bouchbinder, E. A. Brener, I. Barel, M. Urbakh, Slow cracklike dynamics at the onset of frictional sliding, Phys. Rev. Lett. 107 (2011) 235501.

[75] Y. Bar-Sinai, R. Spatschek, E. A. Brener, E. Bouchbinder, Instabilities at frictional interfaces: Creep patches, nucleation, and rupture fronts, Phys. Rev. E 88 (2013) 060403.

[76] Y. Bar-Sinai, R. Spatschek, E. A. Brener, E. Bouchbinder, Velocity-strengthening friction significantly affects interfacial dynamics, strength and dissipation, Sci. Rep. 5 (2015) 7841.

[77] J. C. Comte, P. Tchofo-Dinda, M. Remoissenet, Discrete Burridge-Knopoff model, with exact solitonic or compactlike traveling wave solution, Phys. Rev. E 65 (2002) 026615.

[78] H. P. McKean Jr., Nagumo's equation, Adv. Math. 4 (1970) 209–223.

[79] O. Kresse, L. Truskinovsky, Mobility of lattice defects: discrete and continuum approaches, J. Mech. Phys. Solids 51 (2003) 13051332.

[80] O. Kresse, L. Truskinovsky, Prototypical lattice model of a moving defect: the role of environmental viscosity, Izvestiya, Phys. Solid Earth 43 (2007) 6366.

[81] G. Fáth, Propagation failure of traveling waves in discrete bistable medium, Physica D 116 (1998) 176190.

[82] N. A. Venturi, F. Nori, Marginal stability and chaos in coupled faults modelled by nonlinear circuits, Phys. Rev. Lett. 74 (1995) 74–77.

[83] M. A. Tsyganov, V. N. Biktashev, Classification of wave regimes in excitable systems with linear cross-diffusion, Phys. Rev. E 90 (2014) 062912.

[84] C. F. Kreiner, J. Zimmer, Existence of subsonic heteroclinic waves for the Frenkel-Kontorova model with piecewise quadratic on-site potential, Nonlinearity 24 (2011) 1137.

[85] M. Herrmann, K. Matthies, H. Schwetlick, J. Zimmer, Subsonic phase transition waves in bistable lattices models with small spinodal region, SIAM J. Math. Anal. 45 (2013) 2625–2645.

[86] H. J. Hupkes, D. Pelinovsky, B. Sandstede, Propagation failure in the discrete Nagumo equation, Proceedings of the AMS 139 (2011) 3537–3551.

[87] M. Herrmann, Ground waves in atomic chains with bi-monomial double-well potential, Nonlinear Anal.-Theory Methods Appl. 76 (2013) 41–51.

[88] Y. Earmme, J. Weiner, Dislocation dynamics in the modified Frenkel-Kontorova model, J. Appl. Phys. 48 (1977) 33173341.

[89] V. Celli, N. Flytzanis, Motion of a screw dislocation in a crystal, J. Appl. Phys. 41 (1970) 44434447.

[90] O. Kresse, L. Truskinovsky, Lattice friction for crystalline defects: From dislocations to cracks, J. Mech. Phys. Solids 52 (2004) 25212543.

[91] L. I. Slepyan, A. Cherkaev, E. Cherkaev, Transition waves in bistable structures. II. Analytical solution: wave speed and energy dissipation, J. Mech. Phys. Solids 53 (2005) 407436.

[92] H. J. Hupkes, B. Sandstede, Stability of pulse solutions for the discrete FitzHugh-Nagumo system, Trans. Am. Math. Soc. 365 (2013) 251–301.

[93] A. Carpio, L. Bonilla, Nonlinear stability of oscillatory wave fronts in chains of coupled oscillators, Phys. Rev. E 69 (2004) 046601.

[94] X. Huang, W. C. Troy, Q. Yand, H. Ma, C. R. Laing, S. Schiff, J. Wu, Spiral waves in disinhibited mammalian neocortex, The journal of neuroscience 24 (2004) 9897–9902.

[95] A. P. Muñuzuri, C. Innocenti, J. M. Flesselles, J. M. Gilli, K. I. Agladze, V. I. Krinsky, Elastic excitable medium, Phys. Rev. E 50 (1994) R667–R670.